

AD-A013 736

HIGH RESOLUTION SPECTRAL SURVEY OF MOLECULAR ABSORPTION
IN THE DF LASER REGION - MEASUREMENTS AND CALCULATIONS

Douglas Woods, et al

Science Applications, Incorporated

Prepared for:

Rome Air Development Center
Defense Advanced Research Projects Agency

July 1975

DISTRIBUTED BY:

NTIS

National Technical Information Service
U. S. DEPARTMENT OF COMMERCE

239135

RADC-TR-75-180
Technical Report
July 1975



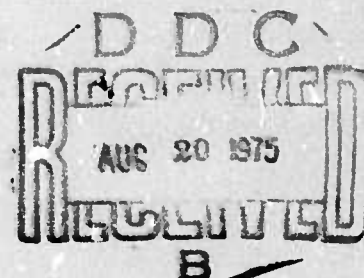
ADA013736

HIGH RESOLUTION SPECTRAL SURVEY OF MOLECULAR
ABSORPTION IN THE DF LASER REGION
MEASUREMENTS AND CALCULATIONS

Science Applications, Inc.

Sponsored by
Defense Advanced Research Projects Agency
ARPA Order No. 1279

Approved for public release;
distribution unlimited.



The views and conclusions contained in this document are those of the authors and should not be interpreted as necessarily representing the official policies, either expressed or implied, of the Defense Advanced Research Projects Agency or the U. S. Government.

Rome Air Development Center
Air Force Systems Command
Griffiss Air Force Base, New York 13441

Reproduced by
NATIONAL TECHNICAL
INFORMATION SERVICE
U S Department of Commerce
Springfield VA 22151

101

This report has been reviewed by the RADC Information Office (OI) and is releasable to the National Technical Information Service (NTIS). At NTIS it will be releasable to the general public including foreign nations.

This report has been reviewed and is approved for publication.

APPROVED:

James W. Cusack
JAMES W. CUSACK
Project Engineer

ACCESSION for		
NTIS	White Section	<input checked="checked" type="checkbox"/>
DEC	Bull Section	<input type="checkbox"/>
UNANNOUNCED		<input type="checkbox"/>
JUSTIFICATION		
BY		
DISTRIBUTION/AVAILABILITY CODES		
Dist.	AVAIL. and/or SPECIAL	
A		

Do not return this copy. Retain or destroy.

HIGH RESOLUTION SPECTRAL SURVEY OF MOLECULAR
ABSORPTION IN THE DF LASER REGION
MEASUREMENTS AND CALCULATIONS

Douglas R. Woods
Robert E. Meredith
Frederick G. Smith
Thomas W. Tuer

Contractor: Science Applications, Inc.
Contract Number: F30602-75-C-0028
Effective Date of Contract: 1 Aug 74
Contract Expiration Date: 31 Jul 75
Amount of Contract: \$93,346.00
Program Code Number: OE20
Period of work covered: 1 Aug 74 - 1 Mar 75

Principal Investigator: Dr. Robert E. Meredith
Phone: 313 662-3261

Project Engineer: James W. Cusack
Phone: 315 330-3145

This research was supported by the Defense
Advanced Research Projects Agency of the
Department of Defense and was monitored by
James W. Cusack (OCSE) Griffiss AFB NY
13441

UNCLASSIFIED

SECURITY CLASSIFICATION OF THIS PAGE (When Data Entered)

REPORT DOCUMENTATION PAGE		READ INSTRUCTIONS BEFORE COMPLETING FORM
1. REPORT NUMBER RADC-TR-75-180	2. GOVT ACCESSION NO.	3. RECIPIENT'S CATALOG NUMBER
4. TITLE (and Subtitle) HIGH RESOLUTION SPECTRAL SURVEY OF MOLECULAR ABSORPTION IN THE DF LASER REGION - MEASUREMENTS AND CALCULATIONS		5. TYPE OF REPORT & PERIOD COVERED Interim Technical Report 1 Aug 74 - 1 Feb 75
7. AUTHOR(s) Douglas Woods Robert Meredith Frederick Smith Thomas Tuer		6. PERFORMING ORG. REPORT NUMBER N/A
9. PERFORMING ORGANIZATION NAME AND ADDRESS Science Applications, Inc. P O Box 328 Ann Arbor MI 48107		8. CONTRACT OR GRANT NUMBER(s) F30602-75-C-0028
11. CONTROLLING OFFICE NAME AND ADDRESS Defense Advanced Research Projects Agency 1400 Wilson Blvd Arlington VA 22209		10. PROGRAM ELEMENT, PROJECT, TASK AREA & WORK UNIT NUMBERS 62301E 12790507
14. MONITORING AGENCY NAME & ADDRESS (if different from Controlling Office) Rome Air Development Center (OCSE) Griffiss AFB NY 13441		12. REPORT DATE July 1975
		13. NUMBER OF PAGES 101
		15. SECURITY CLASS. (of this report) UNCLASSIFIED
		15a. DECLASSIFICATION/DOWNGRADING SCHEDULE N/A
16. DISTRIBUTION STATEMENT (of this Report) Approved for public release; distribution unlimited.		
17. DISTRIBUTION STATEMENT (of the abstract entered in Block 20, if different from Report) Same		
18. SUPPLEMENTARY NOTES RADC Project Engineer: James W. Cusack/OCSE		
19. KEY WORDS (Continue on reverse side if necessary and identify by block number) CH ₄ Spectrum DF Laser Propagation HDO Spectrum Atmospheric Absorption N ₂ O Spectrum Molecular Absorption		
20. ABSTRACT (Continue on reverse side if necessary and identify by block number) The air-broadened spectra of N ₂ O, HDO, and CH ₄ have been measured in the DF laser region between 2545 cm ⁻¹ and 2745 cm ⁻¹ . These measurements were performed at a resolution better than the individual absorption line widths. The measured spectra are compared with synthetic spectra calculated using the AFCRL Atmospheric Absorption Line Parameters Compilation. For N ₂ O, excellent agreement is found between the measured and calculated spectra. The measured HDO lines tend to be stronger and wider than calculated, by factors of 50% and 25%, (Cont'd)		

DD FORM 1473

JAN 73

EDITION OF 1 NOV 65 IS OBSOLETE

UNCLASSIFIED

SECURITY CLASSIFICATION OF THIS PAGE (When Data Entered)

UNCLASSIFIED

SECURITY CLASSIFICATION OF THIS PAGE(When Data Entered)

respectively. However, some lines were much weaker than calculated. The measured CH₄ spectra had many additional lines and was many times stronger than the calculated spectra. Correction of the erroneous line strengths and widths will lead to substantial changes in the calculated molecular line absorption of many DF laser lines.

Molecular line absorption has also been calculated as a function of temperature and altitude for the P₃(8) and P₁(9) DF laser lines using approximate line parameters consistent with the current measurement results. These calculations illustrate significant temperature and altitude effects, and show the importance of using accurate line parameters.

11

UNCLASSIFIED

SECURITY CLASSIFICATION OF THIS PAGE(When Data Entered)

ACKNOWLEDGEMENT

The measurements reported here were performed in cooperation with Professor C. W. Peters and Mr. Daniel H. Leslie of The University of Michigan Physics Department under Subcontract SAI-140-334-00-1. Their substantial contributions to this work are greatly appreciated.

TABLE OF CONTENTS

Acknowledgement.....	ii
Summary.....	iii
List of Figures.....	vi
List of Tables	vii
1. Introduction.....	1
2. Altitude and Temperature Scaling.....	5
3. Instrumentation	19
4. Measured and Synthetic Spectra.....	24
5. Conclusions	35
References	91

FIGURES

1.	Contributors to the Molecular Absorption of the $P_1(9)$ DF Line (Midlatitude Summer, Sea Level)	9
2.	Altitude Dependence of the $P_3(8)$ DF Laser Molecular Line Absorption Coefficient for Various Line Positions	11
3.	Altitude Dependence of the Molecular Line Absorption Coefficient for the $P_3(8)$ DF Line Showing the Major Contributors (Midlatitude Summer)	13
4.	Altitude Dependence of the Molecular Line Absorption Coefficient for the $P_1(9)$ DF Line Showing the Major Contributors (Midlatitude Summer)	14
5.	Altitude Dependence of the Molecular Line Absorption Coefficient for the $P_1(9)$ DF Line Showing the Major Contributors (Midlatitude Winter)	15
6.	Temperature Dependence of the Major Molecular Line Absorption Coefficient Contributors for the $P_1(9)$ and $P_3(8)$ DF Lines.	17
7.	Instrument Optics	20
8.	End View of Double Pass Light Path	20
9.	Data Acquisition System	21
10.	Slit Function	26
11.	Comparison of Narrow Absorption Lines (0.044 cm^{-1} half width) Calculated Using Infinite Resolution with Those Calculated Using the Actual Spectrometer Resolution.	28
12.	Comparison of Narrow Absorption Lines (0.044 cm^{-1} half width) Calculated Using Infinite Resolution with Those Calculated Using the Actual Spectrometer Resolution.	29
13-22.	Measured and Calculated N_2O Spectra	37
23-42.	Measured and Calculated CH_4 Spectra	48
43-63.	Measured and Calculated HDO Spectra	69

TABLES

1. $P_1(9)$ Absorption Coefficients (10^{-3} km^{-1})	8
2. Slit Widths	27

HIGH RESOLUTION SPECTRAL SURVEY OF MOLECULAR ABSORPTION IN THE DF LASER REGION

Measurements and Calculations

1. INTRODUCTION

1.1 Background

Three kinds of measurements are required for a confirmed knowledge of laser molecular absorption in the atmosphere. These are: (1) laser measurements over long paths in the "real world," (2) laser measurements through long paths in the laboratory under simulated atmospheric conditions, and (3) frequency dependent absorption profile measurements from which predictive modeling parameters may be extracted.

The role of field measurements is most obvious. Field measurements provide the greatest protection against surprises when systems are deployed under conditions similar to those of the measurements. They provide the ultimate test of laboratory simulations and of predictive modeling procedures, and eliminate the need to study obscure effects which have a very low probability of affecting atmospheric absorption of laser radiation. The importance of such effects will be easily detected by comparison of field measurement results with expectations based on modeling and simulations.

However, field measurements are expensive and time consuming, and it is impossible to span every combination of temperature, humidity, altitude, laser type and laser line. In fact, for satellite or aircraft borne laser systems the Doppler shift of the laser frequency is sufficient to move the laser frequency on or off absorption lines, thereby rendering fixed frequency measurements inappropriate. In short, while they provide the ideal tests of predictive modeling, they are unsuitable for

independently determining the parameters required for predictive modeling. Of course, a set of parameters could be selected to fit the field measurement results. However, these parameters would be valid only for the limited range of conditions measured in the field, and would be unsuitable for modeling other laser frequencies.

Fixed frequency laboratory measurements eliminate many of the inherent difficulties of field measurements, and they allow the absorption of individual molecular species to be measured separately. Thus, effects due to changes in concentrations can be modeled from these measurements, and to some extent field measurements and spectral measurements can be guided by them. However the characterization of laser absorption over the range of temperatures and pressures encountered in the atmosphere would require a large number of measurements. And even if this were done for each of the lines of a particular laser, these results could not be used to determine the molecular line absorption of another laser operating in the same spectral region. Such measurements determine the absorption only at a small number of monochromatic points (which happen to correspond to laser lines) out of perhaps 20,000 points needed to describe completely the absorption in one spectral region.

The approach being pursued in the current work is to measure directly the frequency dependent absorption profiles, from which modeling parameters for the entire spectral region may be extracted. Once the parameters are known, they can be used to calculate the laser absorption for all combinations of concentration, pressure, and temperature found in the atmosphere. Hence the absorption is defined for all humidities, altitudes, temperatures, and slant ranges. Another advantage of this approach is that it can determine the monochromatic absorption for all frequencies in the region rather than just at a few specific frequencies. The parameters only need to be determined once for a particular region; thus

no additional spectral measurements would be required for each new laser of interest in that region. No additional measurements would be required to determine the change in absorption of laser beams launched from fast aircraft or satellites due to the Doppler shift. Of course, one would not be satisfied in relying completely on predictive analysis. However, when accurate absorption line parameters are available, a very limited set of laboratory and field measurements would be sufficient to provide confidence in the modeling.

In addition to its direct application for laser propagation, the value of predictive analysis in interpreting laboratory and field measurements cannot be overemphasized. In the field, and to a lesser extent in the laboratory, it is difficult or impossible to separate and evaluate all components of molecular absorption. Measurements planning and data analysis therefore ultimately rest on predictive analysis for direction and interpretation. More will be said of this in Section 2.

1.2 Objectives of the Current Program

This investigation has a threefold objective: (1) provide the data base from which predictive laser propagation modeling parameters can be extracted; (2) identify and quantify inadequacies in the current modeling parameters; and (3) determine the sensitivity of altitude and meteorological scaling to the modeling parameters. All three of these objectives are addressed in this interim report. In the following section, the impact of predictive analysis on temperature and altitude scaling is discussed. In that section, the propagation of the $P_1(9)$ and $P_3(8)$ DF lines are predicted as specific examples of the nature of the altitude and temperature scaling problem. In the next three sections, spectral measurements on HDO, CH_4 and N_2O line absorption are presented and comparisons are

made with current predictive calculations (i. e. , synthetic spectra). A specific application to $P_1(7)$ propagation is discussed in the context of the HDO measurements.

2. ALTITUDE AND TEMPERATURE SCALING

2.1 Introduction

As discussed in the previous section, precise predictive modeling is required for at least five applications.

- (1) Planning and interpretation of laboratory fixed-frequency measurements.
- (2) Planning and interpretation of field measurements.
- (3) Scaling to arbitrary conditions for field and laboratory measurements support.
- (4) Scaling to arbitrary conditions for specific engagement scenarios.
- (5) Programmatic decisions such as determining the merits of line selection for a particular device, and evaluating the propagation characteristics of candidate high energy laser devices.

The complicated nature of atmospheric molecular absorption has been discussed in detail in a previous report [1]. In that report, the major individual molecular absorption contributions in the DF region have been computed, and the molecular line, wing, and continuum absorption mechanisms which account for DF laser molecular absorption have been described.

In this report the importance of an accurate knowledge of the molecular absorption line parameters is illustrated by considering the altitude and temperature scaling of the absorption coefficients of the $P_3(8)$ and $P_1(9)$ DF laser lines. These lines are listed as having large output powers [2], and are expected to have fairly low atmospheric absorption coefficients typical of the DF region. This comparison between these two lines is interesting because the absorption coefficients are expected

to have different temperature and altitude dependence. The $P_3(8)$ line has been studied extensively by several groups [3, 4, 5, 6], and the parameters are known accurately for its primary molecular line absorber, N_2O . However for $P_1(9)$ the Air Force Cambridge Research Laboratories (AFCRL) [7] parameters are not reliable. The dominant H_2O line has not been measured, and the current measurements indicate that the important CH_4 and HDO parameters are not accurate. While the CH_4 parameters have been adjusted to be consistent with the measurements in Section 4.4, future changes in the predicted absorption can be expected to arise from changes in the HDO and H_2O line parameters.

It is also important to note that, since this is a study of molecular line absorption, continuum absorption is not considered in this report. If continuum absorption were included, the altitude dependence would be even more dramatic than indicated here since the H_2O continuum absorption depends on the total pressure, as well as on the H_2O concentration which drops very fast with increasing altitude. The N_2 continuum also decreases quickly with altitude since it is related to the square of the pressure.

2.2 Choice of Modeling Parameters for $P_3(8)$ and $P_1(9)$

For the $P_3(8)$ laser line the parameters for the largest absorbers are known quite well. At sea level N_2O absorption is the largest single contributor to molecular absorption, and at higher altitudes or when continuum absorption is not included N_2O absorption is dominant. The current measurements of N_2O profiles and those predicted by the AFCRL [7] strength and width parameters are in perfect agreement (see Section 4.3). Also, the preliminary results of recent measurements by Rao and Heath [3] indicate that for this

particular line, the original DF line position used by AFCRL [7], rather than that of Long and Yin [8], is accurate. The present calculation has used the confirmed AFCRL values for the N_2O line strengths and widths, the AFCRL absorption line frequencies, and the Rao and Heath preliminary laser frequency ($2546.3734 \pm 0.0050 \text{ cm}^{-1}$).

For CH_4 the AFCRL widths and frequencies were used, but the strengths were increased by a factor of 2.85 to be consistent with the measurements reported in Section 4.4.

For the smallest contributor, HDO, the AFCRL values were used unchanged. This undoubtedly leads to an error in the value of the HDO absorption as is discussed in Section 4.5. However, HDO only contributes a very small amount to the overall absorption of $\text{P}_3(8)$ at sea level, and becomes negligible at higher altitudes. The estimated error introduced by the use of these parameters is 4% of the total sea level absorption, and less than 1% at 5 km.

In all of the calculations in this section of the report, the water concentrations and air pressures were determined from the AFCRL standard atmosphere tables [9]. An HDO isotopic fraction of 0.0003 and gas abundances of 0.28 ppm N_2O and 1.6 ppm CH_4 were used.

For the $\text{P}_1(9)$ line the current measurements indicate significant errors exist in the AFCRL parameters. Differences which cause a substantial change in the total molecular line absorption have been approximately included. Those differences which, under all the conditions considered here, cause less than a 20% change in the total molecular line absorption have not been incorporated. The original sea level contributions of various molecules to the line absorption of $\text{P}_1(9)$ were given in our earlier report [1]. These are compared with the revised values in Table 1.

Table 1.

 $P_1(9)$ Absorption Coefficients (10^{-3} km^{-1})

Frequency (cm^{-1})	H ₂ O	HDO	N ₂ O	CH ₄	H ₂ O cont.	N ₂ cont.	Total	
2691.41	6.13	11.52	- -	0.30	22.32	0	40.27	Original
2691.61	40.97	12.23	- -	8.51	22.34	0	84.05	Revised

To illustrate the source of the values better and the effect of the changes in the absorption coefficients, detailed plots of significant contributing line absorption, continuum absorption, and total absorption coefficients are shown in Figure 1 for the AFCRL parameters.

The absorption lines in that plot are designated as follows:

H	H ₂ O line
D	HDO line
M	CH ₄ line
1, 2, 3...	1st, 2nd, 3rd... contributing line in order of ascending frequency.

The primary cause of the differences between the "original" and "revised" absorption coefficients is the use of Rao and Heath's [3] preliminary DF laser frequencies. This leads to a 7 fold increase in the predicted H₂O absorption. Also, the use of modified CH₄ line strengths which are consistent with the measurements reported in Section 4.4, along with the new frequencies, leads to an increase in the CH₄ absorption. The data in Figure 37 show a factor of 2.62 increase in the peak absorption for the unresolved doublet which is the principle source of CH₄ absorption. This, coupled with the near coincidence of the CH₄ line center with the revised laser frequency, results in a factor of 30 increase in the methane absorption coefficient. The net result is an increase of more than a factor

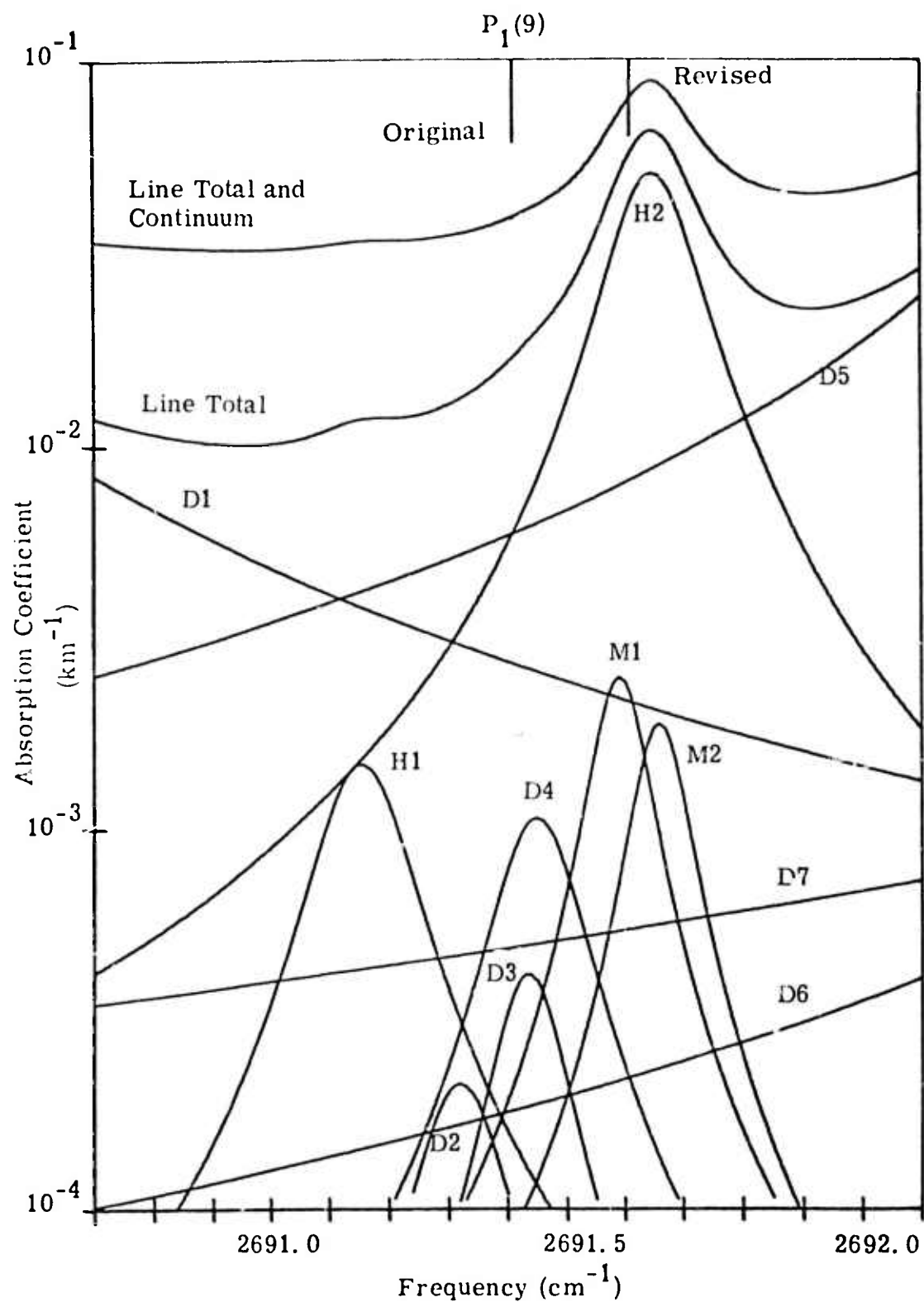


Figure 1. Contributors to the Molecular Absorption of the $P_1(9)$ DF Line (Midlatitude Summer, Sea Level) [1]

of two in the midlatitude summer total absorption, and an increase of the CH_4 contribution to 0.01 km^{-1} .

In the scaling calculations for $P_1(9)$, the AFCRL values for CH_4 line widths and frequencies were used unchanged while the strength values were increased by a factor of 2.62. The AFCRL values were also used for the H_2O and HDO parameters. Some of these values undoubtedly need to be revised also. However, the measurements reported in Section 4.6 indicated that while changes in the HDO parameters are required, they will not lead to a large change in the total calculated absorption for this laser line. H_2O line parameters have not been measured. If the H_2O absorption is much less than predicted, then the changes in the HDO parameters could be important. The preliminary $P_1(9)$ laser frequency value of $2691.6075 \pm 0.0050 \text{ cm}^{-1}$ was used [3].

2.3 Altitude Scaling of Molecular Line Absorption-- $P_3(8)$ and $P_1(9)$

Figure 2 shows the altitude scaling from 0 to 10 km for the molecular line absorption of the $P_3(8)$ DF laser line when the midlatitude summer atmospheric model [9] is assumed. Also shown on the figure are hypothetical curves that would be valid if the laser line were exactly at the N_2O line center, or if the laser line were located in the line wing where the line profile is proportional to the square of the pressure. These have been normalized to give the correct absorption at sea level. The circle in the figure gives the fixed frequency measurement by Mills and Long [5, 10]. This value is the sum of their measurements of HDO and N_2O . It lies below the calculated absorption by an amount which corresponds to the CH_4 absorption which has not been reported by Mills and Long for this line. Note that while the fixed frequency measurement confirms the

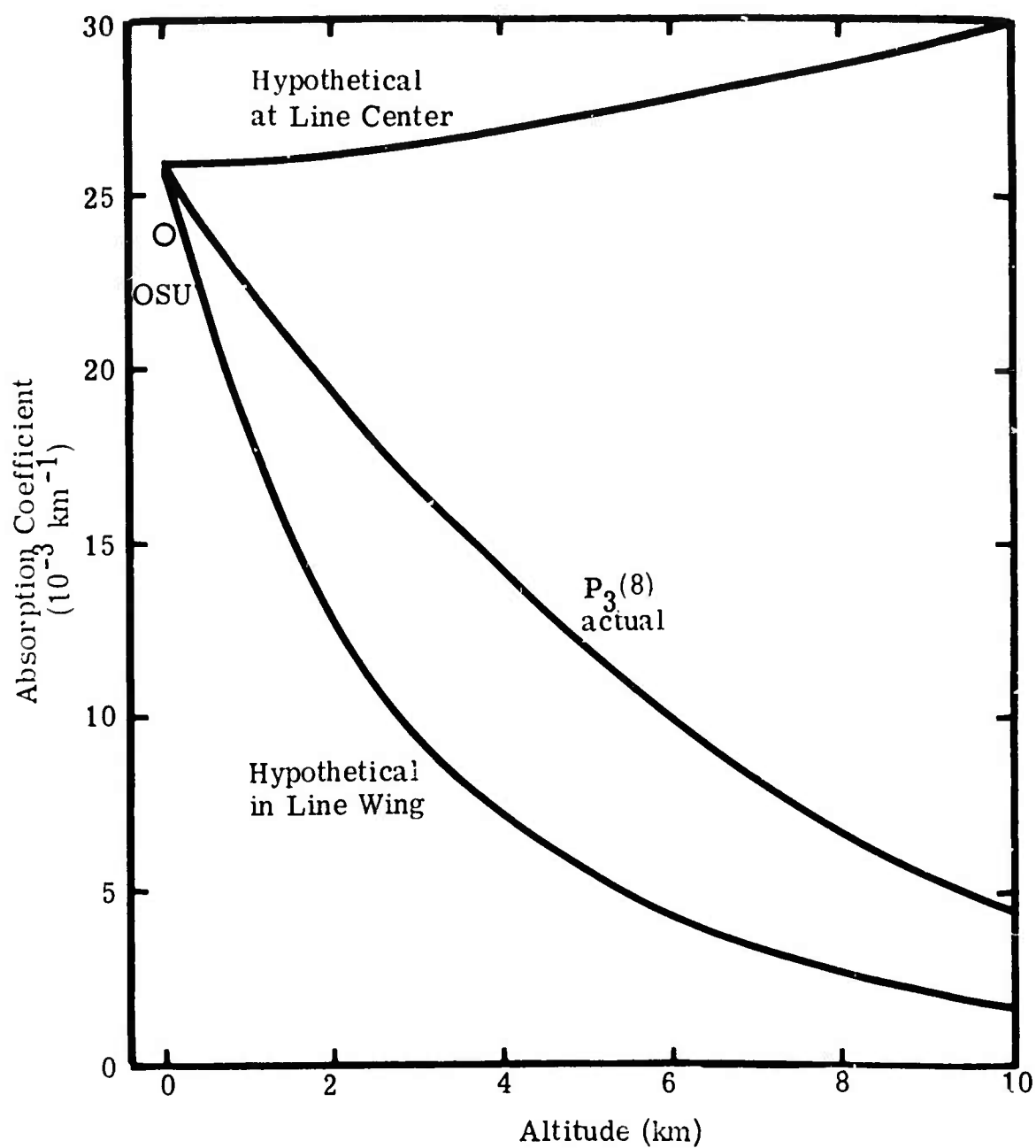


Figure 2. Altitude Dependence of the $P_3(8)$ DF Laser Molecular Line Absorption Coefficient for Various Line Positions.

sea level calculation, line parameter information (strengths, widths, and frequencies) is required to perform altitude scaling.

The line absorption for each individual constituent is scaled from 0 to 10 km in Figure 3. Again the measurements by Mills and Long [5, 10] are given by circles. The validity of the current modeling approach is confirmed by the excellent agreement with measurements when accurate parameters are available for the calculations. This is the case for N_2O where the absorption coefficient of $.0214 \text{ km}^{-1}$ agrees very well with the calculated value of $.02169 \text{ km}^{-1}$. The need for accurate parameters is demonstrated in Figure 3 for the case of HDO. It can be seen that there is a factor of two difference between the absorption measured by Mills and Long, and the HDO calculations based on AFCRL parameters which are now known to be in error (see Section 4.5).

While $P_3(8)$ is an example of a line where essentially a single function determines the altitude dependence, $P_1(9)$ is an example of a line whose altitude dependence is determined by the sum of dramatically different altitude functions which were only shown hypothetically for $P_3(8)$. The $P_1(9)$ altitude scaling for the midlatitude summer model is shown in Figure 4. All molecular line absorption contributions are included. In this case the $P_1(9)$ laser line lies near the center of a CH_4 line. Thus the CH_4 absorption persists as the altitude is increased, while the HDO and H_2O absorption falls off very quickly with increasing altitude.

The striking new importance of CH_4 is illustrated in Figure 5 where the midlatitude winter [9] propagation of $P_1(9)$ is plotted. In this case the sea level absorption by CH_4 is about the same as that of water vapor, while propagation at higher altitudes is dominated by CH_4 and remains nearly the same as for the summer model.

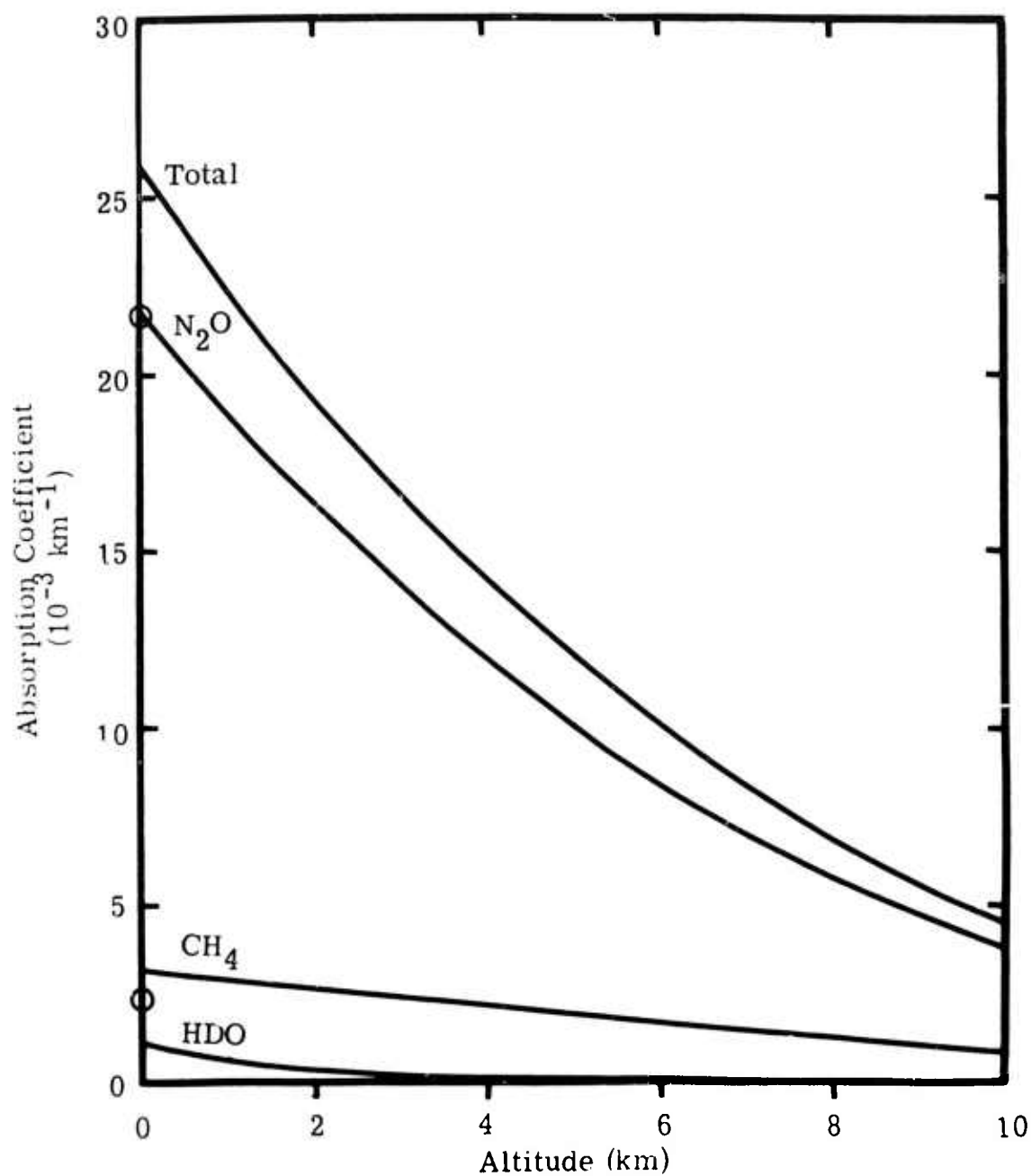


Figure 3. Altitude Dependence of the Molecular Line Absorption Coefficient for the $P_3(8)$ DF Line Showing the Major Contributors (Midlatitude Summer)

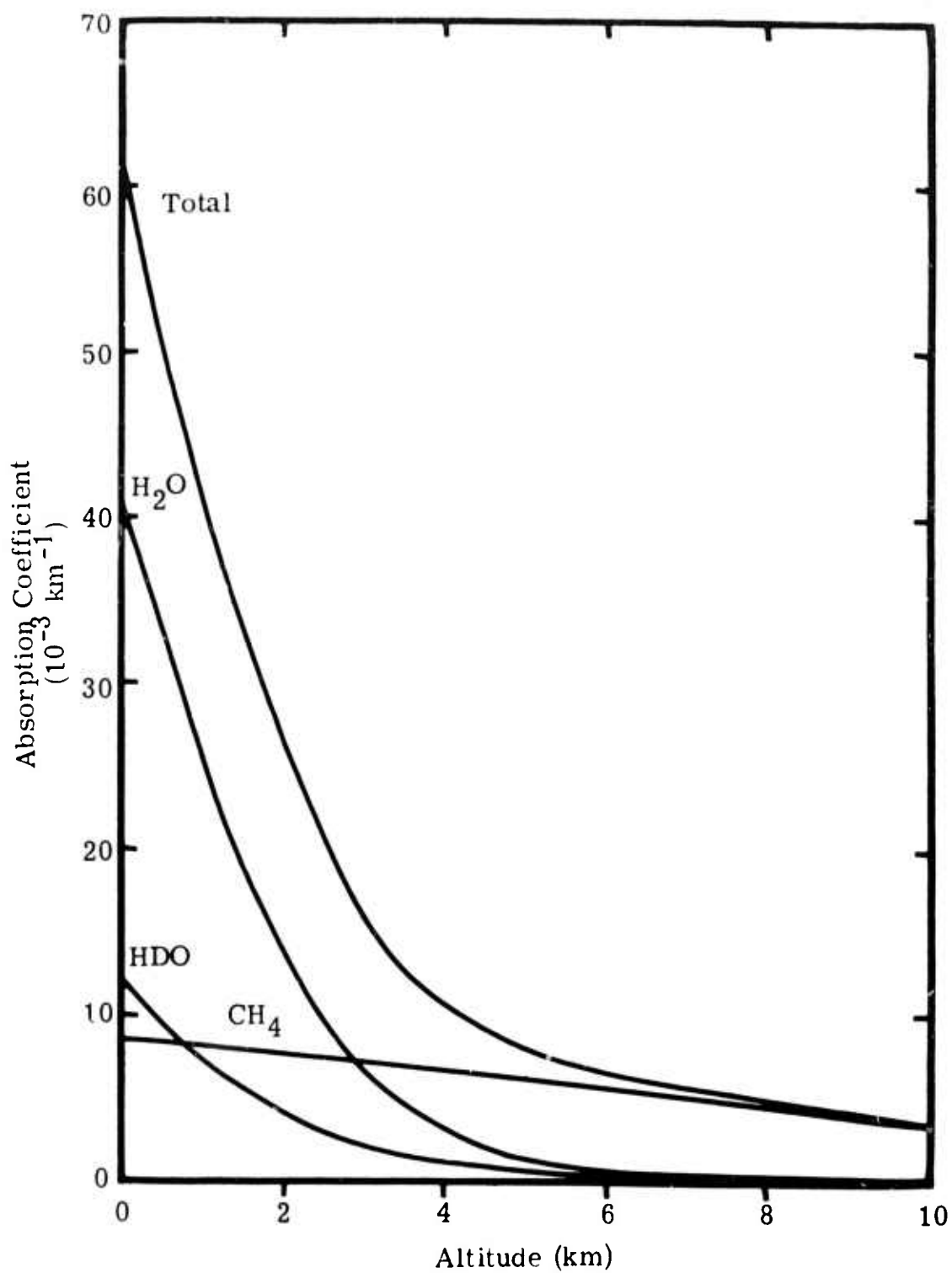


Figure 4. Altitude Dependence of the Molecular Line Absorption Coefficient for the $P_1(9)$ DF Line Showing the Major Contributors (Midlatitude Summer)

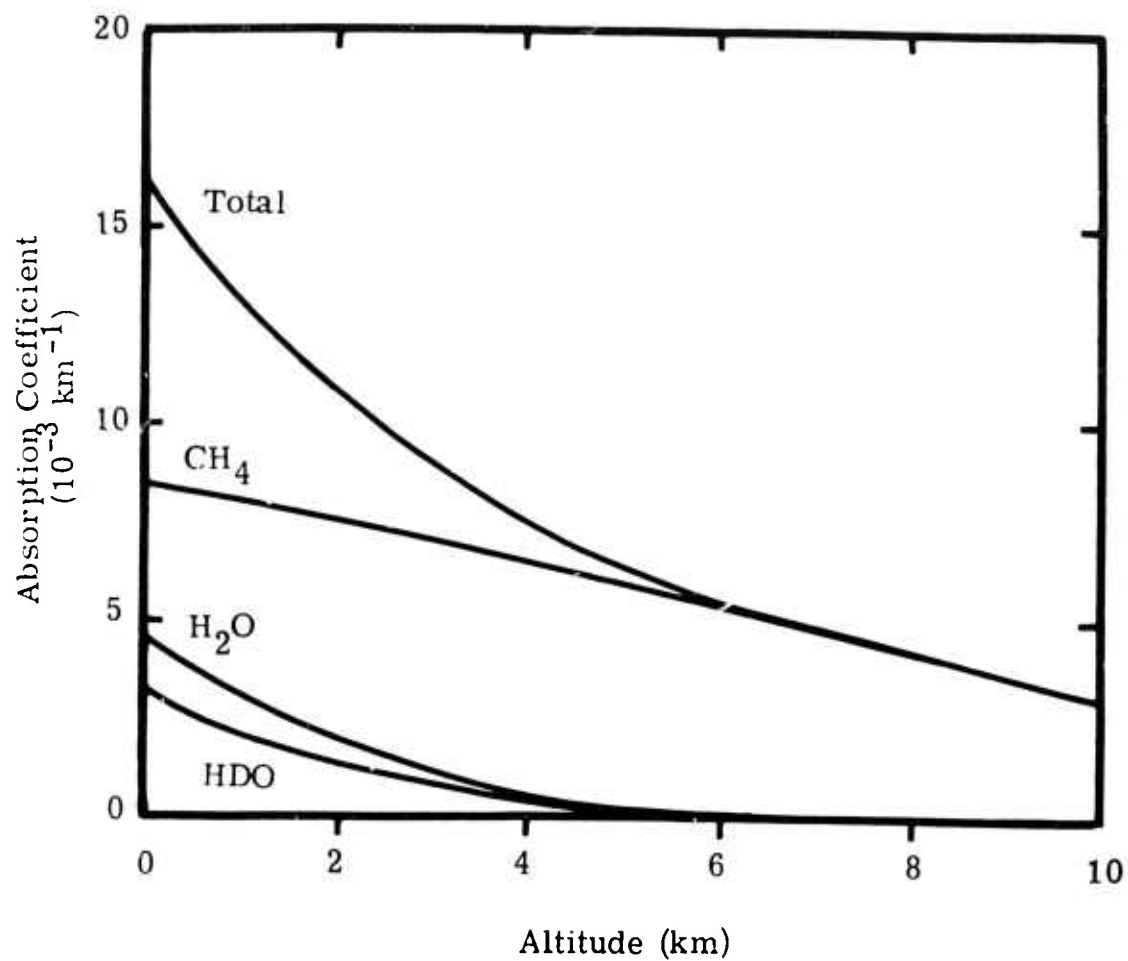


Figure 5. Altitude Dependence of the Molecular Line Absorption Coefficient for the $P_1(9)$ DF Line Showing the Major Contributors (Midlatitude Winter)

2.4 Temperature Scaling of Molecular Line Absorption-- $P_3(8)$ and $P_1(9)$

While both temperature and pressure changes are included in the altitude scaling, the temperature can also change significantly at a particular altitude. Thus temperature scaling is important independent of altitude scaling.

The conditions and parameters used for these calculations were the same as discussed in Section 2.3. The water concentration assumed was 14 gm/m^3 . Figure 6 shows the temperature dependence of molecular line absorption of the $P_3(8)$ and $P_1(9)$ DF laser lines, over a normal range of temperatures at sea level. The contrast is striking. Since the H_2O absorption line originates from a "hot" band, its initial energy level has a high value, and it is thus very temperature sensitive. The initial energy levels of N_2O and CH_4 are much lower, and they therefore are not so temperature sensitive. Note, however, that each of these molecule's absorption still has a different quantitative scaling law.

A constant concentration has been used for all the constituents in Figure 6. Thus the water concentrations used at lower temperatures are not attainable due to condensation. This would lead to an even sharper drop in the absorption under actual atmospheric conditions due to changes in the water concentration.

2.5 General Considerations

H_2O lines, as well as HDO line and H_2O continuum, play a significant part in our understanding of DF laser propagation. H_2O lines absorb trace amounts at almost all DF frequencies, and are a competing or majority line contributor for a half-dozen or so DF lines according to the current AFCRL tabulation. It is important to note

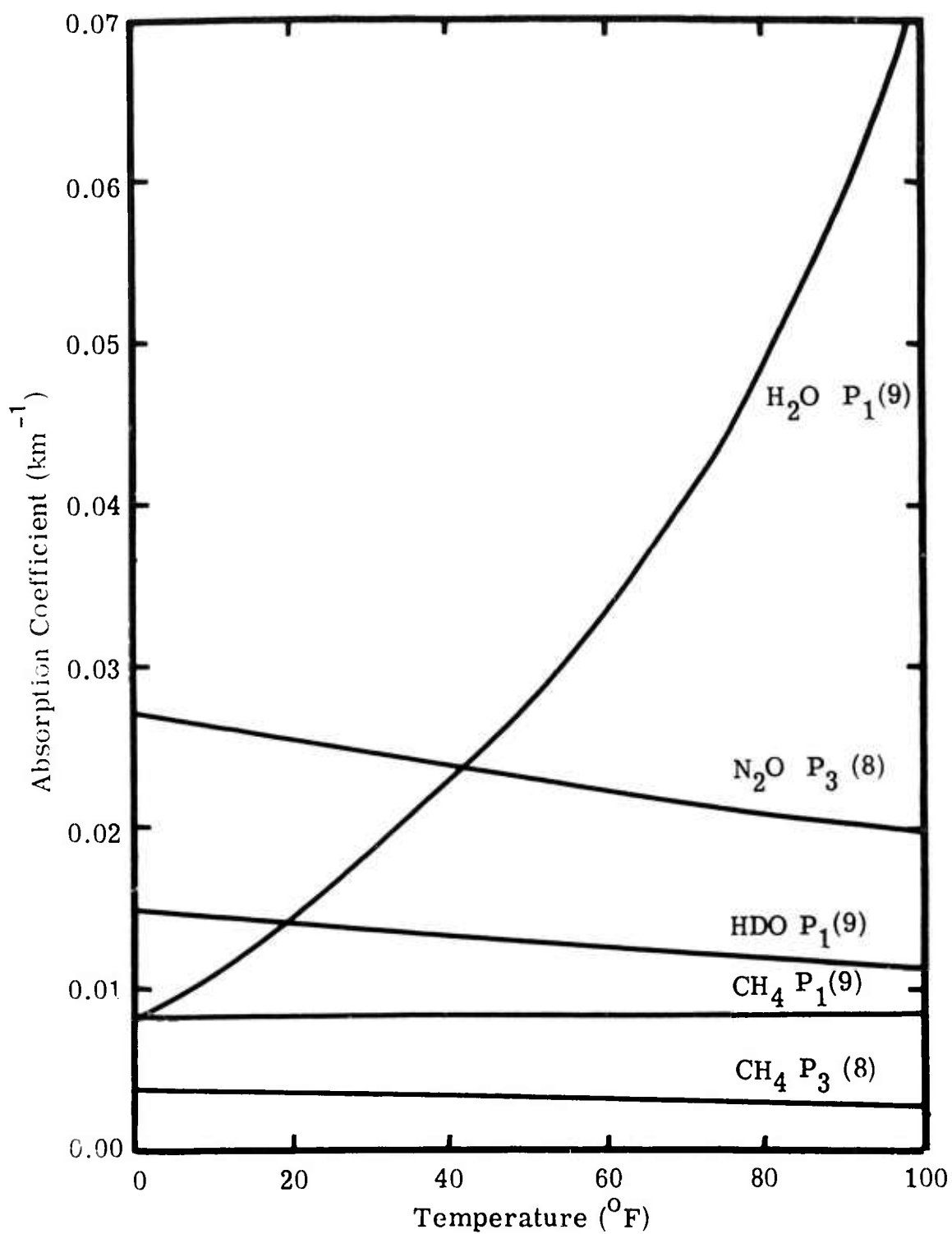


Figure 6. Temperature Dependence of the Major Molecular Line Absorption Coefficient Contributors for the $P_1(9)$ and $P_3(8)$ DF Lines.

that the distinction between H_2O lines, HDO lines, and H_2O continuum has great physical significance, and the need to distinguish them is much more than for mere bookkeeping. As shown above, H_2O lines in this region tend to scale in a much different way than do HDO lines or the H_2O continuum.

The distinction between H_2O line absorption, and H_2O continuum and HDO absorption is also important for the interpretation of experimental data. H_2O line absorption is naturally weak on a per molecule basis, as contrasted to HDO which is weak in the atmosphere by virtue of small natural abundance. For this reason, H_2O cannot be enriched in the laboratory for easy observation, as can HDO. Indeed, H_2O lines in this region, like H_2O continuum, can be observed in the laboratory only with instrumentation capable of measuring absorption coefficients of order 0.01 km^{-1} . This fact also has considerable impact on attempts to measure the H_2O continuum. If one uses water with a "normal" amount of deuteration, the HDO contribution can be subtracted out if HDO absorption is separately known. However, H_2O lines and H_2O continuum are indistinguishable by fixed frequency, constant temperature measurements.

In conclusion, the separate consideration of absorption contributors is important for scaling and measurements interpretation. This can be done only by carefully separating the absorption of the several background contributors: HDO lines, H_2O lines, H_2O continuum and the D_2O lines which necessarily occur in enriched HDO samples.

3. INSTRUMENTATION

3.1 Spectrometer Description

The data were obtained with a 3 meter focal length, double passed, Ebert spectrometer at the University of Michigan Physics Department. A diagram of the spectrometer optics is given in Figures 7 and 8. The grating used had 300 grooves per millimeter and was blazed at 3.0 micrometers. An InSb detector was used with an internal cold filter. The source was a Nernst glower.

3.2 Data Acquisition System

A block diagram of the data acquisition system is given in Figure 9. The analog signal was recorded on a strip chart recorder and also digitized by a 4-1/2 digit, digital panel meter. The digital signal was transmitted to a data terminal using a Nation Wide Electronics Data Logger. The data terminal was a Texas Instruments 733 ASR with a digital cassette tape recorder. The digital signal was recorded on the cassette tapes and could subsequently be retransmitted to any computer available over the telephone lines. In this study the University of Michigan's IBM 370/168 computer system was used. A FORTRAN computer program was used to normalize and scale the spectra, subtract off the zero offset and produce a calibrated plot.

3.3 Performance

A resolution of 0.043 cm^{-1} was obtained with a rms signal-to-noise ratio of 360 and a time constant of 1.3 seconds. The stray and scattered radiation was determined to be less than 2% by observing 100% absorbing methane lines.

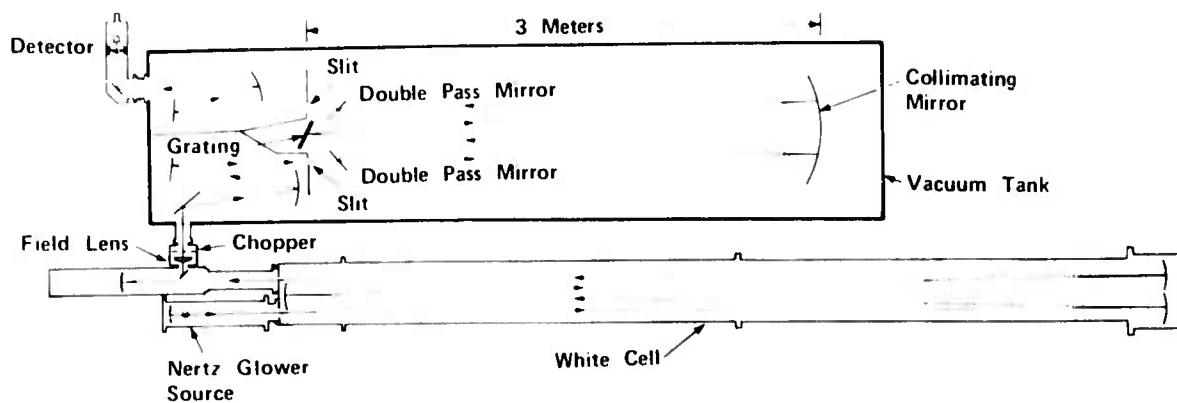


Figure 7. Instrument Optics

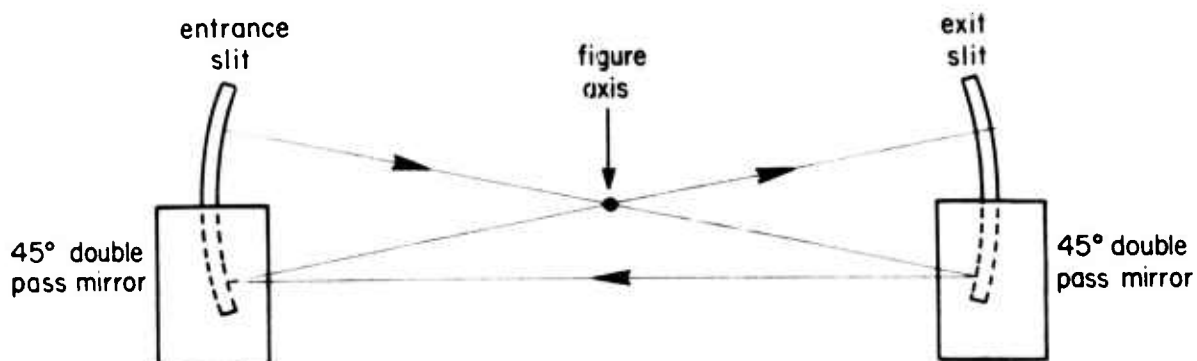


Figure 8. End View of Double Pass Light Path

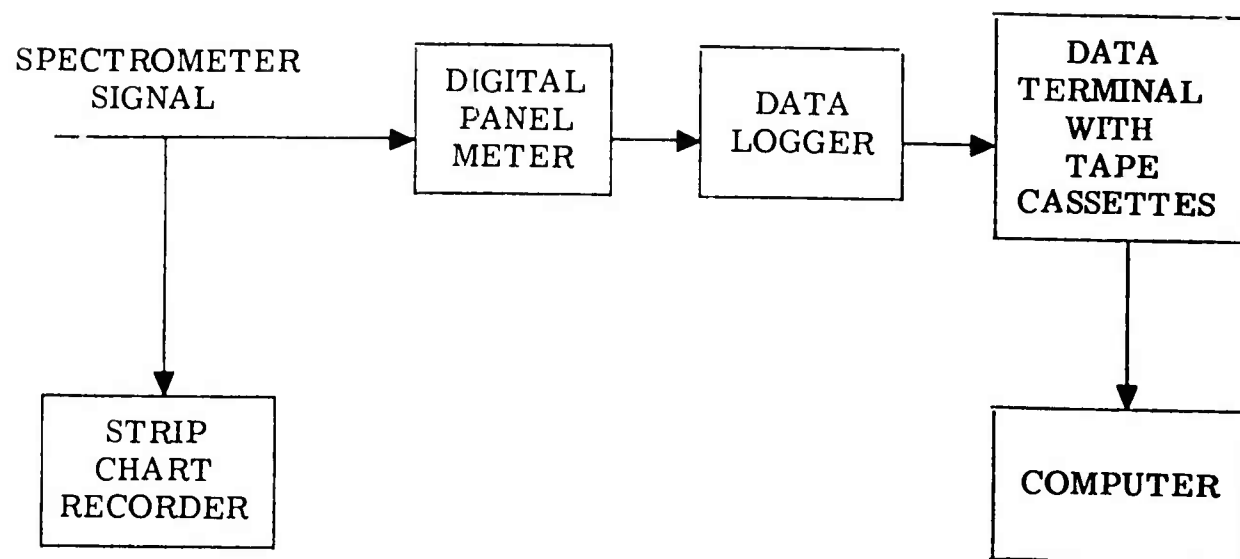


Figure 9. Data Acquisition System

3.4 White Cell

A $4.988 \pm .002$ meter White cell (see Figure 7) was used to obtain gas sample path lengths of 20 to 100 meters. The actual path used depended on the particular measurement being made. The amount of gas sample admitted to the White cell was measured with a capacitance manometer with an accuracy better than 1%. A Wallace & Tiernan absolute pressure gauge was used to measure the total pressure of air and gas sample with an accuracy better than 2%. In the case of the HDO measurement, the total amount of water in the cell was also monitored with a dew point hygrometer and found to be consistent with the initial fill pressure admitted to the cell.

3.5 Gas Samples

The methane was obtained from Air Products and Chemicals Inc. and had a purity of 99%. The N_2O was purchased from Matheson. It was premixed with nitrogen and had a concentration of $2.06 \pm .04\%$. The D_2O was manufactured by Merck Sharp and Dohme Canada Limited. It had an atomic purity of 99.7% deuterium. The normal water was obtained from the University of Michigan Chemical Stores distilled water supply. It was assumed that the ' H_2O ' contained the normal isotopic abundance of deuterium. While this assumption may be in error by 10% [11] the resulting error in the HDO concentration used is negligible. The HDO sample was obtained by mixing liquid D_2O and H_2O . The cell was filled by putting the proper amount of this liquid into a glass boiler and boiling its entire contents into the White cell. The concentration of HDO in the cell was calculated using the gas equilibrium constant of 3.506 derived by Spencer, Denault, and Takimoto [4].

$$3.506 N_{H_2O} N_{D_2O} = N_{HDO}^2$$

For the measurements made with a HDO pressure of 0.2002 torr and 0.0205 torr the total water pressure was 9.39 torr and 8.78 torr respectively.

4. MEASURED AND SYNTHETIC SPECTRA

4.1 Measured Spectra

The molecular absorption spectra have been measured for N_2O , CH_4 and HDO in the region between 2545 cm^{-1} and 2745 cm^{-1} . The figures containing the spectra are located at the end of this report. The measurements were made at temperatures between 298°K and 300°K , and at a total pressure of one atmosphere. The measured spectra have been normalized and plotted on the same scale as the synthetic spectra which are discussed in Section 4.2. The frequency scale on the measured spectra was determined from a least-squares fit of the grating equation using the frequencies given [7] for each species measured. The measurement of the relative frequencies of adjacent lines is accurate to better than 0.01 cm^{-1} . However the absolute frequencies of the lines have not been measured. The frequency scale on the spectra displayed in Figures 13 through 63 should only be used to determine approximate positions of lines and to measure the relative frequencies of adjacent lines.

The 100% transmission points were determined from the troughs between the measured absorption lines. Where the synthetic spectra showed that the troughs corresponded to a few percent less than 100% transmission, a correction was made using the trough transmission of the synthetic spectra. Thus the trough transmission has not been independently measured. The zero transmission point was determined by placing a flag in the beam. This signal level was then corrected for 2% scattered and impure radiation. The accuracy of the measured absorption relative to the absorption at another point on the same figure and within 2 cm^{-1} is better than 2% of full scale. The absolute accuracy of the absorption including errors in the 100% transmission point is better than 5%, and in most cases, better than 2% of full scale

4.2 Synthetic Spectra

Synthetic spectra have been generated in the region between 2545 cm^{-1} and 2745 cm^{-1} for N_2O , CH_4 and HDO . The parameters from the AFCRL Atmospheric Absorption Line Parameters Compilation [7] were used to generate the monochromatic transmission spectra for a temperature of 300°K . These spectra were then convolved with the spectrometer slit function to generate spectra with the exact appearance of spectra observed with the spectrometer. The spectrometer slit function (i. e. , spectral bandpass profile) was approximated by a trapezoid as shown in Figure 10. The width of the approximate slit function was set equal to the width of the actual spectrometer slit function. The particular widths used at different frequencies are given in Table 2.

The distortion of the real absorption spectra by the spectrometer slit function is very small for the resolution used in this study. This can be seen in Figures 11 and 12 by comparing the transmission spectra as it appears before and after it is convolved with the approximated spectrometer slit function. The first figure is for a relatively narrow absorption line and the second figure is for a wide line.

The positions of the major DF laser lines are also plotted on the synthetic spectra. These frequencies are based on preliminary results from measurements being made by Rao and Heath [3]. They are believed to be accurate to $.005\text{ cm}^{-1}$.

4.3 N_2O Spectra

The measured N_2O spectrum is compared with the calculated synthetic spectrum in Figures 13 through 19 located at the end of this report. The agreement appears perfect. Since the agreement is so close,

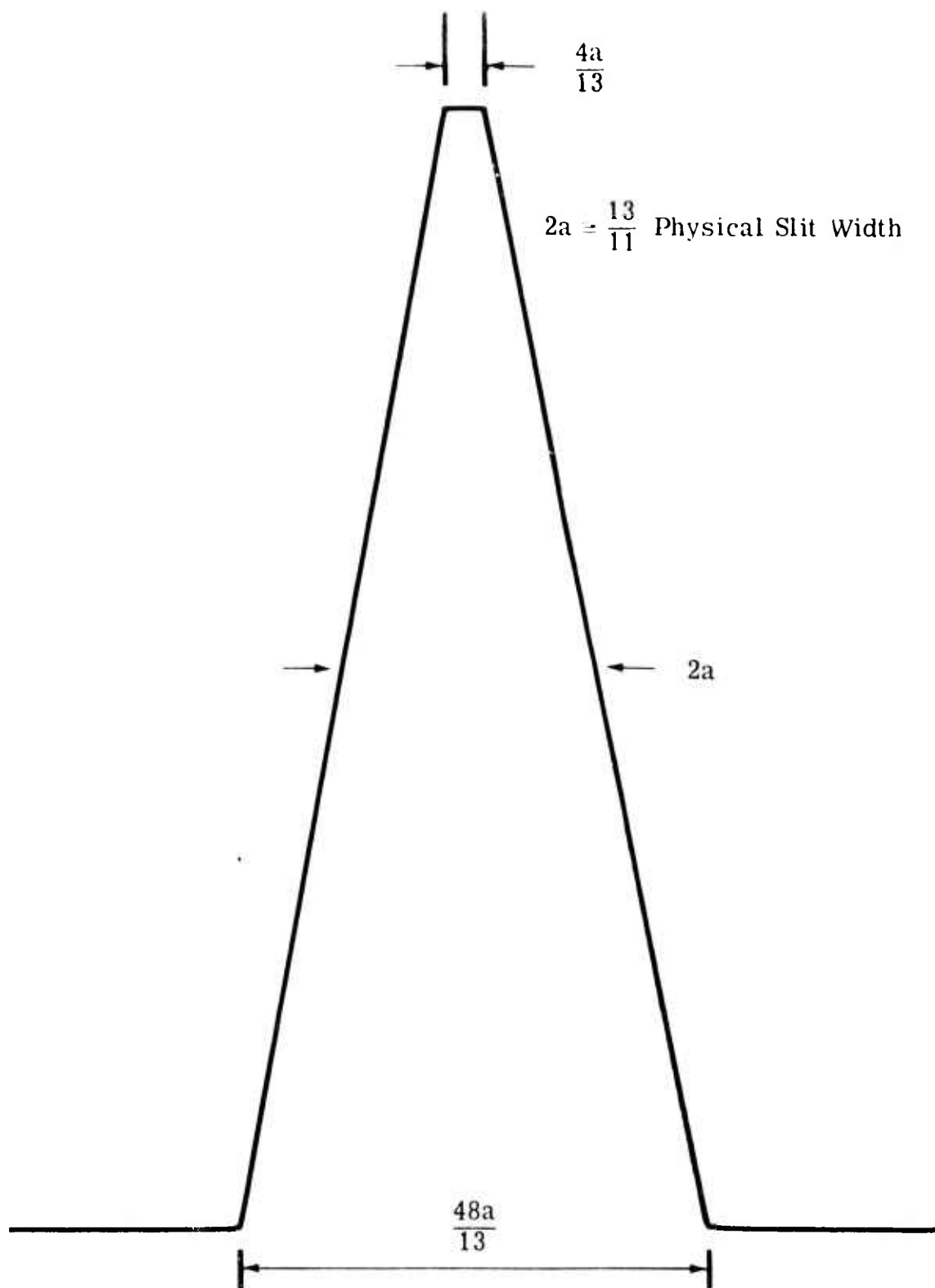


Figure 10. Slit Function

Table 2.
Slit Widths

$\bar{\nu}(\text{cm}^{-1})$	$2a(\text{cm}^{-1})$
2450	.0390
2460	.0394
2470	.0398
2480	.0403
2490	.0407
2500	.0411
2510	.0415
2520	.0419
2530	.0424
2540	.0428
2550	.0432
2560	.0437
2570	.0441
2580	.0445
2590	.0449
2600	.0454
2610	.0458
2620	.0462
2630	.0467
2640	.0471
2650	.0476
2660	.0480
2670	.0485
2680	.0489
2690	.0494
2700	.0498
2710	.0503
2720	.0507
2730	.0512
2740	.0516
2750	.0521

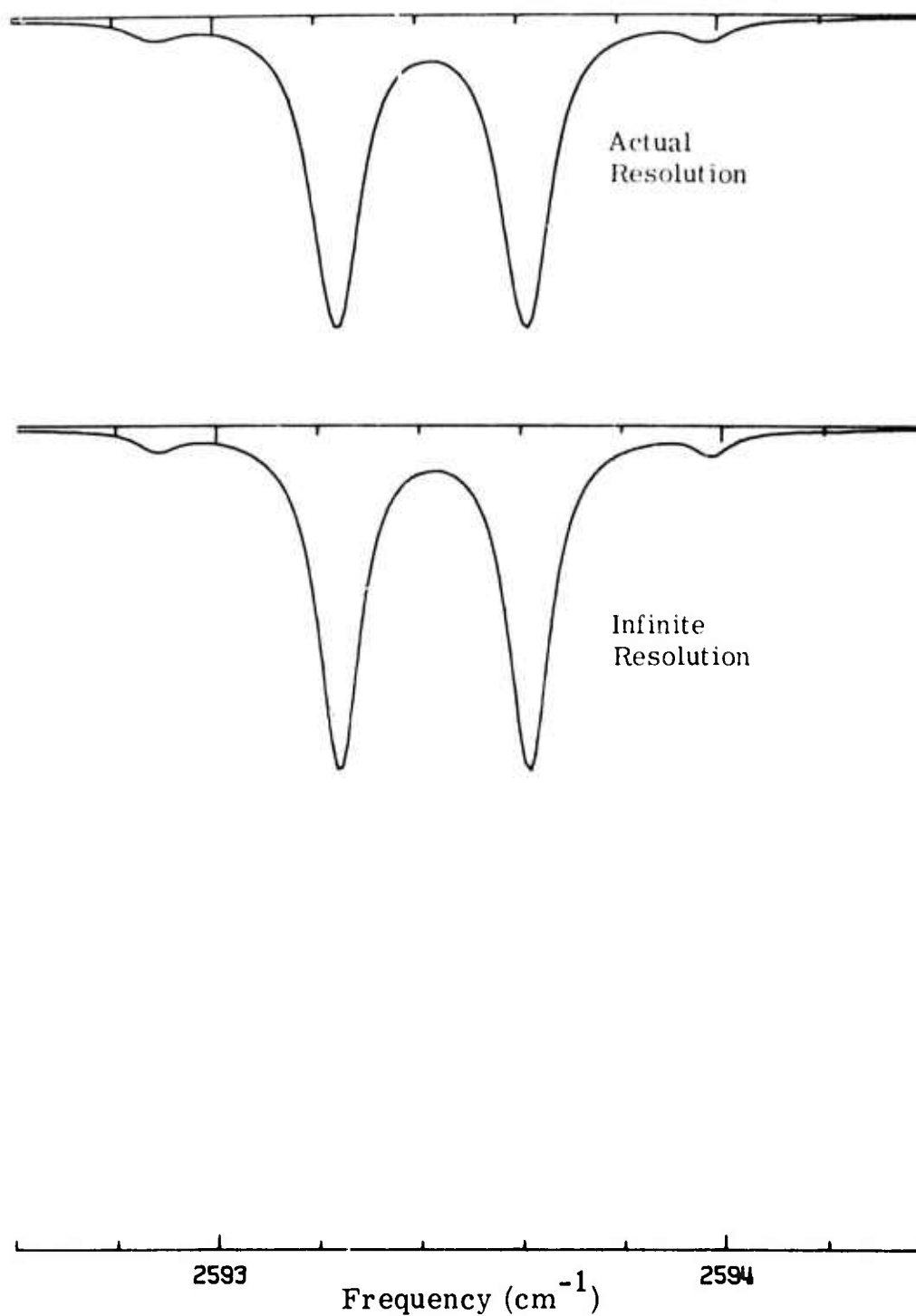


Figure 11. Comparison of Narrow Absorption Lines (0.044 cm^{-1} half width) Calculated Using Infinite Resolution with Those Calculated Using the Actual Spectrometer Resolution.

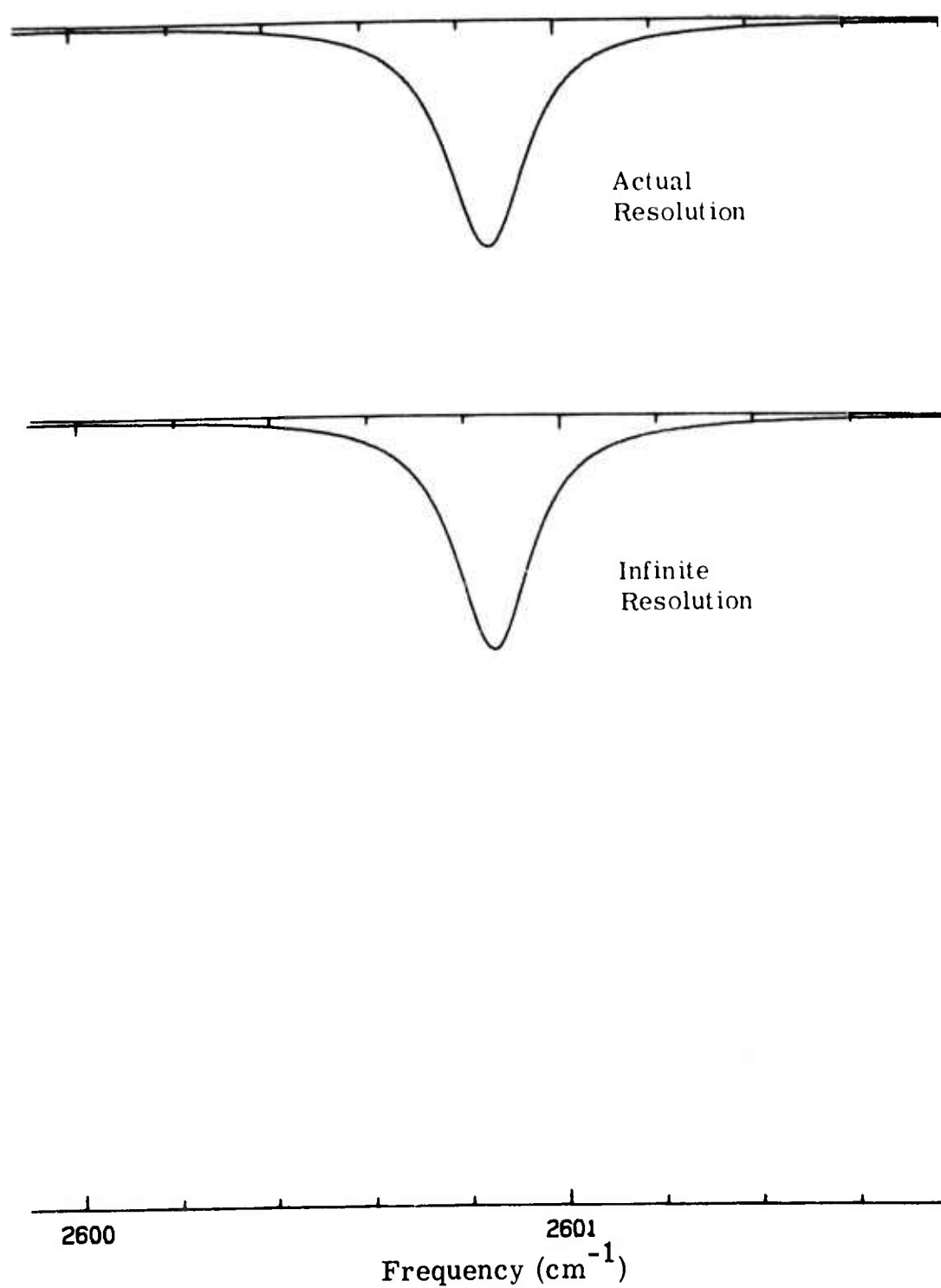


Figure 12. Comparison of Narrow Absorption Lines (0.044 cm^{-1} half width) Calculated Using Infinite Resolution with Those Calculated Using the Actual Spectrometer Resolution.

three expanded scale plots are given for the principal absorption lines influencing the $P_2(10)$, $P_3(7)$, and $P_3(8)$ DF laser lines. These are shown in Figures 20, 21, and 22. From these it can clearly be seen that the calculated absorption is within a few percent of actual absorption. Thus the current values for the widths and strengths of these lines must be correct. However, because the frequency calibration for the measurements was taken from the positions of the N_2O lines themselves, the agreement of these spectra confirms the relative positions of adjacent lines but not the absolute positions. Thus any differences observed between the calculated absorption and monochromatic DF laser measurements are most likely due to errors in the relative frequencies of the laser and the absorption lines.

For the determination of DF laser absorption by N_2O , the most important remaining measurement is the evaluation of the relative spacings between the DF and N_2O lines. Two less important effects also need to be checked. First, the trough absorption between N_2O lines should be spot checked. Errors found here would have their largest effects on $P_3(6)$, but might also lead to 10% corrections to the N_2O absorption coefficients at other important DF laser lines. Secondly, the $2\nu_1 + 2\nu_2 \leftarrow 2\nu_2$ N_2O band is significant for $P_3(6)$. For this laser line the N_2O absorption coefficient is less than 3% of the total at midlatitude summer, sea level conditions, but under dry conditions N_2O absorption is important. At frequencies below 2575 cm^{-1} other N_2O bands are important for atmospheric absorption, but most currently important DF laser lines lie above this frequency.

4.4 CH_4 Spectra

The measured CH_4 spectrum is compared with the calculated synthetic spectrum in Figures 23 through 42. There is little agreement between these spectra. The measured spectrum varies from typically

two times stronger than the calculated spectrum for the low frequency end of the region to ten times stronger for the high frequency end. However, the difference in the strengths is not a simple function of frequency. Quite the contrary, the factors of two to ten times are only rough averages and do not apply to individual lines. There are also numerous cases where the measured spectra show lines which are not included in the calculated spectra such as at 2647 cm^{-1} in Figure 33, and in Figure 40. There are no CH_4 lines in the AFCRL compilation for the region covered in Figure 40 although we observe lines in that region. There are also cases where the predicted lines are not observed in the measured spectrum such as at 2648.6 cm^{-1} in Figure 33. In some of the spectra such as Figure 32, it is difficult to see any similarity between the measurements and calculations.

Of particular interest is the absorption of the $P_1(9)$ laser line shown in Figure 37. The latest value [3] for the $P_1(9)$ DF laser frequency places it exactly on the center of the unresolved CH_4 doublet at 2691.61 cm^{-1} . But the peak height of the observed CH_4 lines is 2.62 times stronger than predicted. This factor of 2.6, coupled with the new laser line position leads to an increase in the expected methane absorption by a factor of 30 over the value predicted using the AFCRL parameters. This higher methane absorption ($.00851\text{ km}^{-1}$) agrees well with the measurements of Spencer [4] ($.00752\text{ km}^{-1}$). Spencer's slightly smaller observed value is expected since his measurements were made on self-broadened CH_4 . Because the self-broadened width of CH_4 is greater than the air broadened width, the lines are wider under Spencer's measurement conditions and thus, the peak absorption is less. The generally good agreement with Spencer's absorption measurement tends to confirm the creditability of the current measurements, the Rao and Heath frequencies, and the modeling procedures.

Another line of some interest is the $P_3(8)$ line at 2546.4 cm^{-1} . The line primarily responsible for methane absorption at this frequency is 2.85 times stronger at the peak than given by AFCRL. While CH_4 still remains a minor contributor to molecular absorption of the $P_3(8)$ laser line, this increase brings its contribution to about 10% of the sea level absorption coefficient.

4.5 HDO Spectra

The measured HDO spectrum is compared with the synthetic spectrum in Figures 43 through 53. These spectra were obtained with an enhanced abundance of HDO, hence D_2O was also present (see Section 3.5). The possible presence of D_2O absorption lines was investigated by comparing transparent regions of the HDO spectrum with the spectrum of pure D_2O . It was found that the only significant D_2O lines were in the region between 2725 cm^{-1} and 2745 cm^{-1} . Where the D_2O lines have not been completely obscured they have been identified in the figures. The HDO line at 2728 cm^{-1} appears similar to the identified D_2O lines, however it has been checked carefully and is not D_2O .

On first inspection, the HDO measurements seem to confirm the synthetic spectra. However a closer examination reveals differences which lead to roughly a factor of two change in the absorption of most DF laser lines. The measured absorption peaks and line widths generally appear to be stronger and wider by about 25%. This difference tends to be greatest for the lower frequencies and becomes substantially less beyond 2700 cm^{-1} . How these relatively small changes in the AFCRL parameters, lead to a 100% increase in laser absorption coefficient becomes readily apparent from considerations of the Lorentz absorption line expression.

$$k = \frac{S\gamma}{\pi[(\nu - \nu_0)^2 + \gamma^2]}$$

where: k = absorption coefficient
 S = absorption line strength
 γ = absorption line width
 ν_0 = absorption line frequency
 ν = observation frequency

At the line peak

$$k = \frac{S}{\pi\gamma}$$

or $S = k_p \pi\gamma$

Thus if the peak absorption coefficient is larger by a factor of 1.25, and the line width (γ) is larger by a factor of 1.25 the line strength (S) is larger by a factor of 1.56.

However most of the laser lines lie well out in the wings of HDO lines. That is, the difference between the laser and absorption line frequencies is much greater than the absorption line half width. For this case:

$$k_{\text{wing}} \cong S\gamma \frac{1}{\pi(\nu - \nu_0)^2}$$

Because the values of S and γ are larger by factors of 1.56 and 1.25 respectively, k_{wing} is larger by a factor of 1.95. Of course the exact increase for a particular line will depend on the change in the specific parameters than influence that line. However, the above considerations do explain some of the measurements reported by Mills and Long [10]. They reported measured HDO absorption coefficients for the $P_3(6)$, $P_3(7)$ and $P_3(8)$ DF laser lines which were a factor of two larger than previously predicted.

While this effect should be important for a majority of the DF laser lines, it does not dominate all of them. A number of DF laser lines lie

close enough to HDO absorption lines that they are sensitive to the relative frequencies of the laser and absorption lines. Also DF laser lines lie at higher frequencies where the AFCRL parameter are more accurate. Thus, analysis of the exact effect of HDO on DF laser transmission will require a detailed study.

Not all of the measured absorption lines are stronger than the values given by AFCRL [7]. Some are dramatically weaker. This can be seen in Figure 62 at 2727.5 cm^{-1} and at 2729 cm^{-1} . Other examples are seen in Figure 63 at 2735.6 cm^{-1} , 2740.4 cm^{-1} and 2742.9 cm^{-1} . The case at 2742.9 cm^{-1} is of particular interest since this line had been expected to dominate the absorption of the $P_1(7)$ DF laser line. However, this absorption line is so weak that it appears to be missing. Thus the absorption of the $P_1(7)$ line will be much less than previously predicted. The exact HDO absorption for $P_1(7)$ is obscured by the adjacent D_2O absorption line, and will require more detailed measurements. However, the absorption for this laser line is at least a factor of two less than previously predicted.

5. CONCLUSIONS

5.1 Scaling

Changes in altitude and temperature can each individually cause large changes in the molecular line absorption of laser radiation. These variations can be accurately calculated when the absorption line parameters are accurately known. However, it is important to know the precise source of the absorption because different sources, scale differently. The three sources of water absorption, H_2O continuum, H_2O lines and HDO lines each scale differently. The temperature dependence of absorption lines with high ground state energies (hot bands) scale dramatically differently than lines with low ground state energies.

5.2 N_2O

The current values of the N_2O absorption line strengths and widths are accurate for the principle lines of the $2\nu_1$ band at 3.90 micrometers (2563.5 cm^{-1}). This is the primary N_2O band responsible for the absorption of DF laser radiation in the atmosphere. Confirmation of the relative frequencies of the DF laser lines and the N_2O absorption lines is the most important remaining measurement required for N_2O .

5.3 CH_4

The current line parameter values given by the AFCRL data tape [7] for CH_4 in the region between 2545 cm^{-1} and 2745 cm^{-1} are the most erroneous of any of the species in this region. The strengths of the lines are typically 5 times as strong as the values on the data tape. The relative intensities are also different, and numerous lines are not included on the data tape. In some regions even the qualitative appearances of the measured and calculated spectra are completely different.

Clearly methane will require a substantial amount of investigation to eliminate these discrepancies.

5.4 HDO

In the region between 2545 cm^{-1} and 2745 cm^{-1} the HDO line strengths and widths tend to be larger than predicted by factors of 1.56 and 1.25 respectively. This leads to typical increases of the calculated absorption coefficient by a factor of two for many of the DF laser lines. However some of the HDO absorption lines are much weaker than predicted. In the case of the $P_1(7)$ DF laser line this leads to dramatically less absorption than previously predicted. Thus new line widths and strengths need to be compiled for the HDO lines in the DF laser region. The relative differences in frequency between the DF laser lines and HDO lines are also needed.

Measured and Calculated

N_2O Spectra

Figures 13 - 22

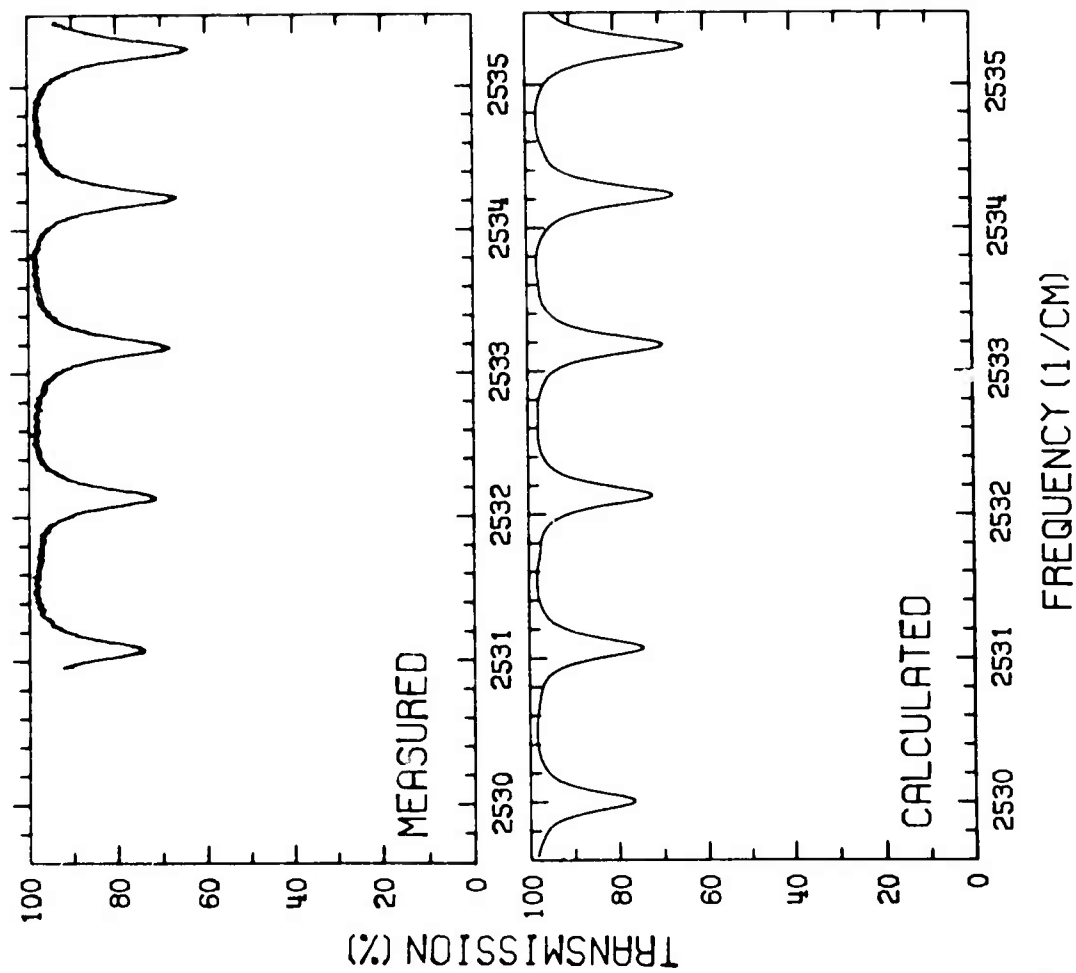


Figure 13. Comparison of Measured and Calculated N_2O Spectra .
(20 meter path; 0.150 Torr N_2O ; 760 Torr Air; 300°K)

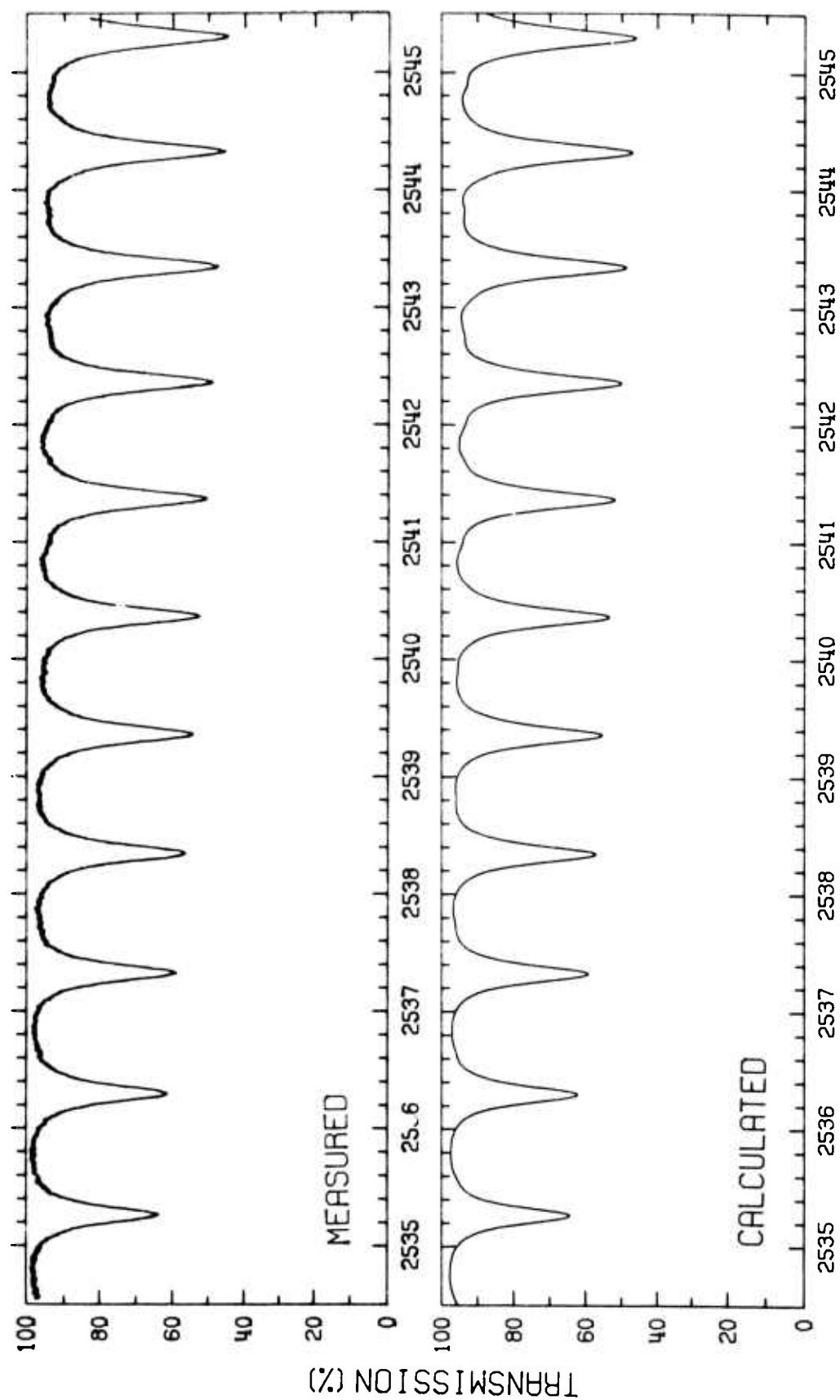


Figure 14. Comparison of Measured and Calculated N_2O Spectra
(20 meter path; 0.150 Torr N_2O ; 760 Torr air; 300°K)

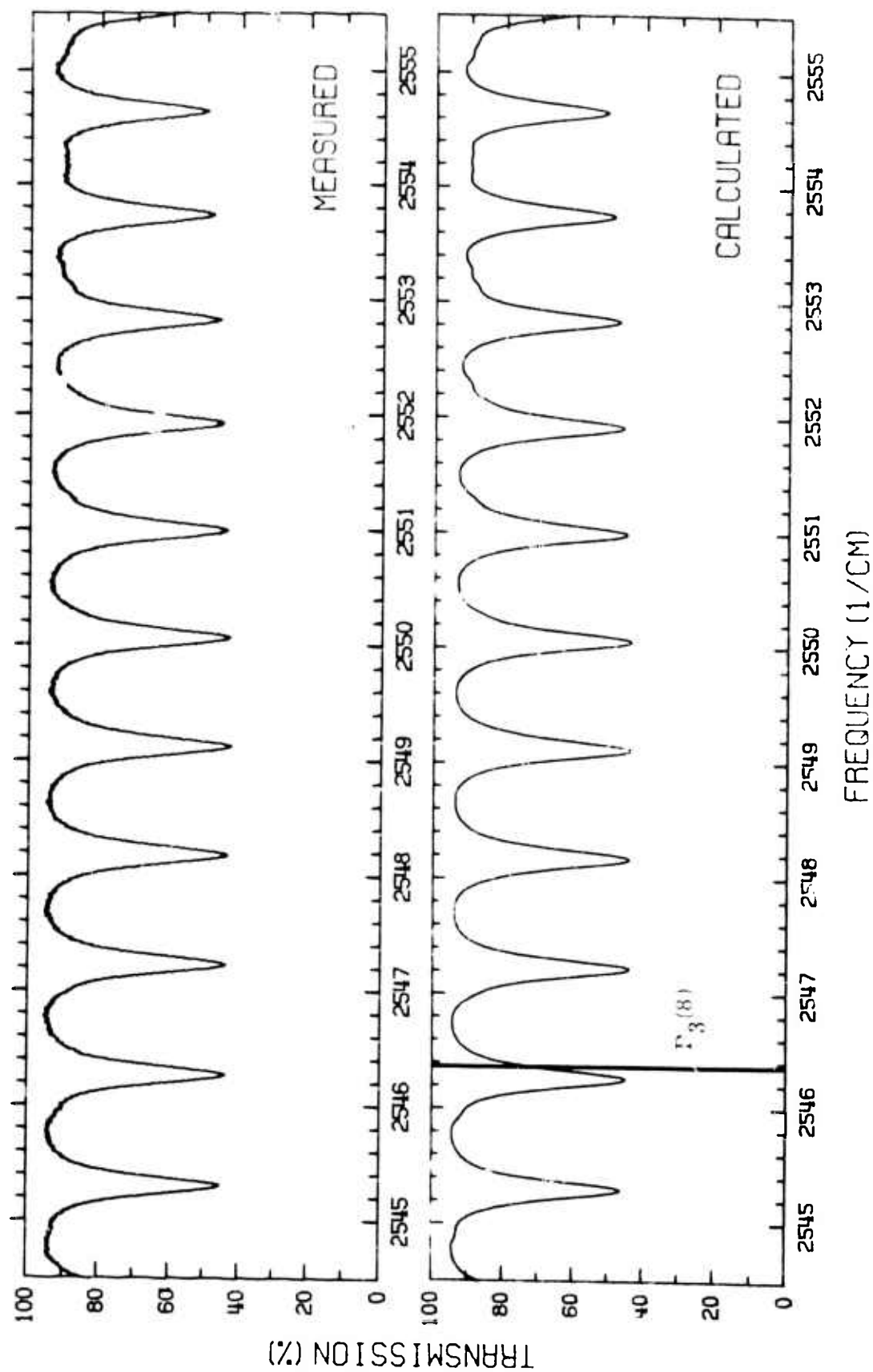


Figure 15. Comparison of Measured and Calculated N_2O Spectra
(20 meter path; 0.150 Torr N_2O ; 760 Torr air; 300°K)

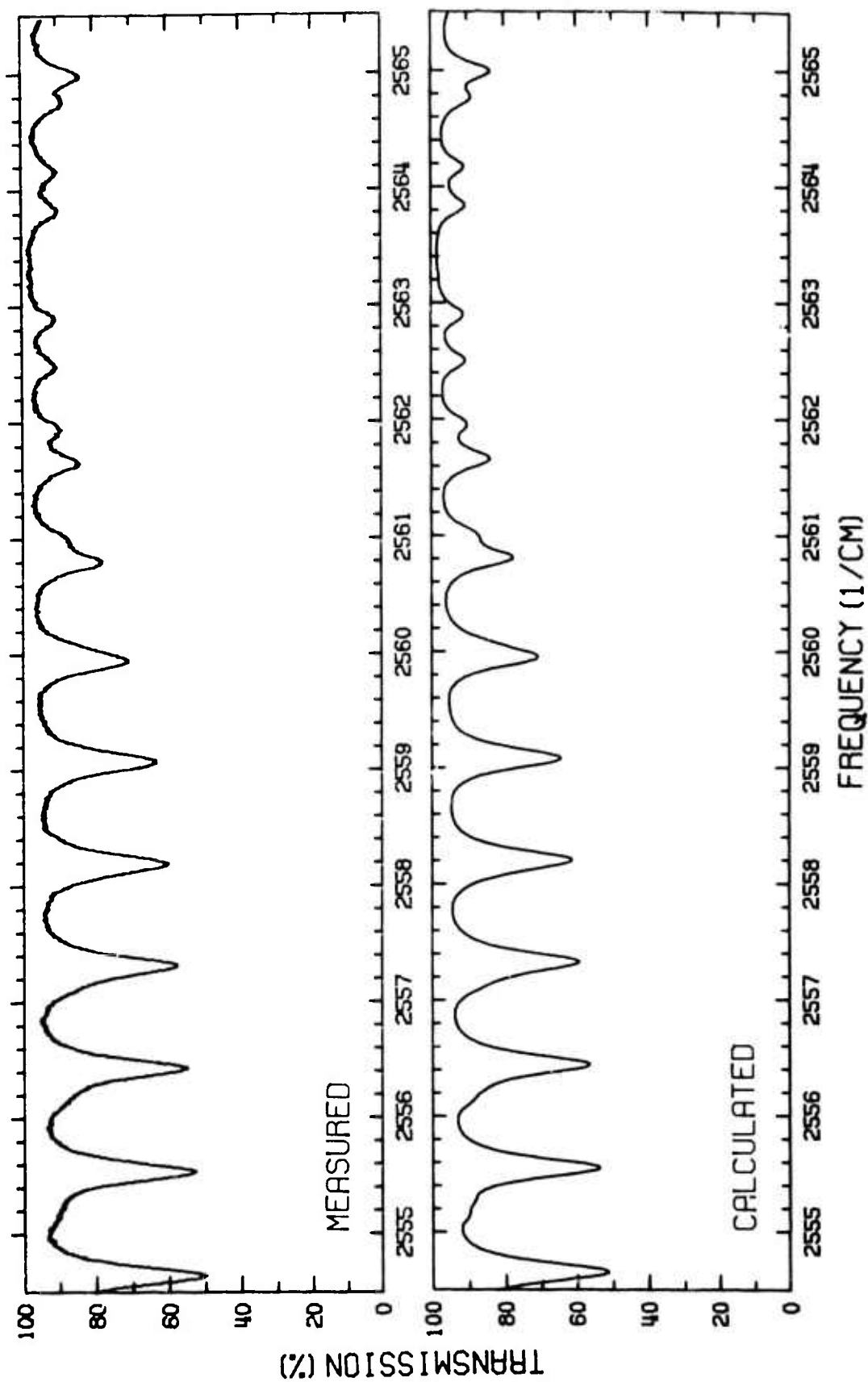


Figure 16. Comparison of Measured and Calculated N_2O Spectra
(20 meter path; 0.150 Torr N_2O ; 760 Torr air; 300°K)

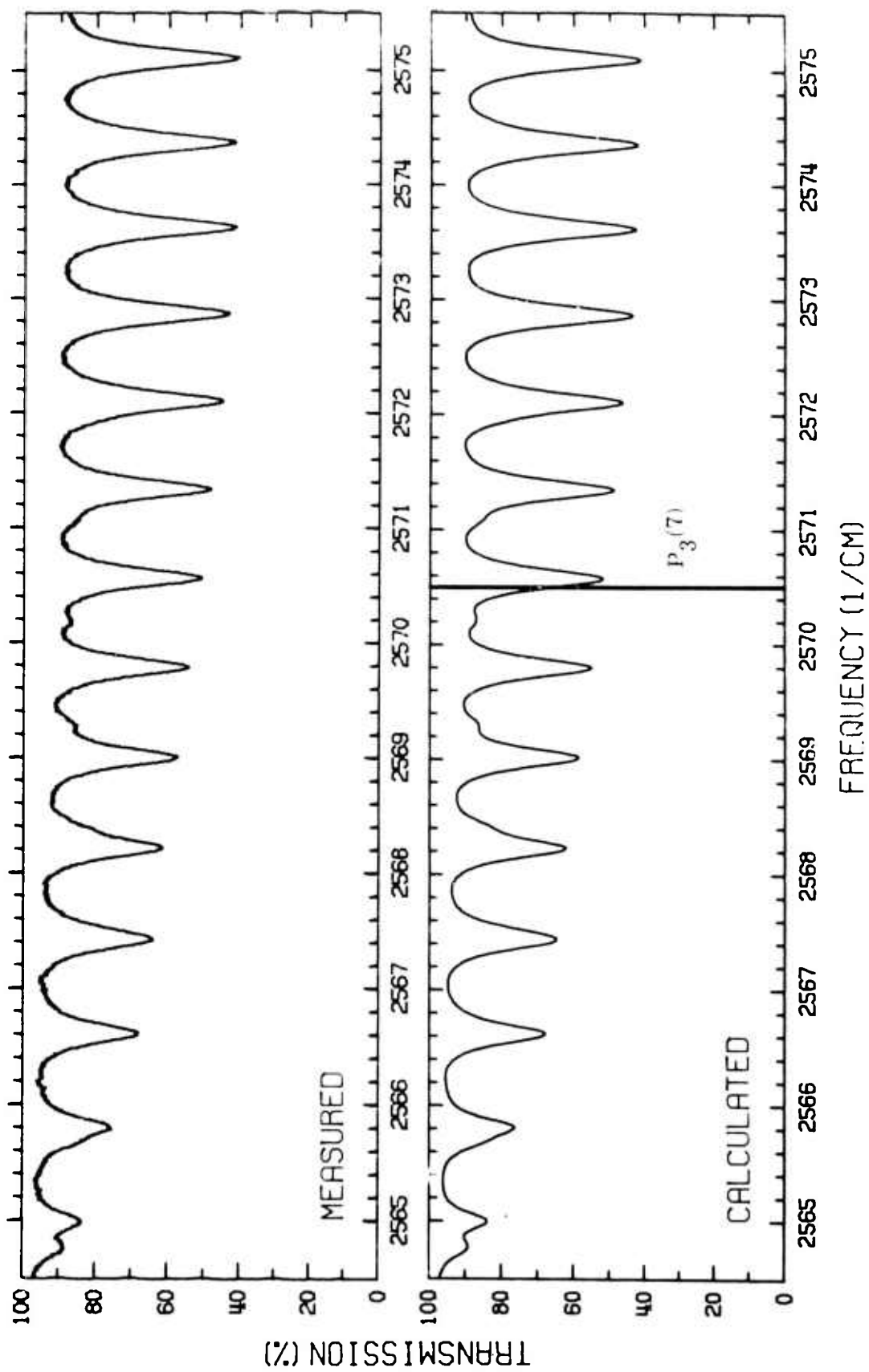


Figure 17. Comparison of Measured and Calculated N_2O Spectra
(20 meter path: 0.150 Torr N_2O ; 760 Torr air; 300°K)

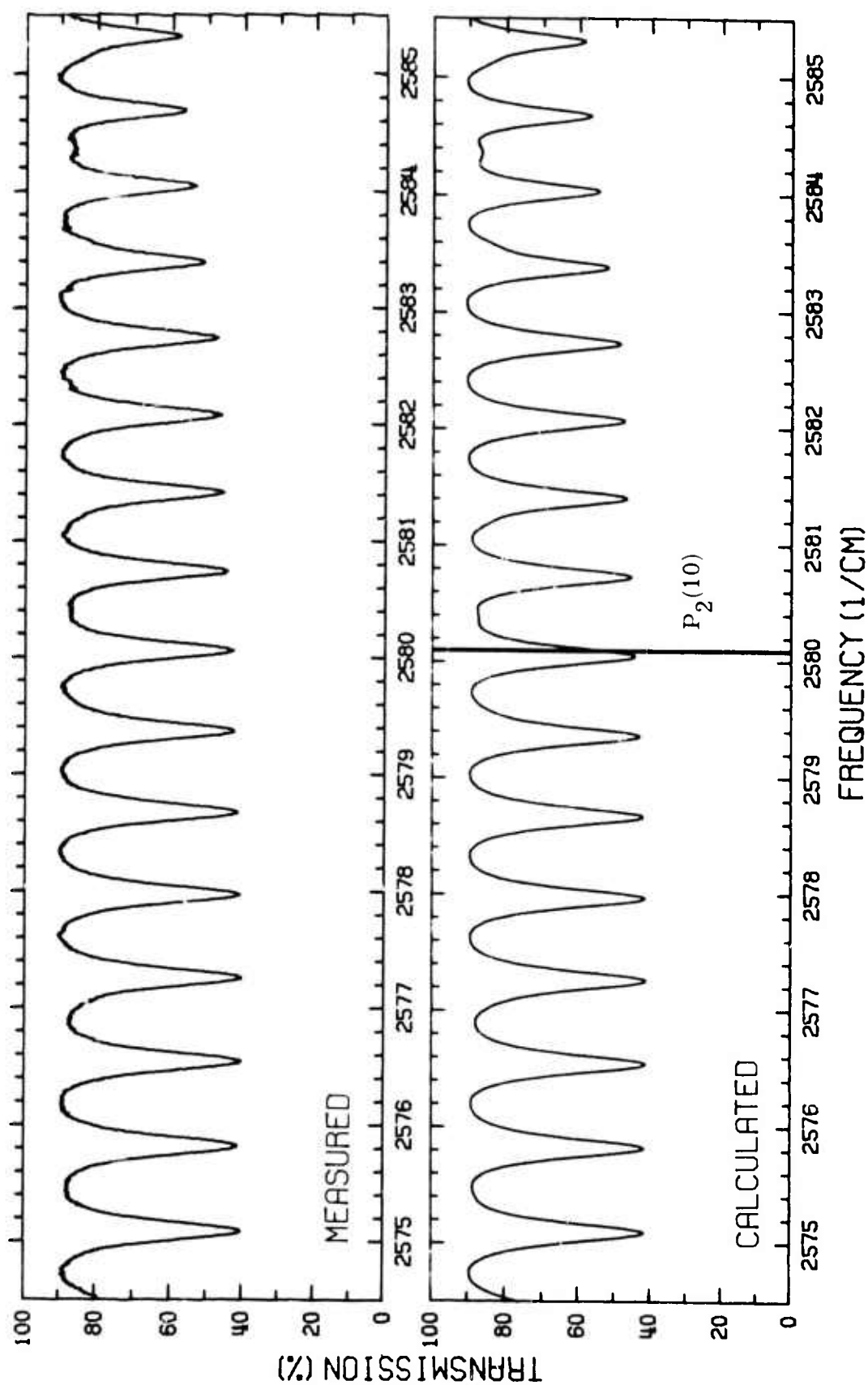


Figure 18. Comparison of Measured and Calculated N_2O Spectra
(20 meter path; 0.150 Torr N_2O ; 760 Torr air; 300°K)

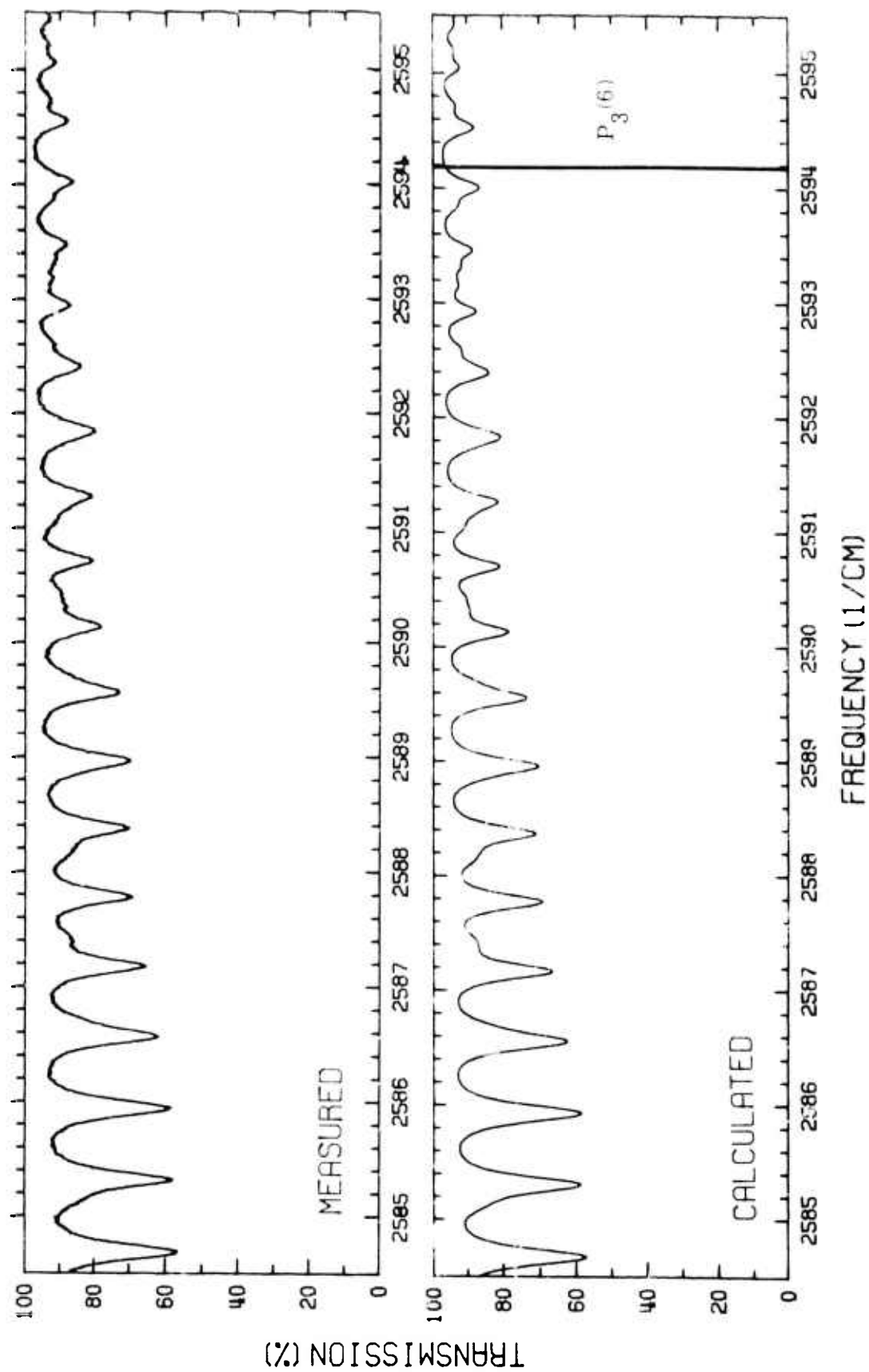


Figure 19. Comparison of Measured and Calculated N_2O Spectra
(20 meter path: 0.150 Torr N_2O : 760 Torr air: 390°K)

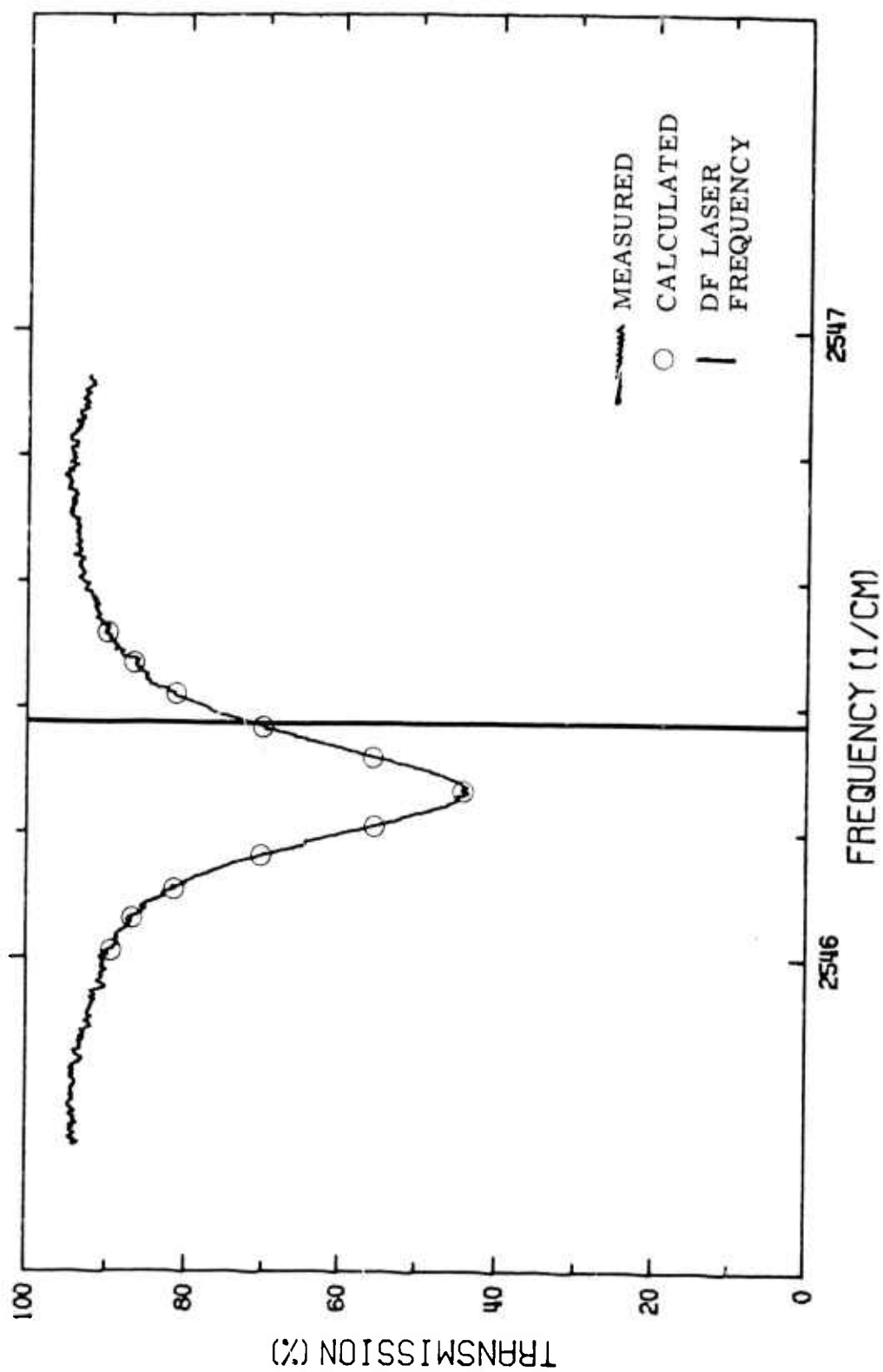


Figure 20. Comparison of Measured and Calculated Absorption Near the $P_3(8)$ DF Laser Line.
(20 meter path; 0.150 Torr N_2O ; 760 Torr air; 300°K)

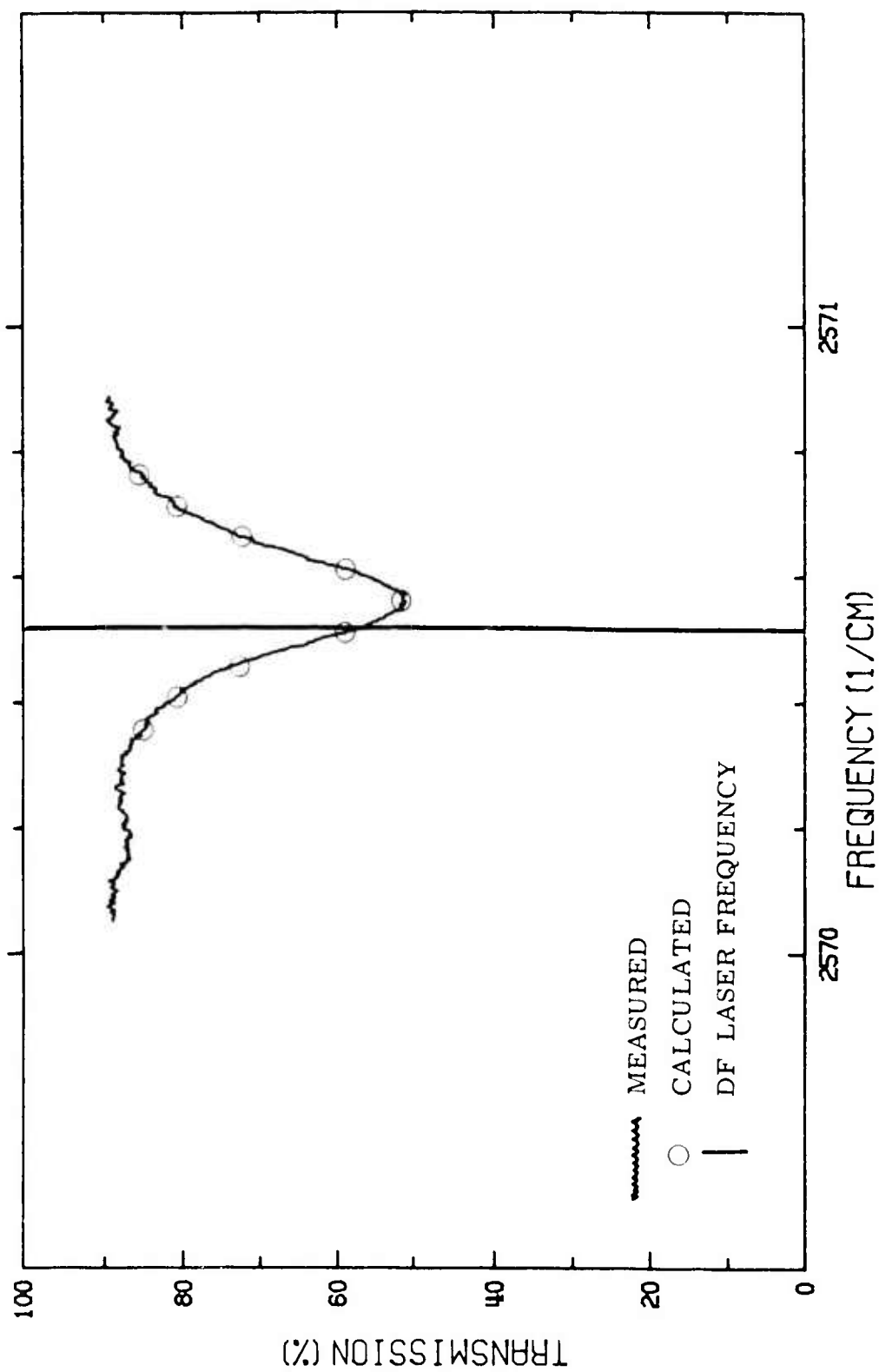


Figure 21. Comparison of Measured and Calculated Absorption Near the $P_3(7)$ DF Laser Line.
(20 meter path; 0.150 Torr N_2O ; 760 Torr air; 300°K)

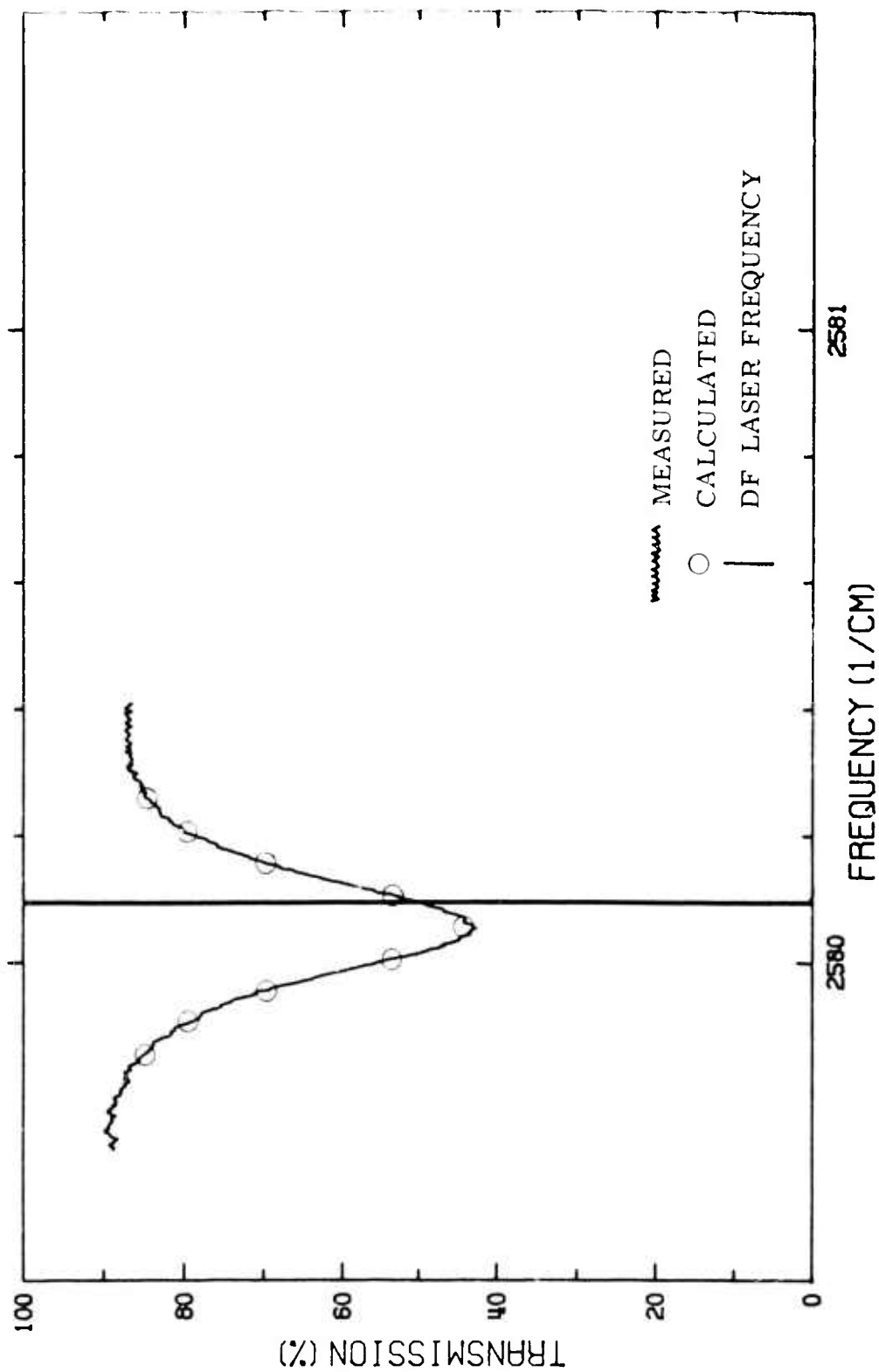


Figure 22. Comparison of Measured and Calculated Absorption Near the $P_2(10)$ DF Laser Line.
(20 meter path; 0.150 Torr N_2O ; 760 Torr air; 300°K)

Measured and Calculated

CH_4 Spectra

Figures 23 - 42

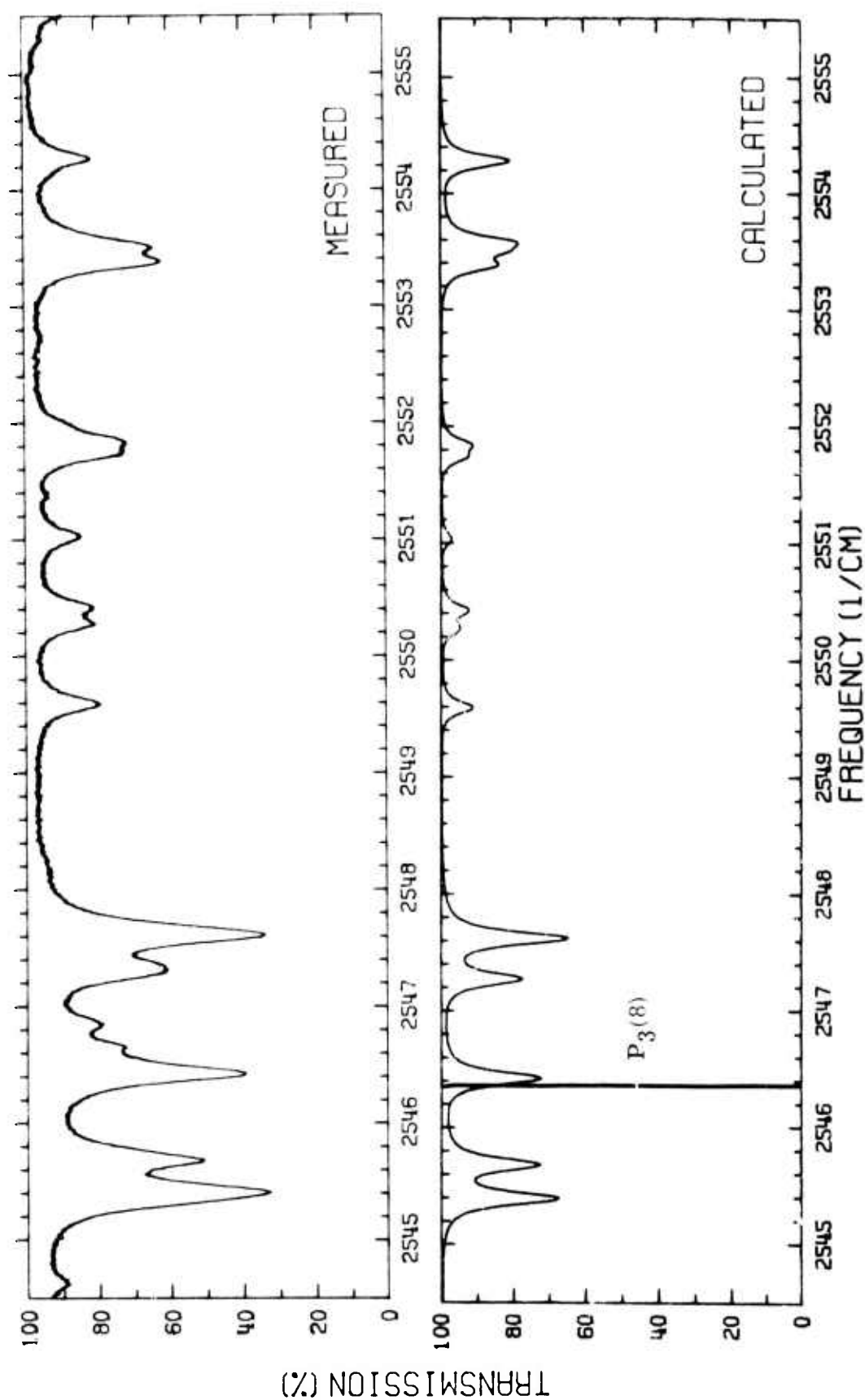


Figure 23. Comparison of Measured and Calculated CH_4 Spectra.
(40 meter path; 6 Torr CH_4 ; 754 Torr air; 300°K)

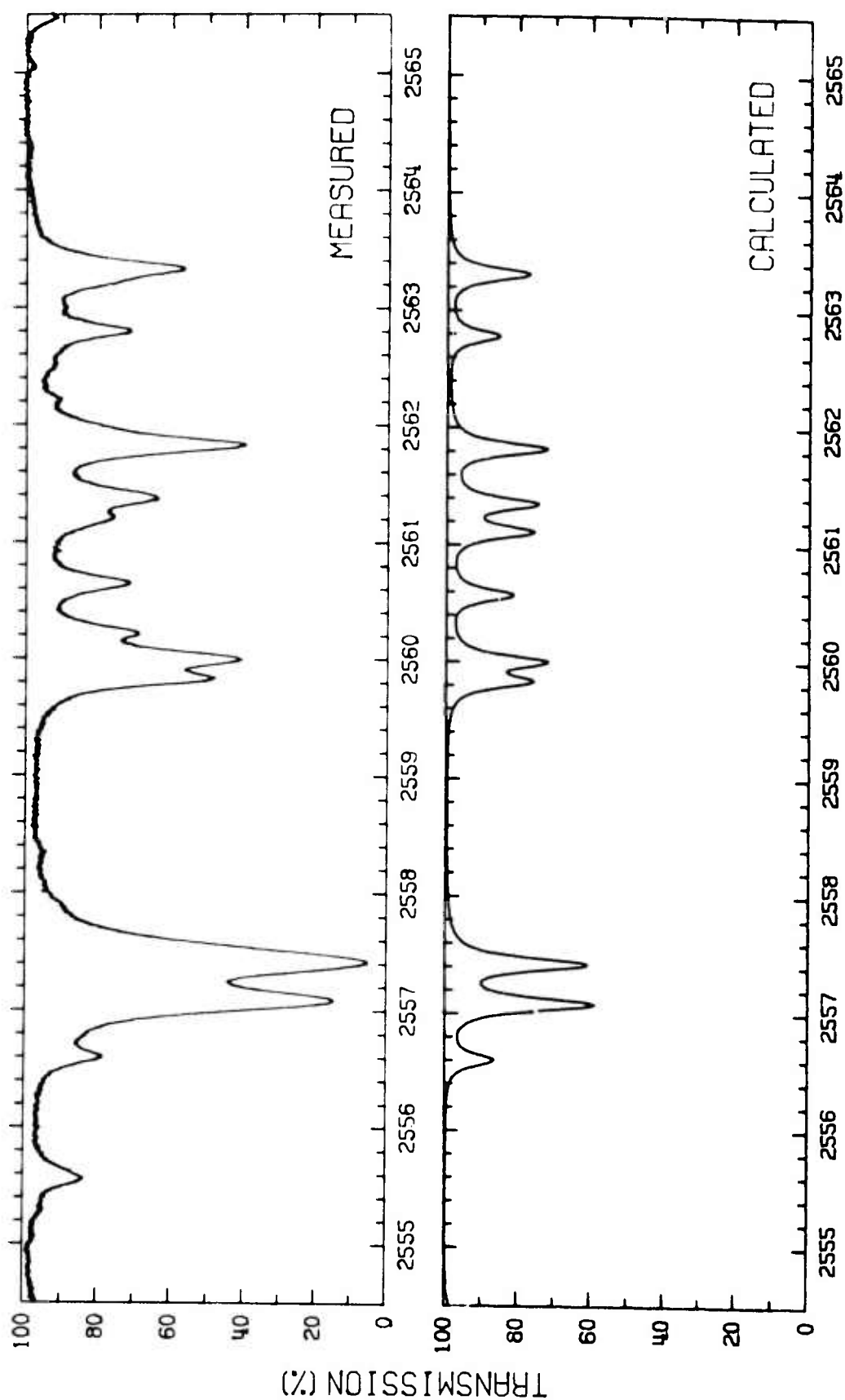


Figure 24. Comparison of Measured and Calculated CH_4 Spectra.

(40 meter path: 6 Torr CH_4 ; 754 Torr air; 300°K)

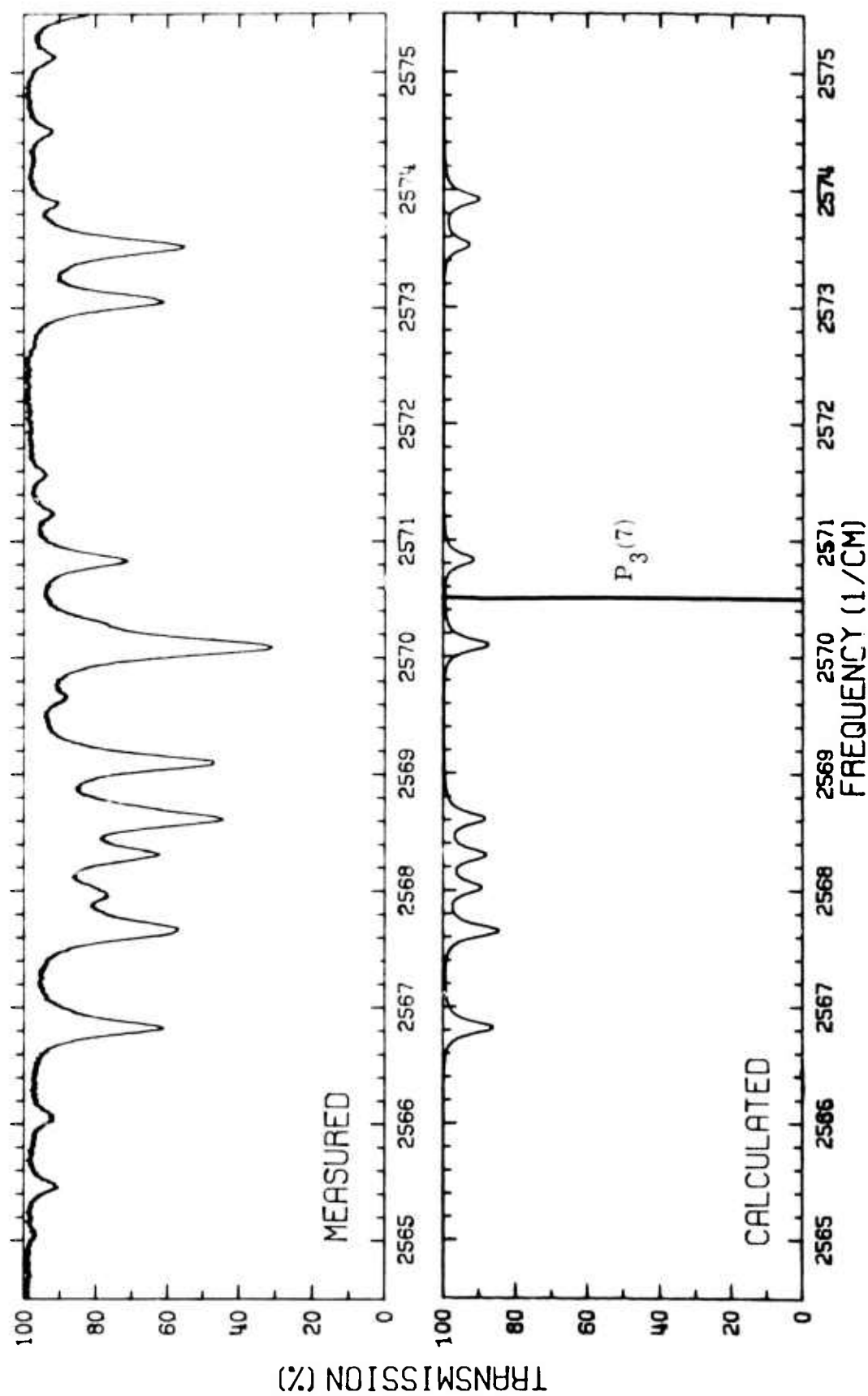


Figure 25. Comparison of Measured and Calculated CH_4 Spectra.
 (40 meter path; 6 Torr CH_4 ; 754 Torr air; 300°K)

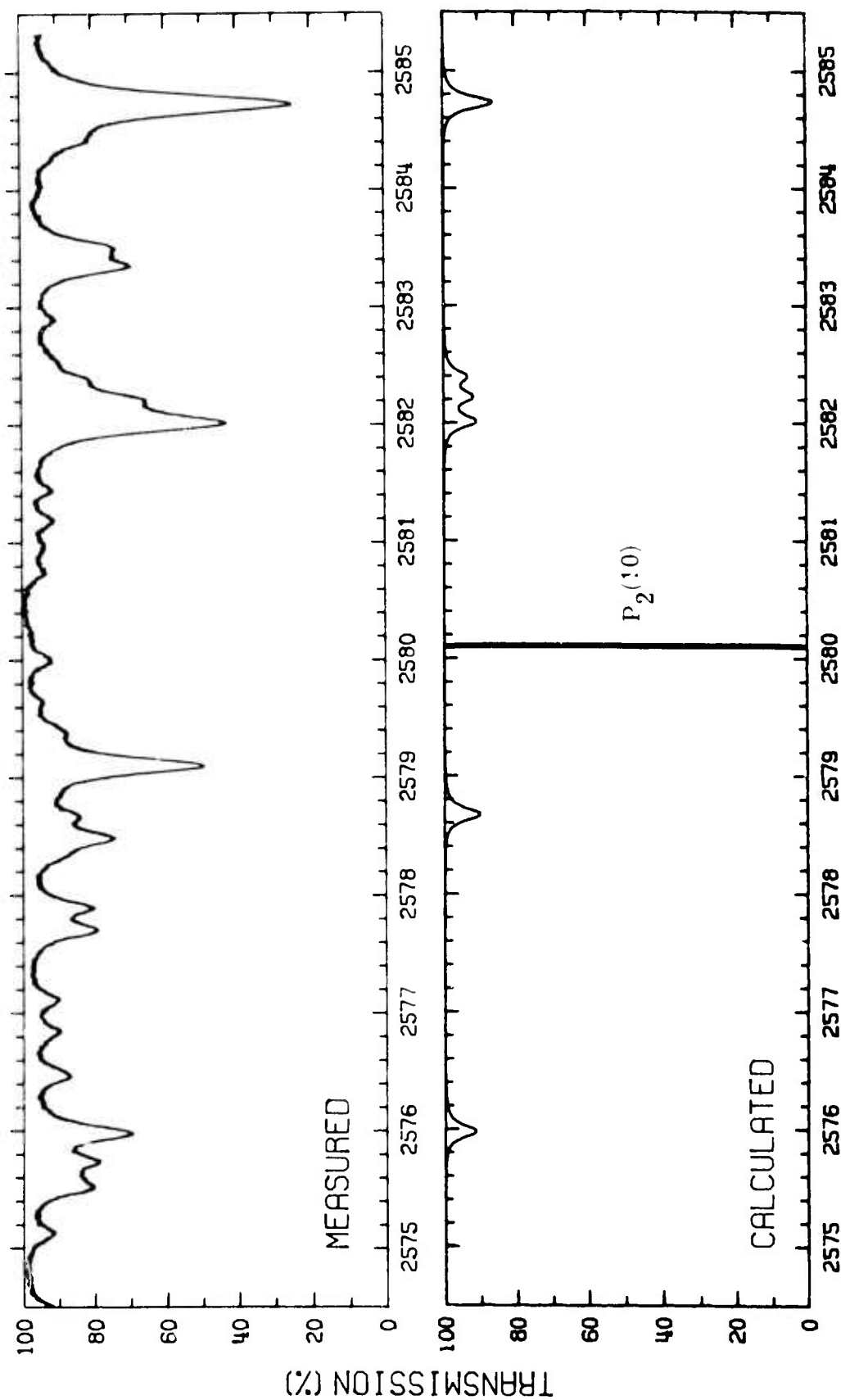


Figure 26. Comparison of Measured and Calculated CH_4 Spectra.
(40 meter path; 6 Torr CH_4 ; 754 Torr air; 300°K)

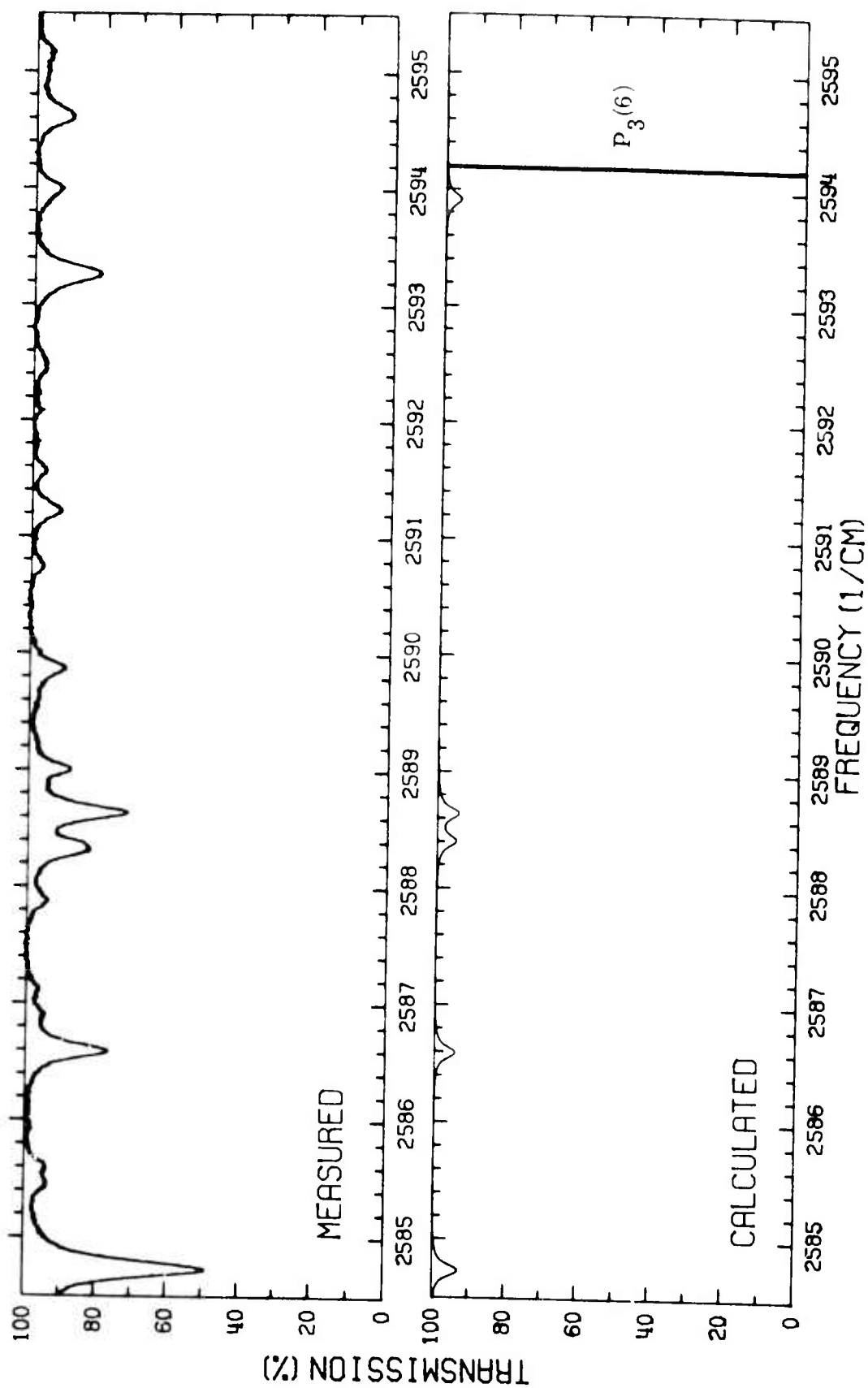


Figure 27. Comparison of Measured and Calculated CH_4 Spectra.
(20 meter path; 6 Torr CH_4 ; 754 Torr air; 300°K)

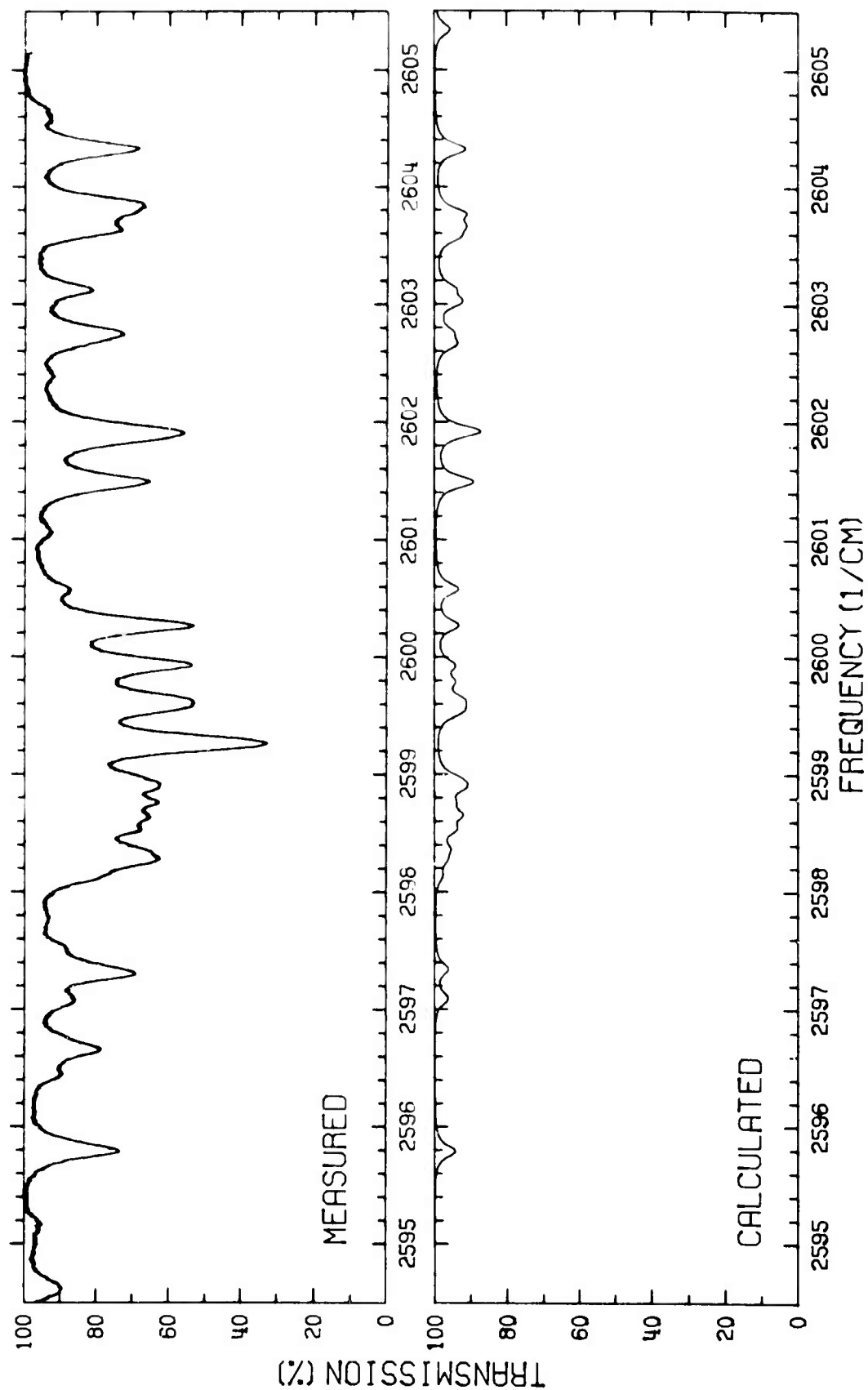


Figure 28. Comparison of Measured and Calculated CH_4 Spectra.
(20 meter path: 6 Torr CH_4 ; 754 Torr air; 300°K)

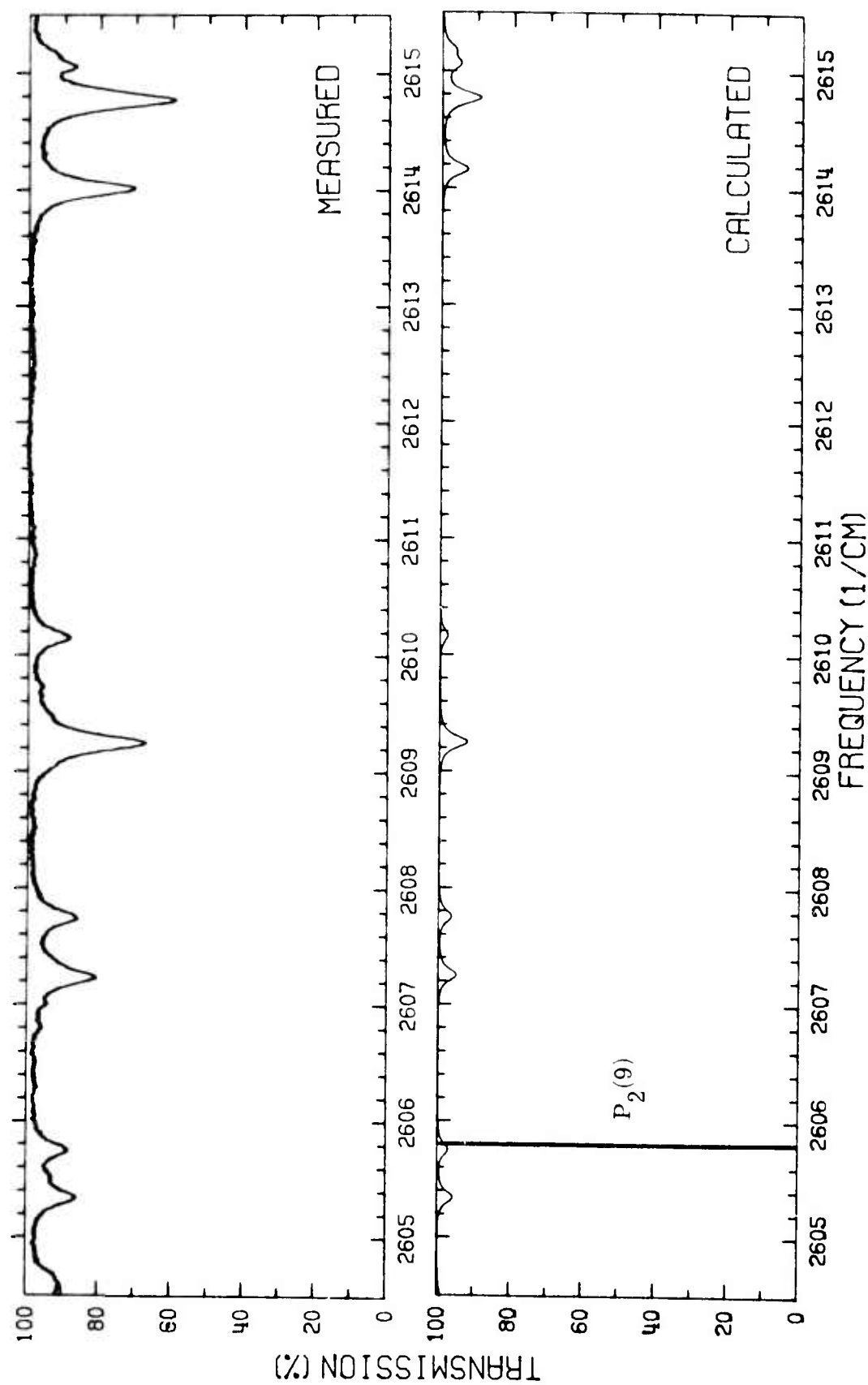


Figure 29. Comparison of Measured and Calculated CH_4 Spectra.
(20 meter path; 6 Torr CH_4 ; 754 Torr air; 300°K)

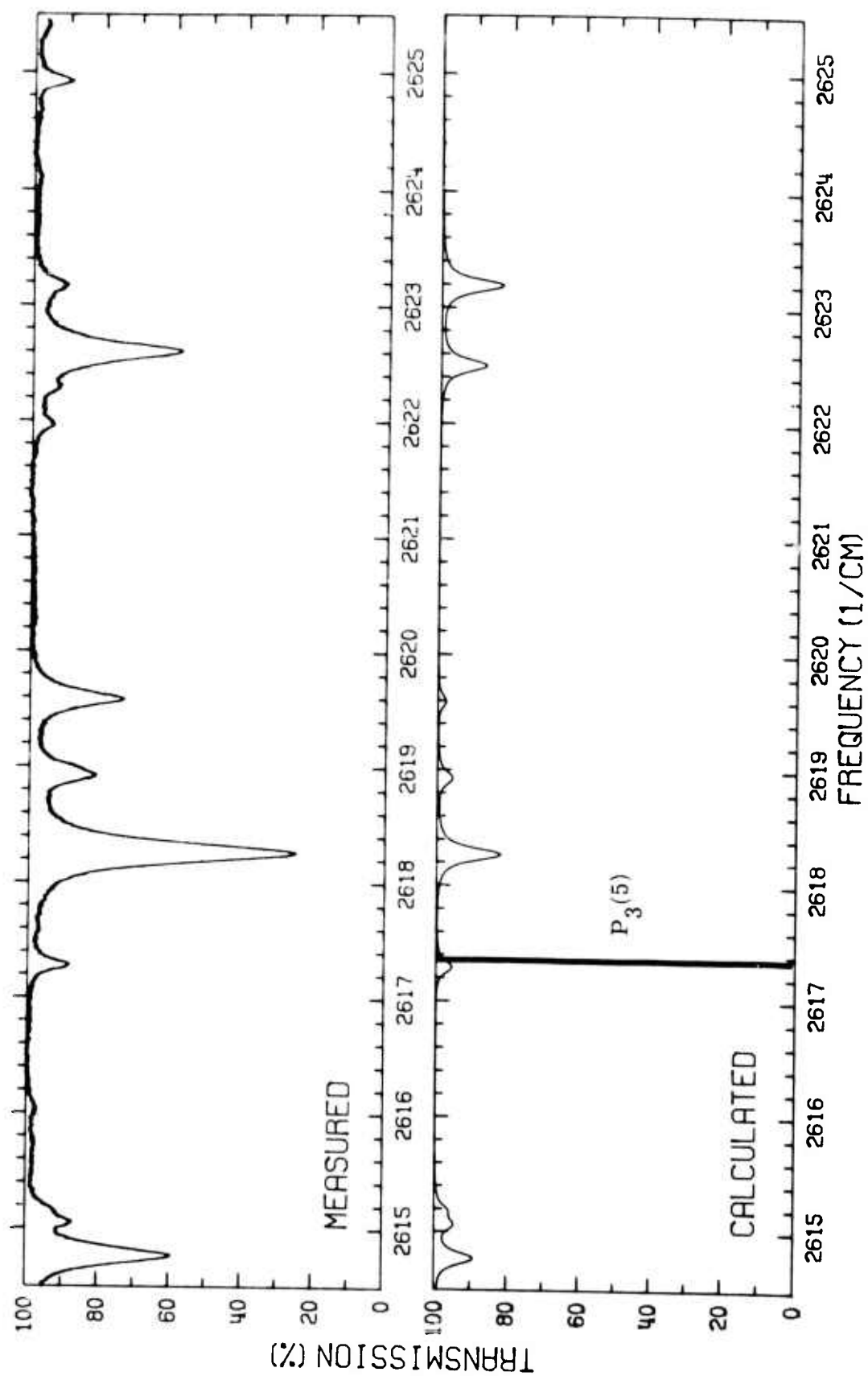


Figure 30. Comparison of Measured and Calculated CH₄ Spectra.
(20 meter path; 6 Torr CH₄; 754 Torr air; 300°K)

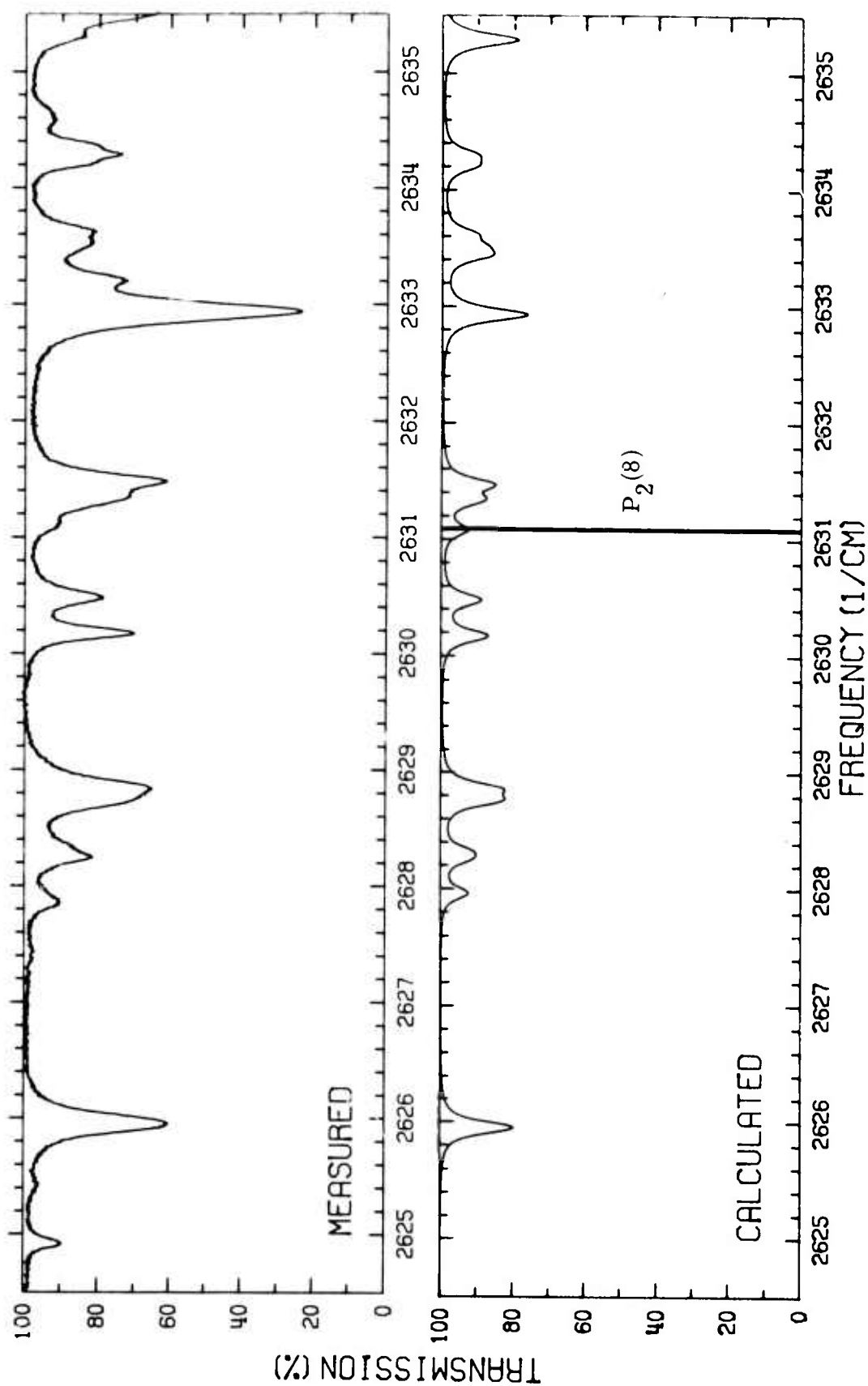


Figure 31. Comparison of Measured and Calculated CH_4 Spectra.
(20 meter path; 6 Torr CH_4 ; 754 Torr air; 300°K)

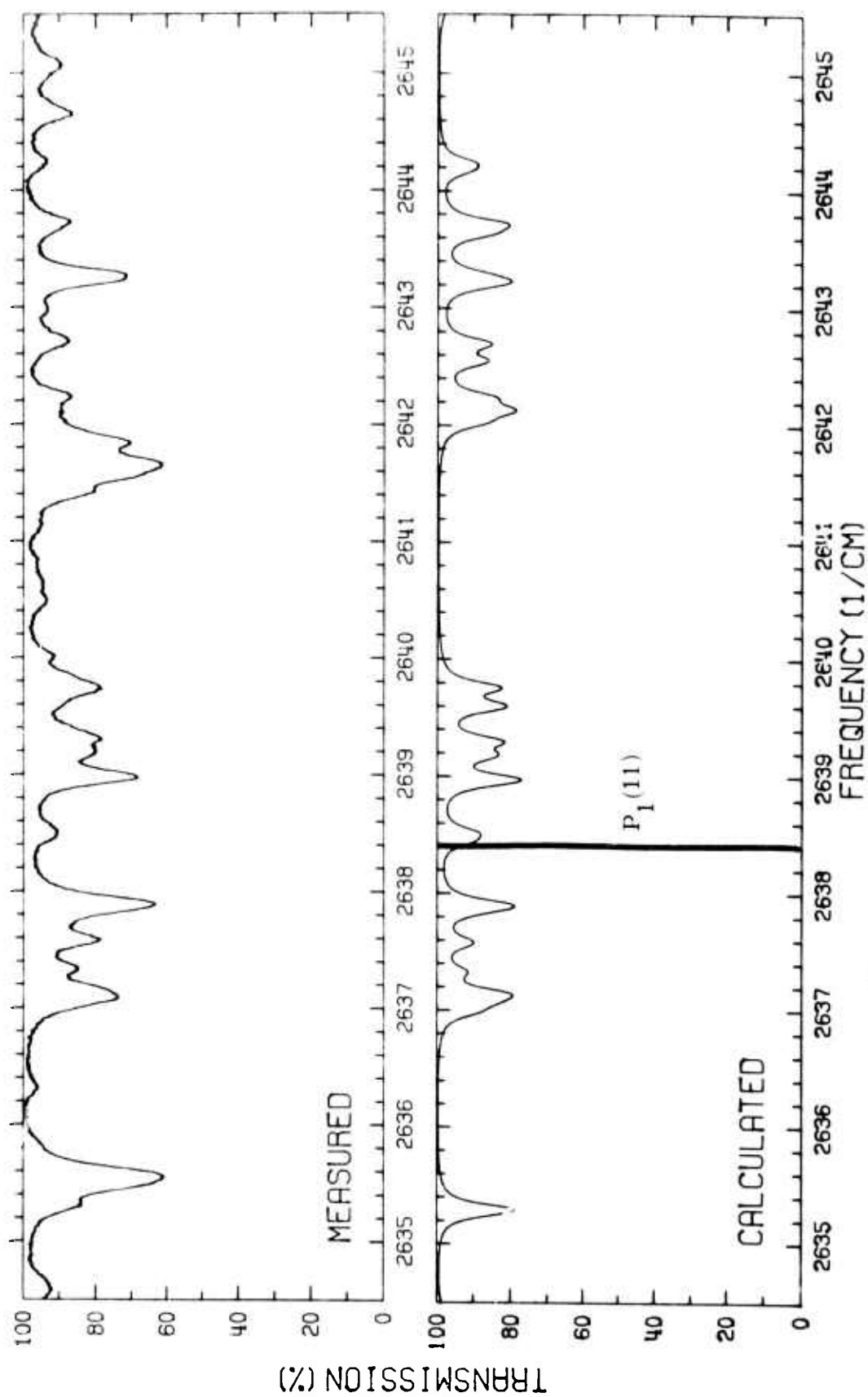


Figure 32. Comparison of Measured and Calculated CH_4 Spectra.
(20 meter path; 6 Torr CH_4 ; 754 Torr air; 300°K)

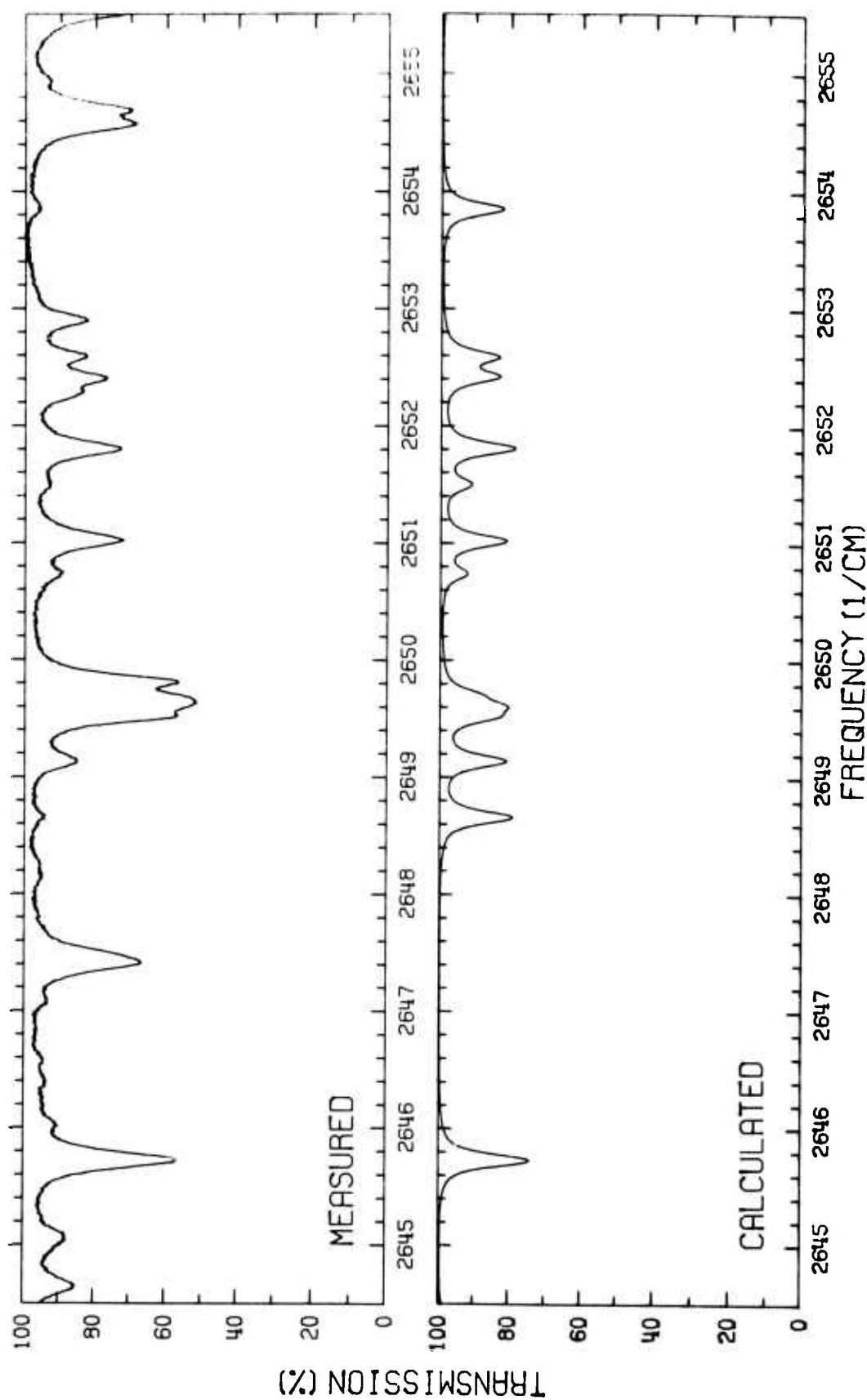


Figure 33. Comparison of Measured and Calculated CH_4 Spectra.
(20 meter path; 6 Torr CH_4 ; 754 Torr air; 300°K)

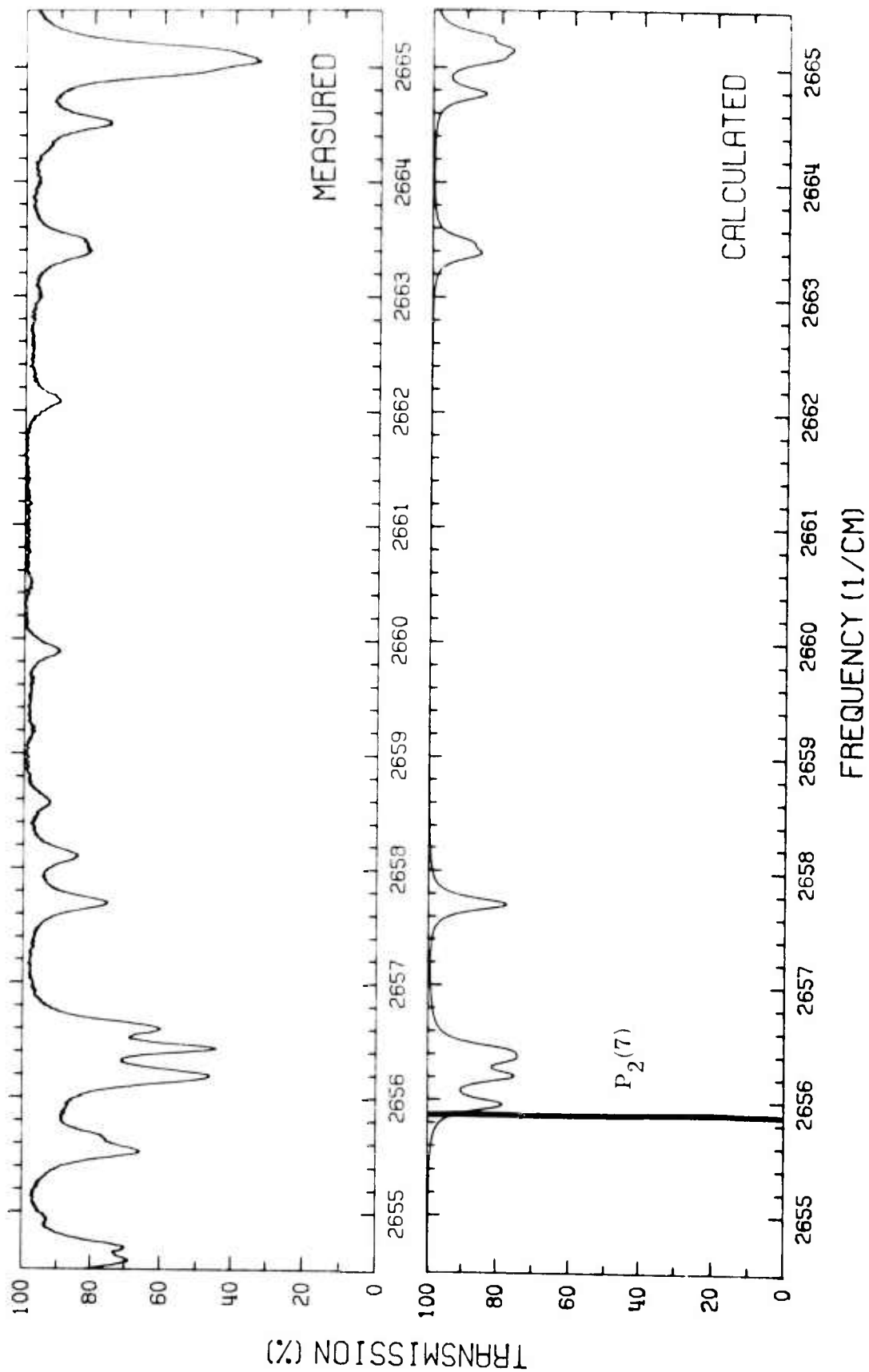


Figure 34. Comparison of Measured and Calculated CH_4 spectra.
(20 meter path; 6 Torr CH_4 ; 754 Torr air; 300°K)

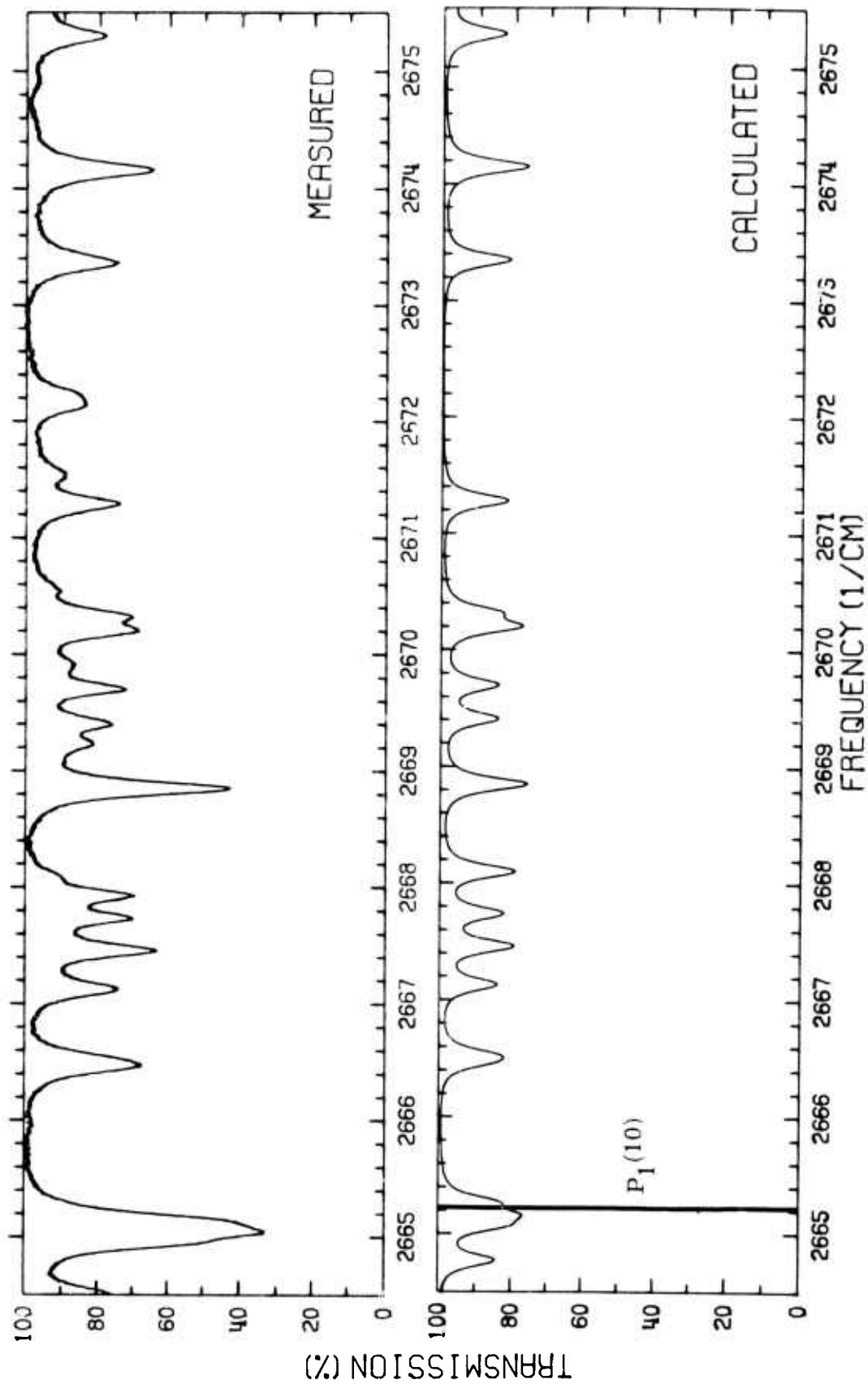


Figure 35. Comparison of Measured and Calculated CH_4 Spectra.
(20 meter path; 6 Torr CH_4 ; 754 Torr air; 300°K)

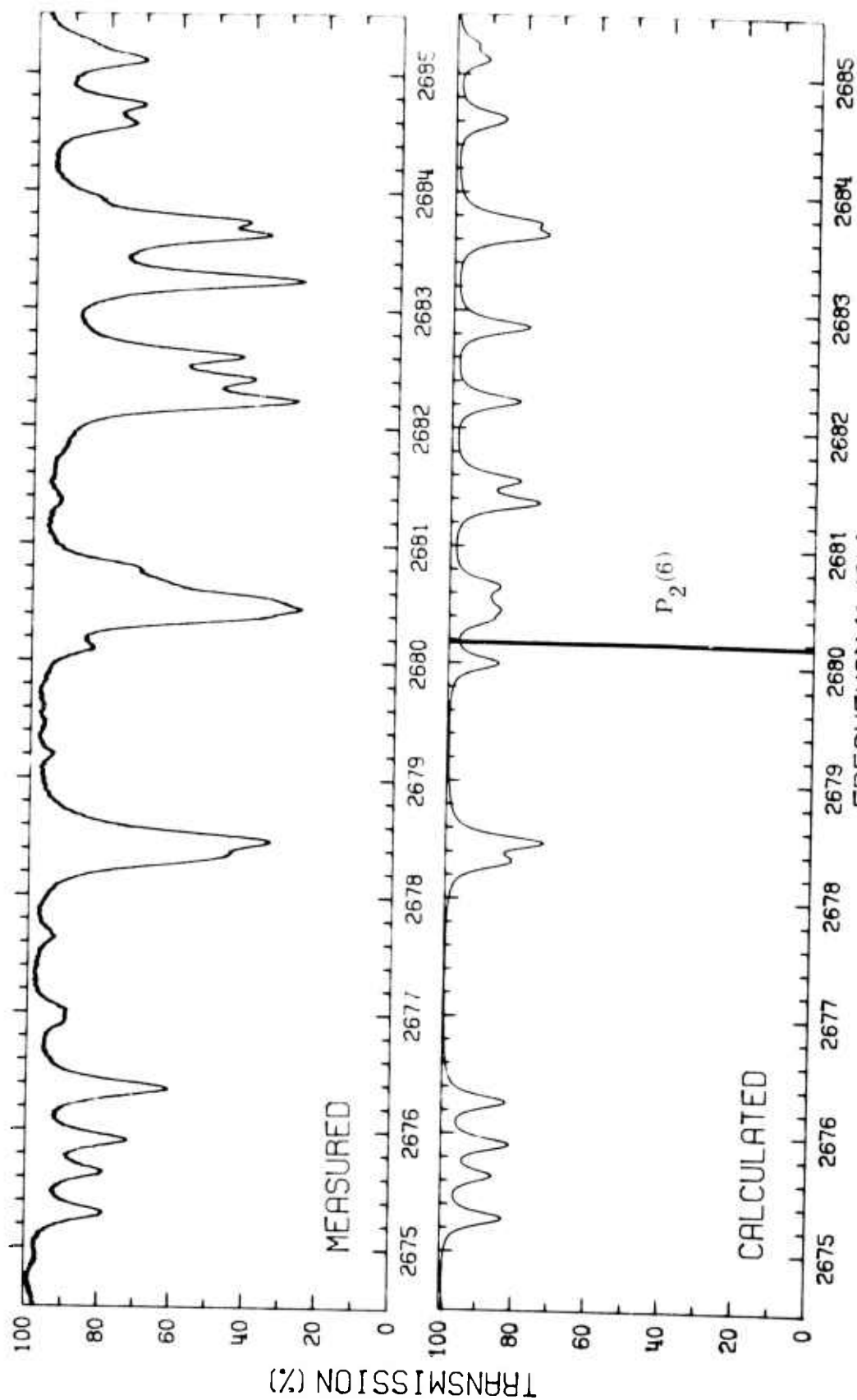


Figure 36. Comparison of Measured and Calculated CH₄ Spectra.
(20 meter path; 6 Torr CH₄; 754 Torr air; 300°K)

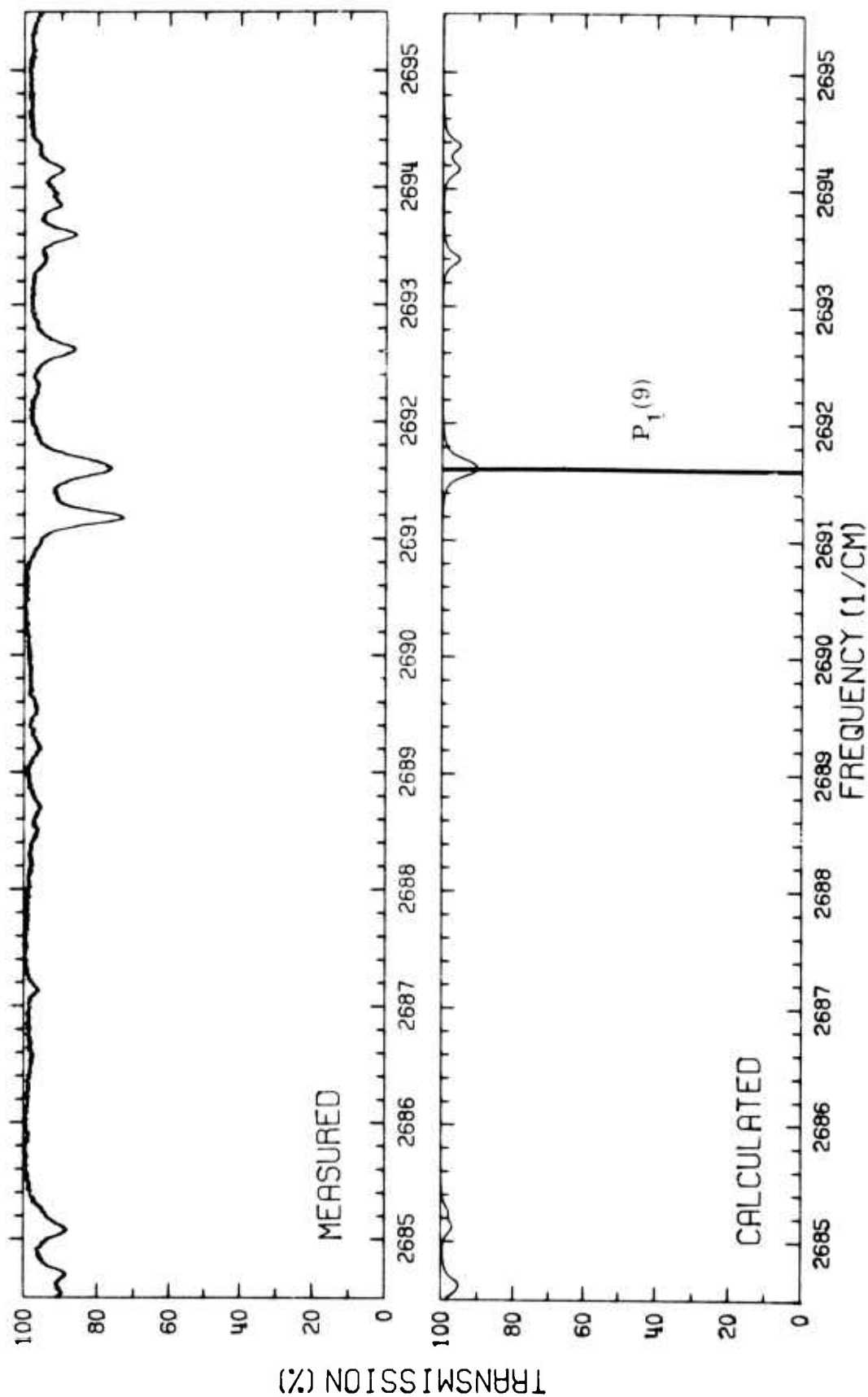


Figure 37. Comparison of Measured and Calculated CH_4 Spectra.
(40 meter path; 1.00 Torr CH_4 ; 759 Torr air; 300°K)

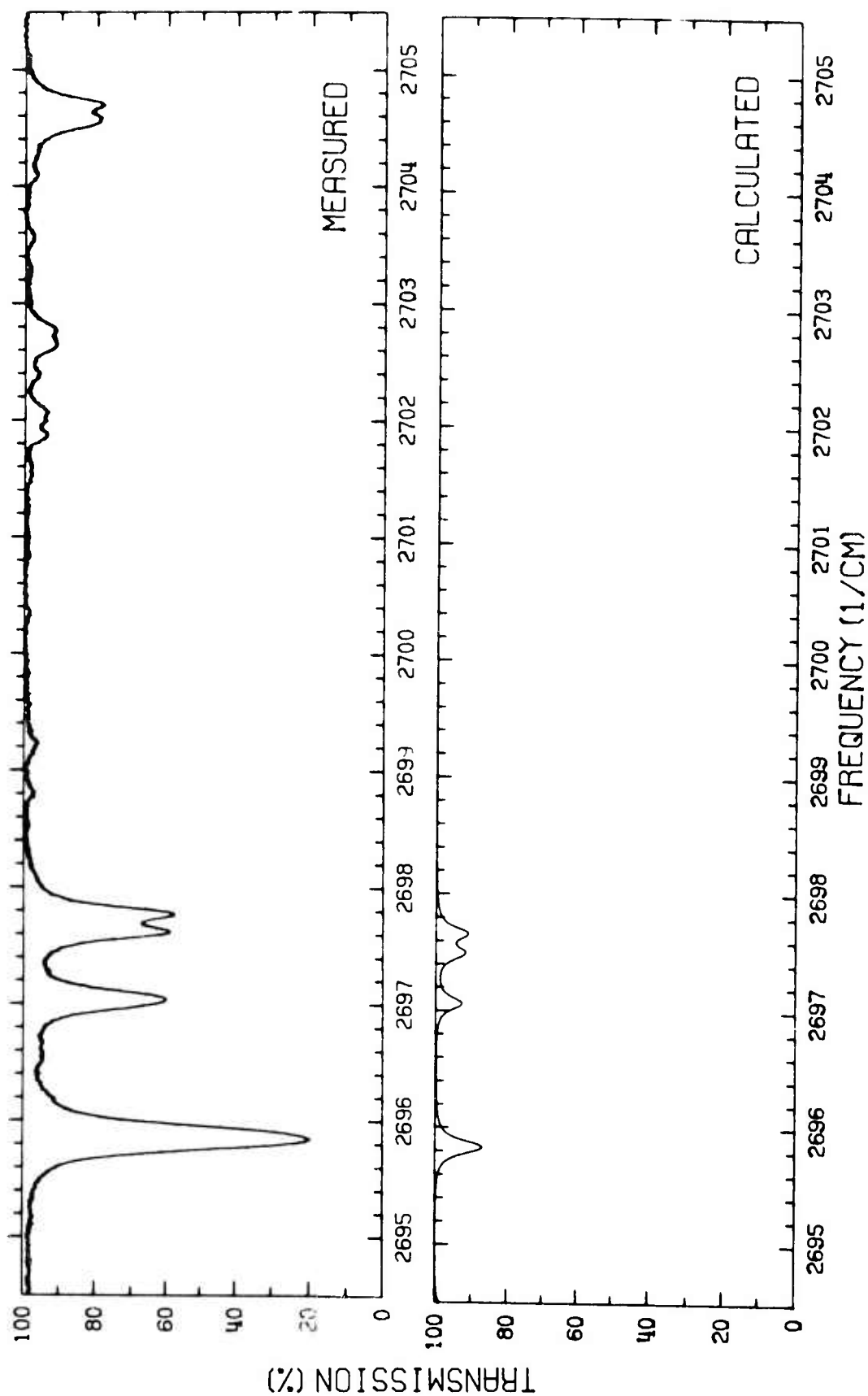


Figure 38. Comparison of Measured and Calculated CH_4 Spectra.
(40 meter path; 1.00 Torr CH_4 ; 759 Torr air; 300°K)

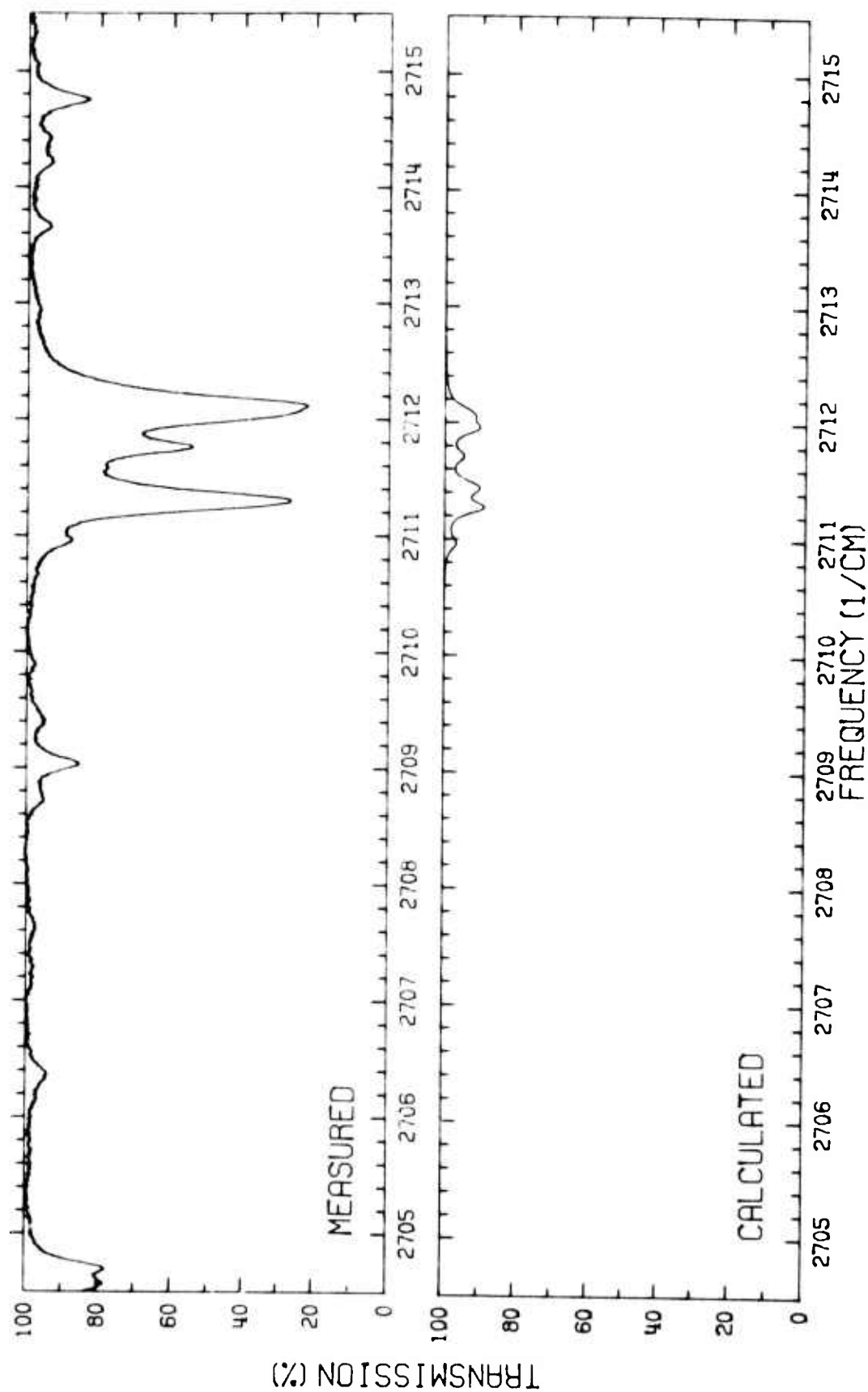


Figure 39. Comparison of Measured and Calculated CH_4 Spectra.
(40 meter path; 1.00 Torr CH_4 ; 759 Torr air; 300°K)

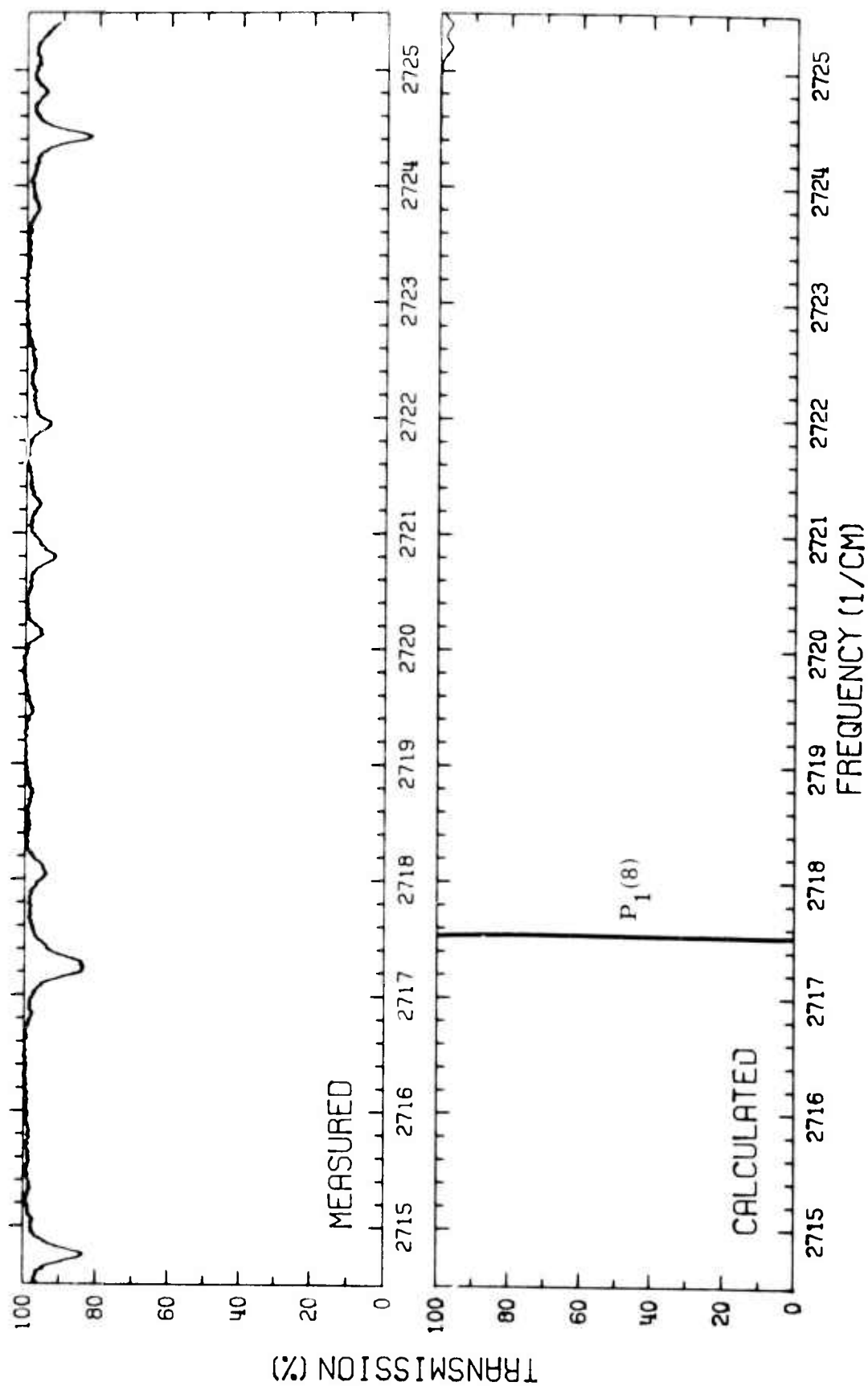


Figure 40. Comparison of Measured and Calculated CH_4 Spectra.
 (40 meter path; 1.00 Torr CH_4 ; 759 Torr air; 300°K)

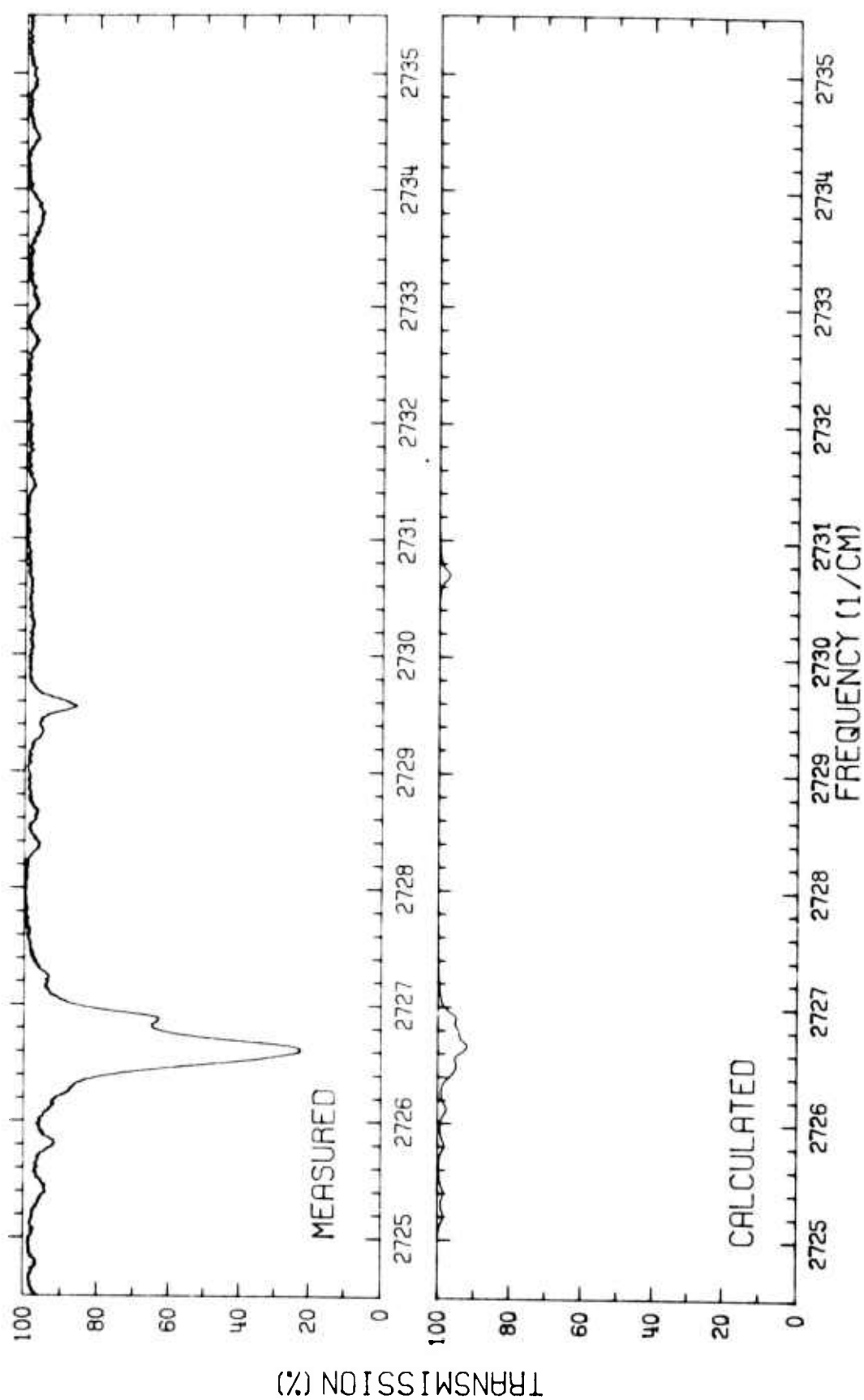


Figure 41. Comparison of Measured and Calculated CH_4 Spectra.
(20 meter path; 1.00 Torr CH_4 ; 759 Torr air; 300°K)

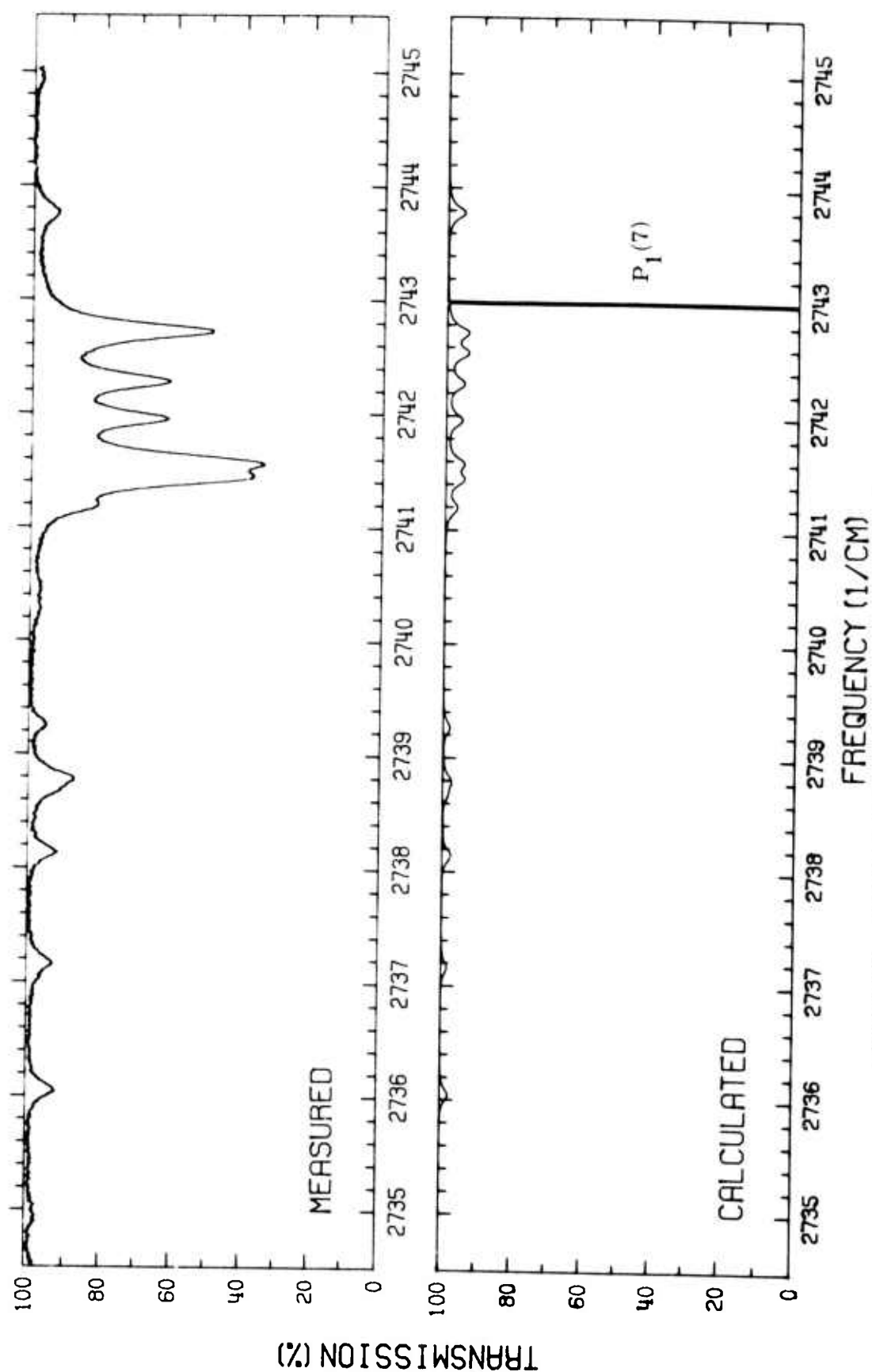


Figure 42. Comparison of Measured and Calculated CH_4 Spectra.
(20 meter path; 1.00 Torr CH_4 ; 759 Torr air; 300°K)

Measured and Calculated
HDO Spectra

Figures 43 - 63

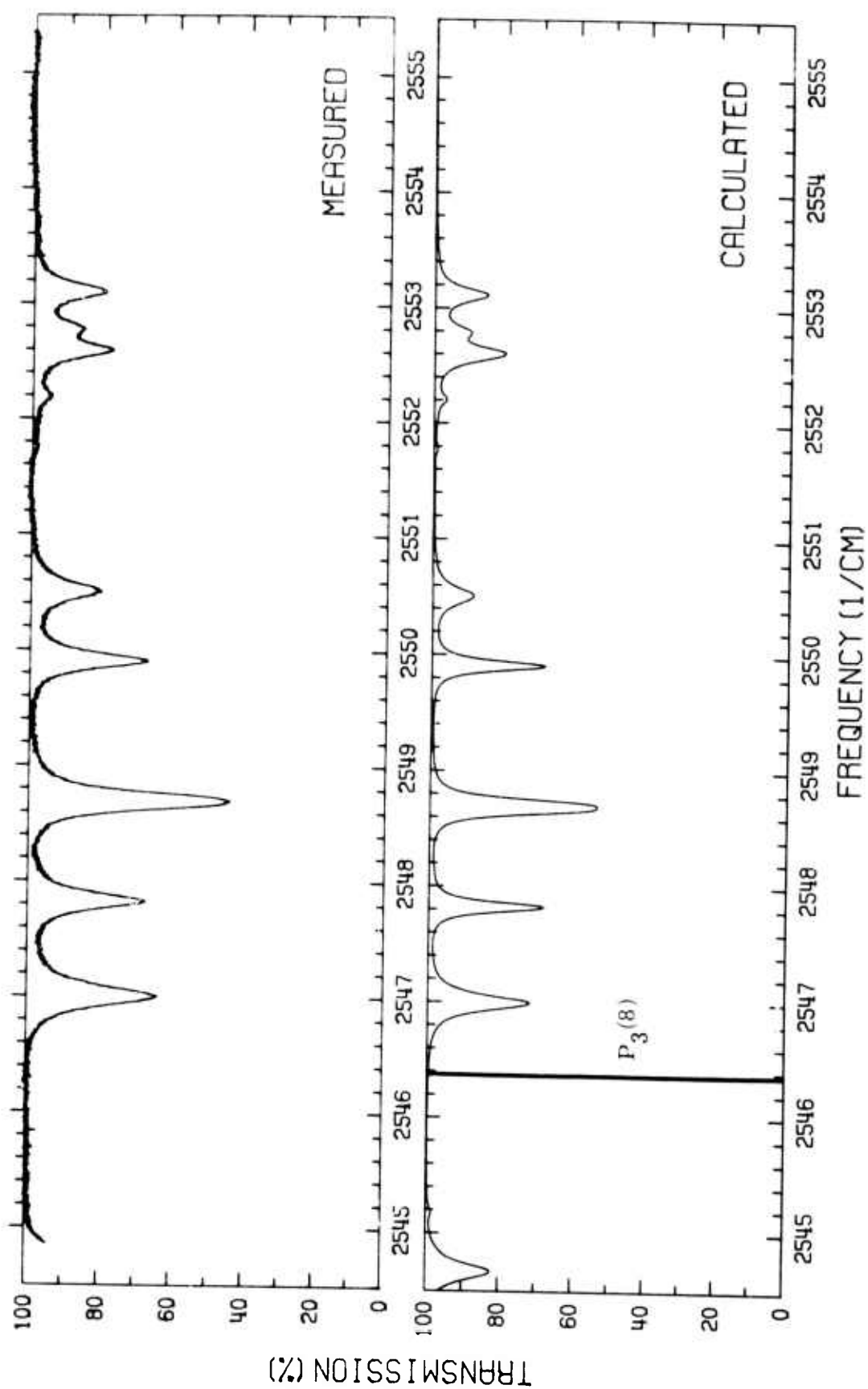


Figure 43. Comparison of Measured and Calculated HDO Spectra.
 (100 meter path; .2002 Torr HDO; 760 Torr air; 300°K)

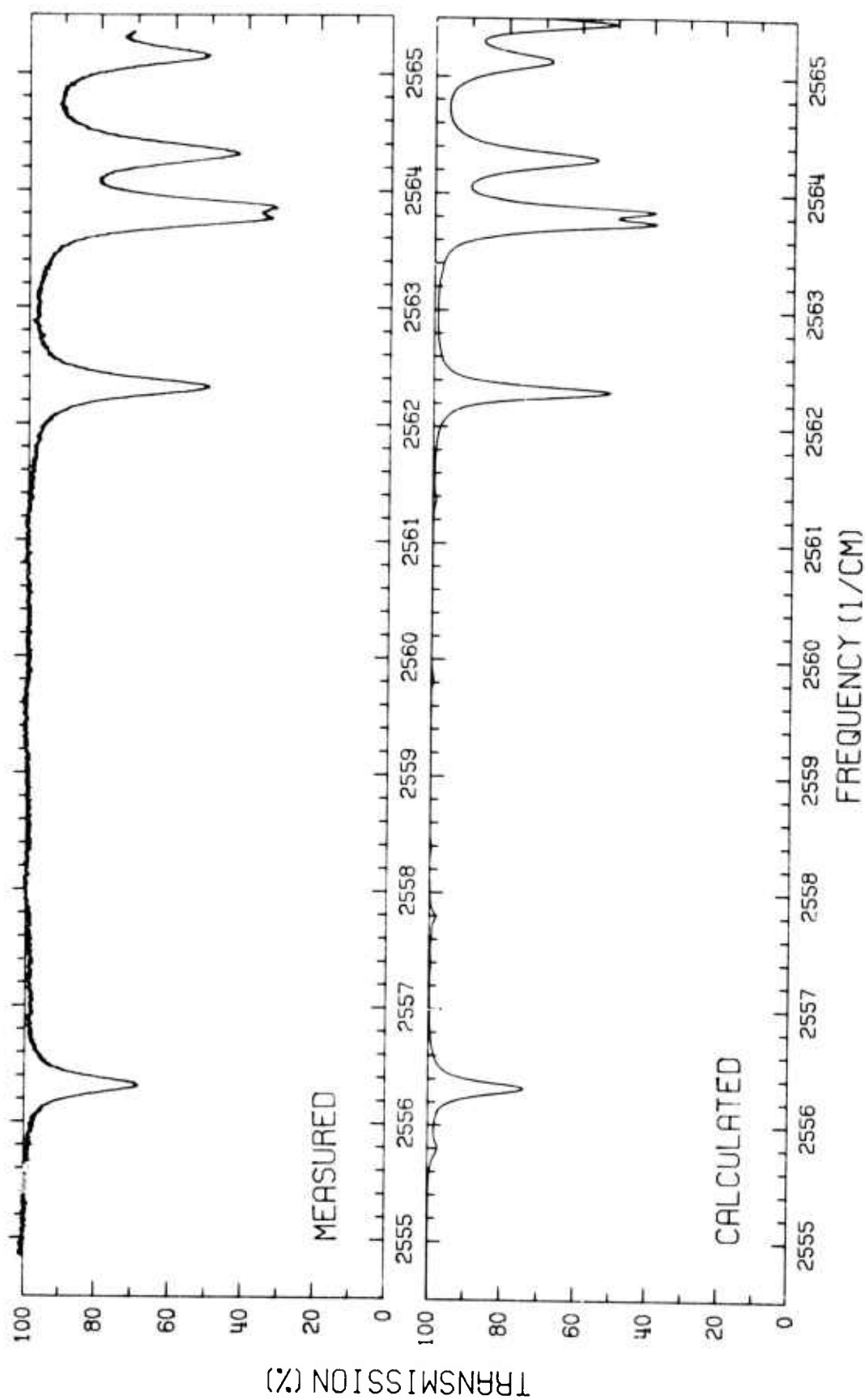


Figure 44. Comparison of Measured and Calculated HDO Spectra.
(100 meter path; .2002 Torr HDO; 760 Torr air; 300°K)

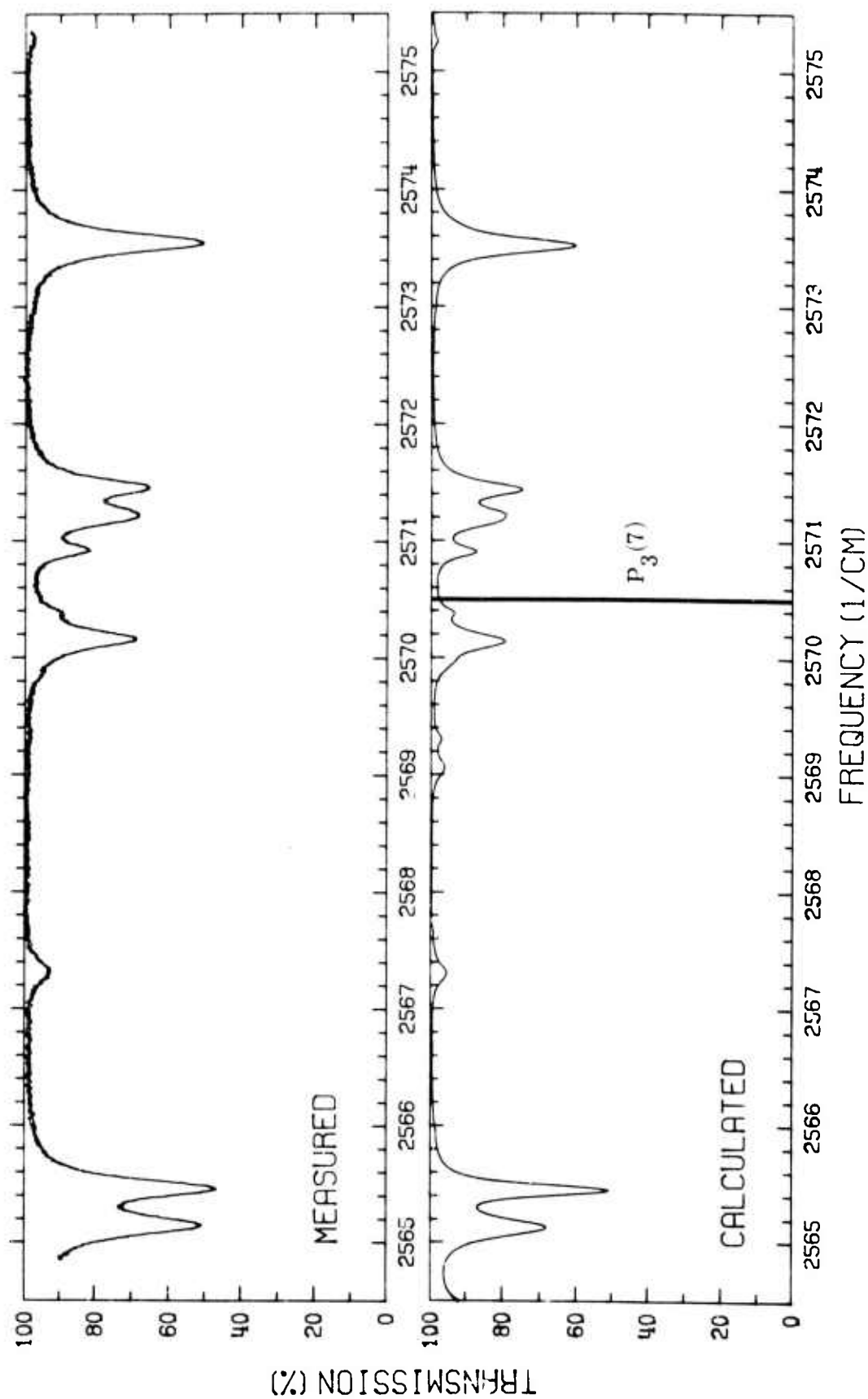


Figure 45. Comparison of Measured and Calculated HDO Spectra.
(100 meter path; .2002 Torr HDO; 760 Torr air; 300°K)

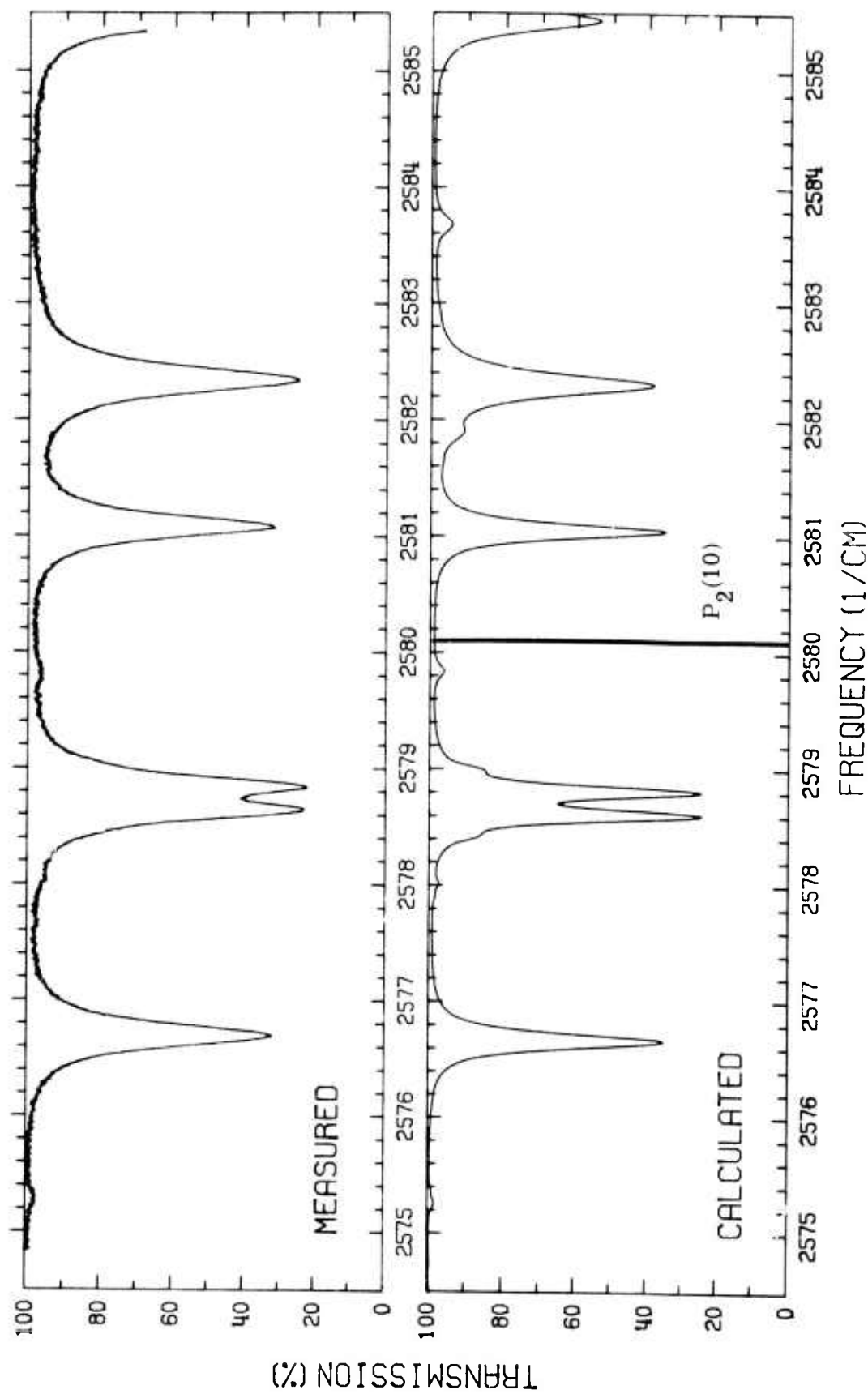


Figure 46. Comparison of Measured and Calculated HDO Spectra.
(100 meter path; .2002 Torr HDO; 760 Torr air; 300°K)

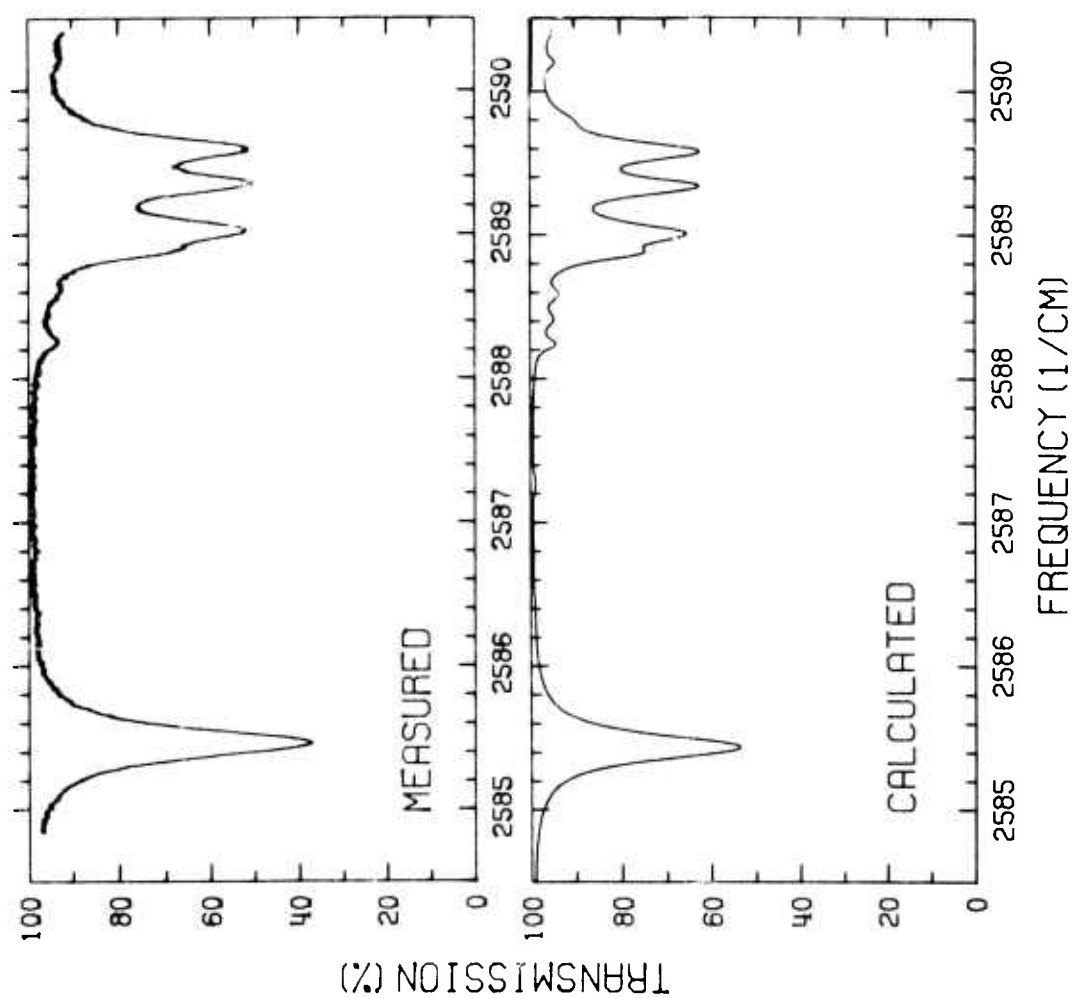


Figure 47. Comparison of Measured and Calculated HDO Spectra.
(100 meter path; .2002 Torr HDO; 760 Torr air; 300°K)

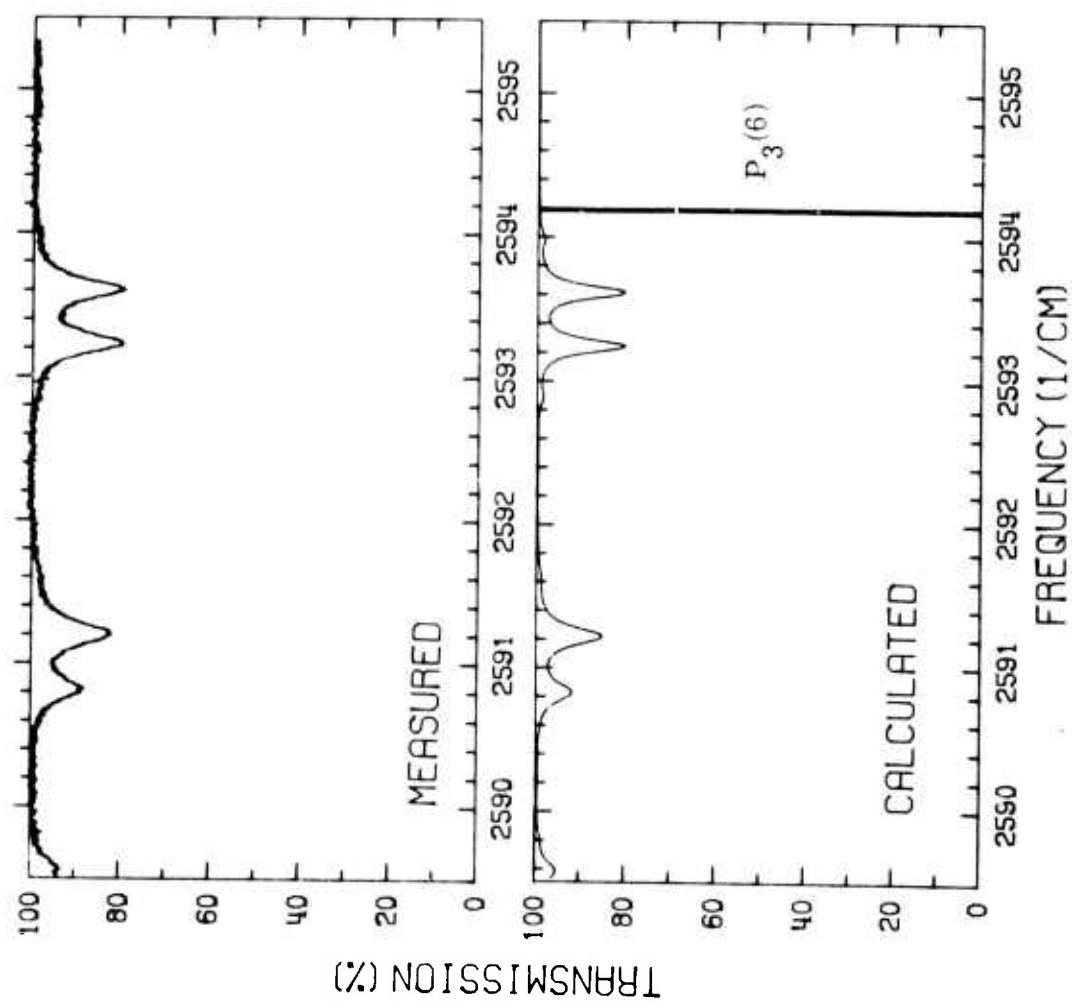


Figure 48. Comparison of Measured and Calculated HDO Spectra.
(100 meter path; .0205 Torr HDO; 760 Torr air; 300°K)

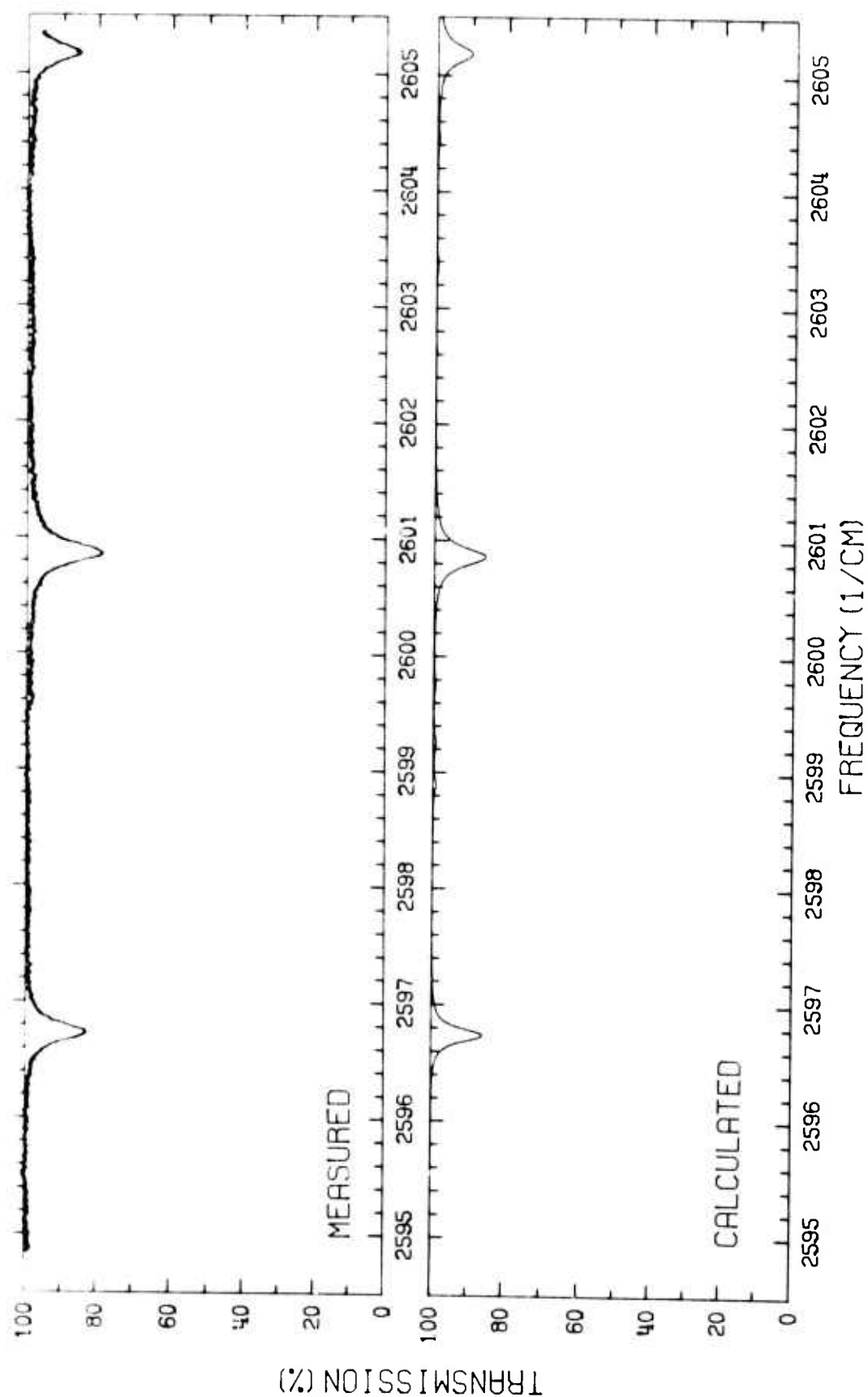


Figure 49. Comparison of Measured and Calculated HDO Spectra.
(100 meter path; .0205 Torr HDO; 760 Torr air; 300°K)

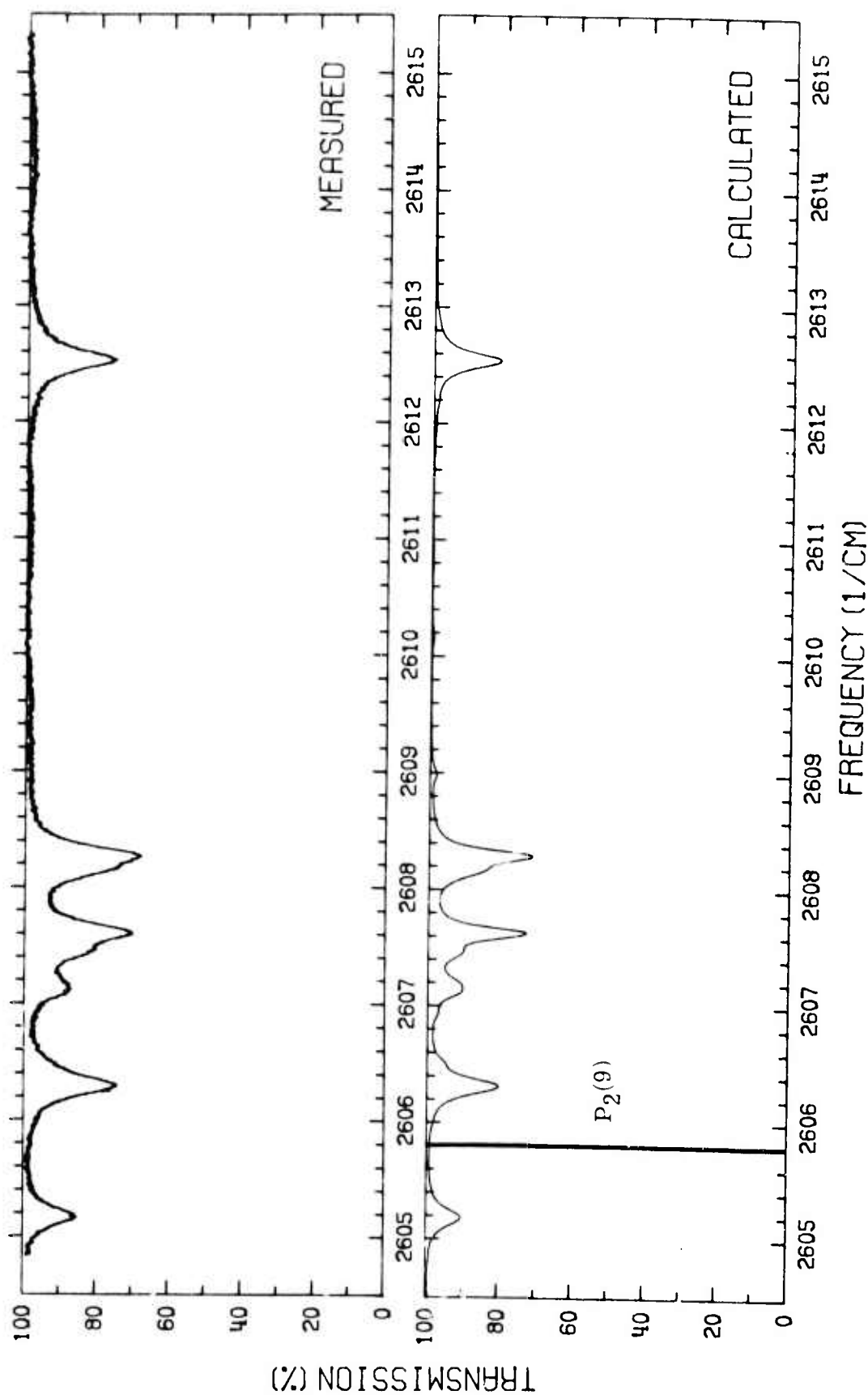


Figure 50. Comparison of Measured and Calculated HDO Spectra.
(100 meter path; .0205 Torr HDO; 760 Torr air; 300°K)

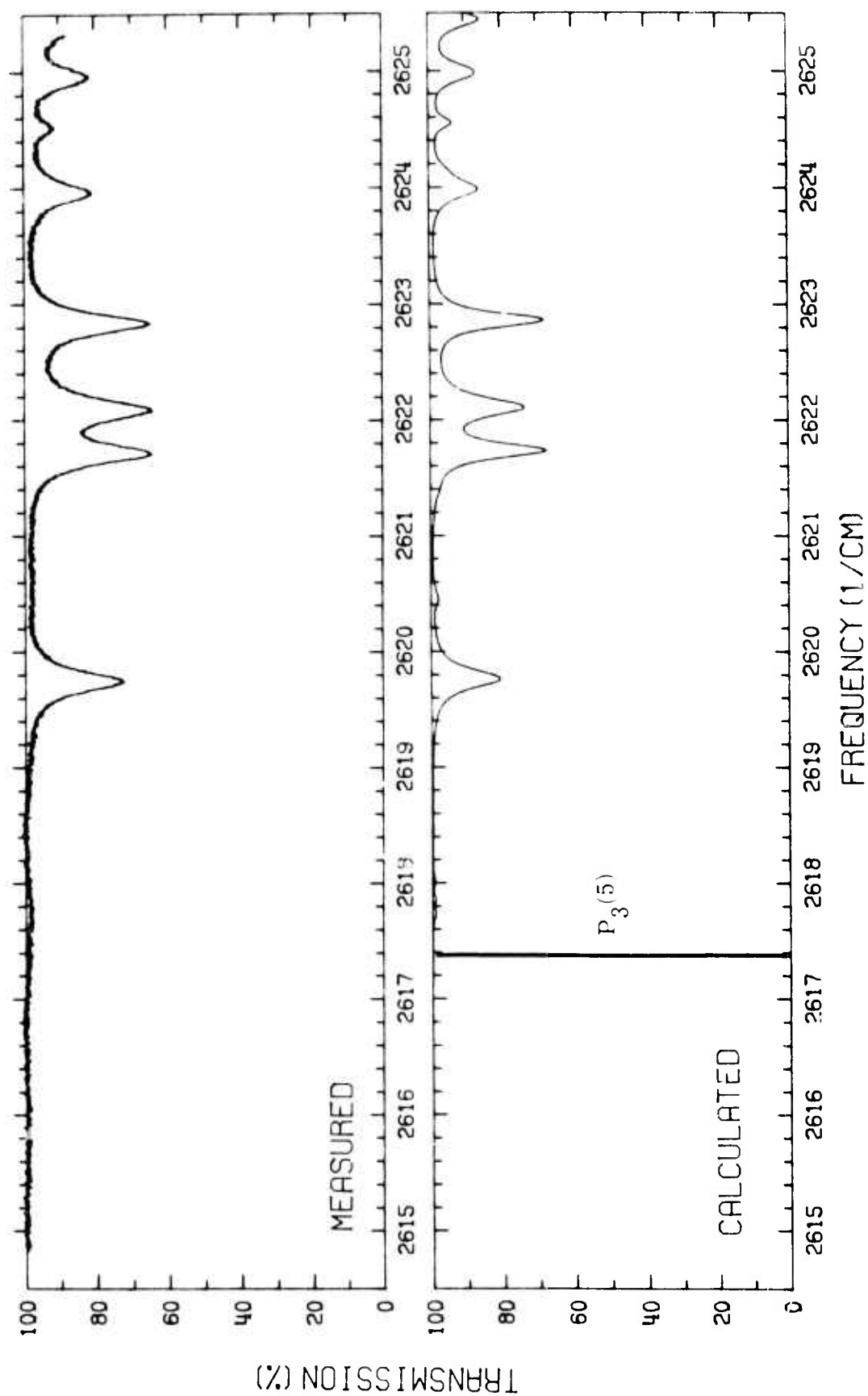


Figure 51. Comparison of Measured and Calculated HDO Spectra.
(100 meter path; .0205 Torr HDO; 760 Torr air; 300°K)

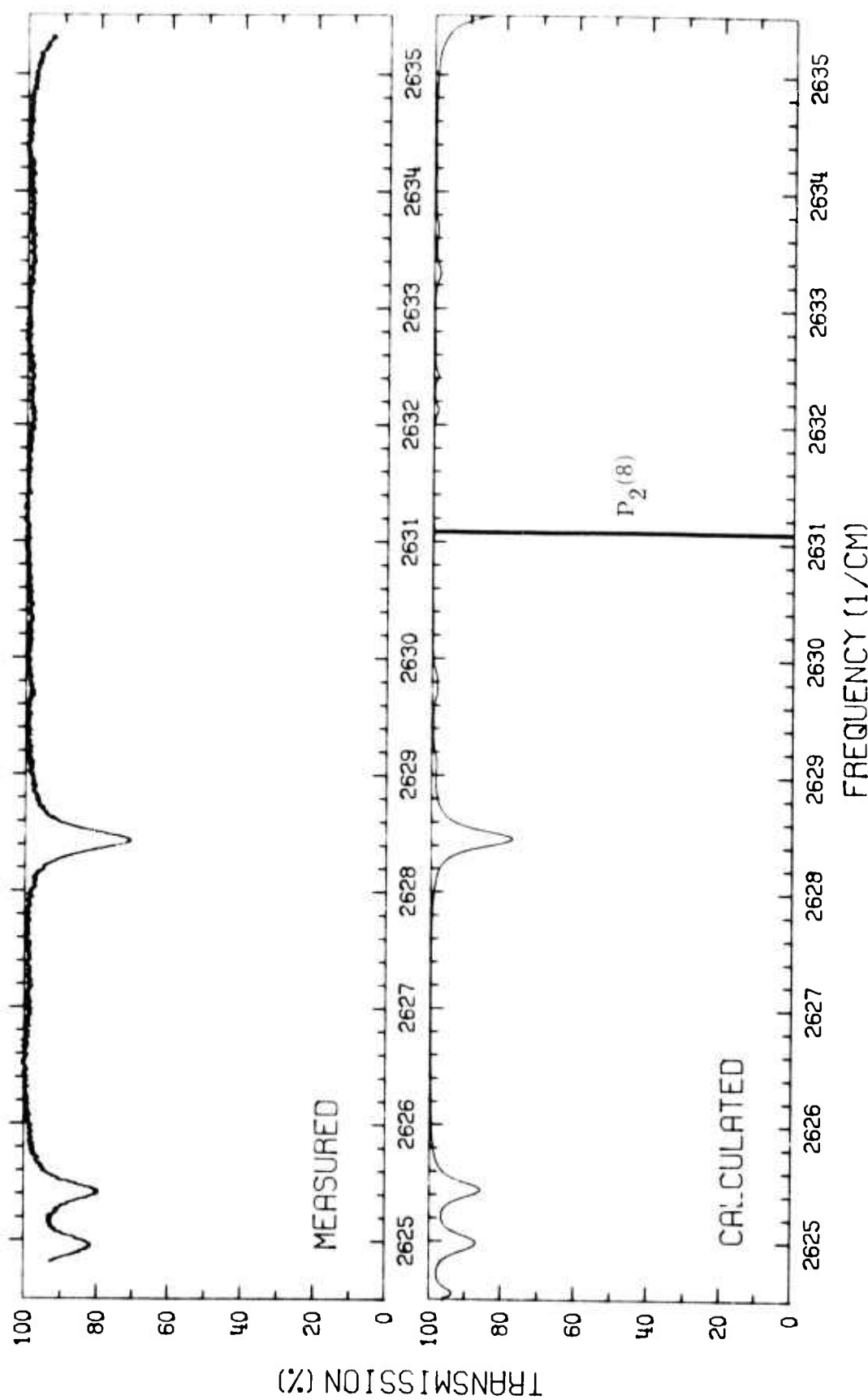


Figure 52. Comparison of Measured and Calculated HDO Spectra.
(100 meter path; .0205 Torr HDO; 760 Torr air; 300°K)

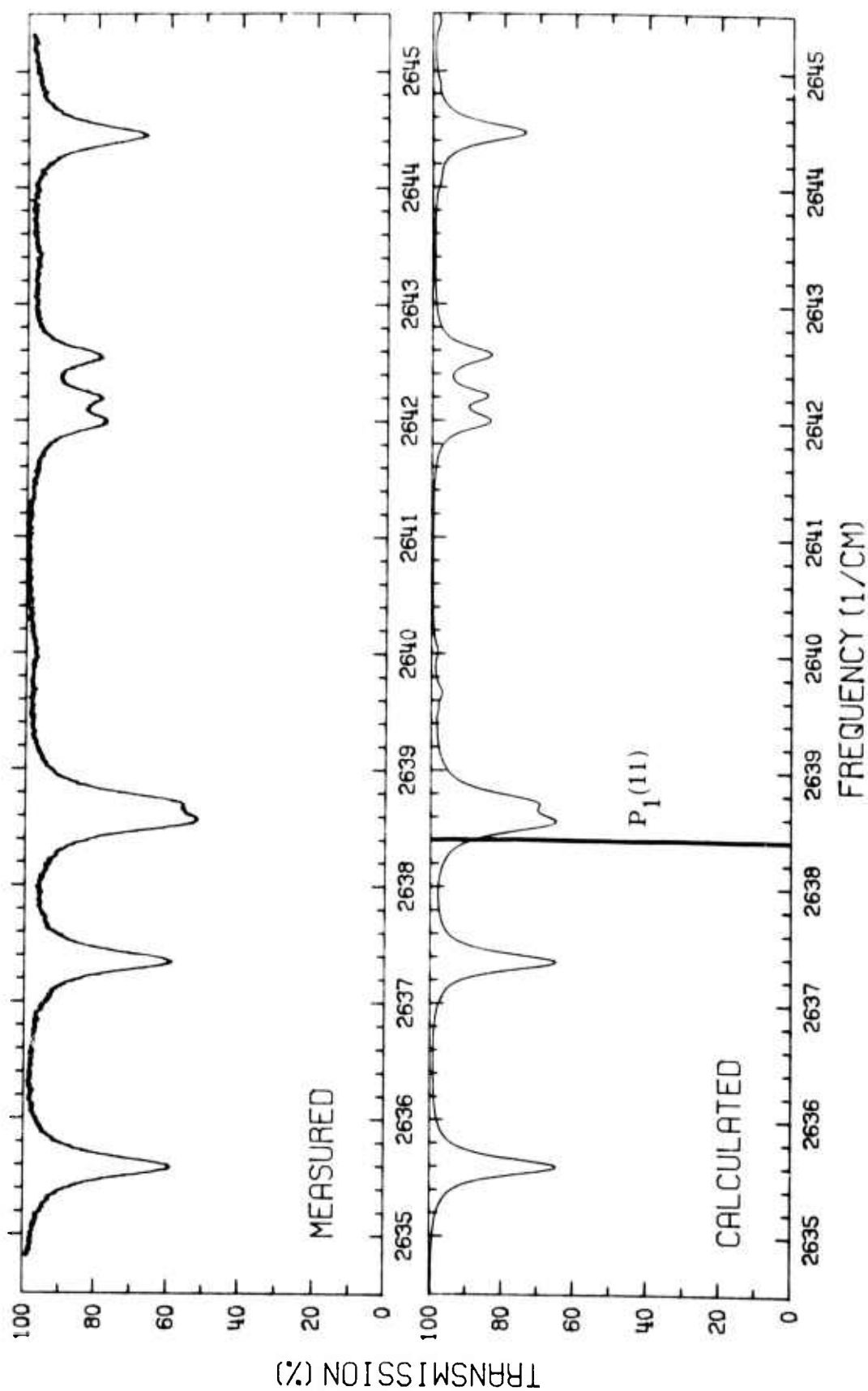


Figure 53. Comparison of Measured and Calculated HDO Spectra.
(100 meter path; .0205 Torr HDO; 760 Torr air; 300°K)

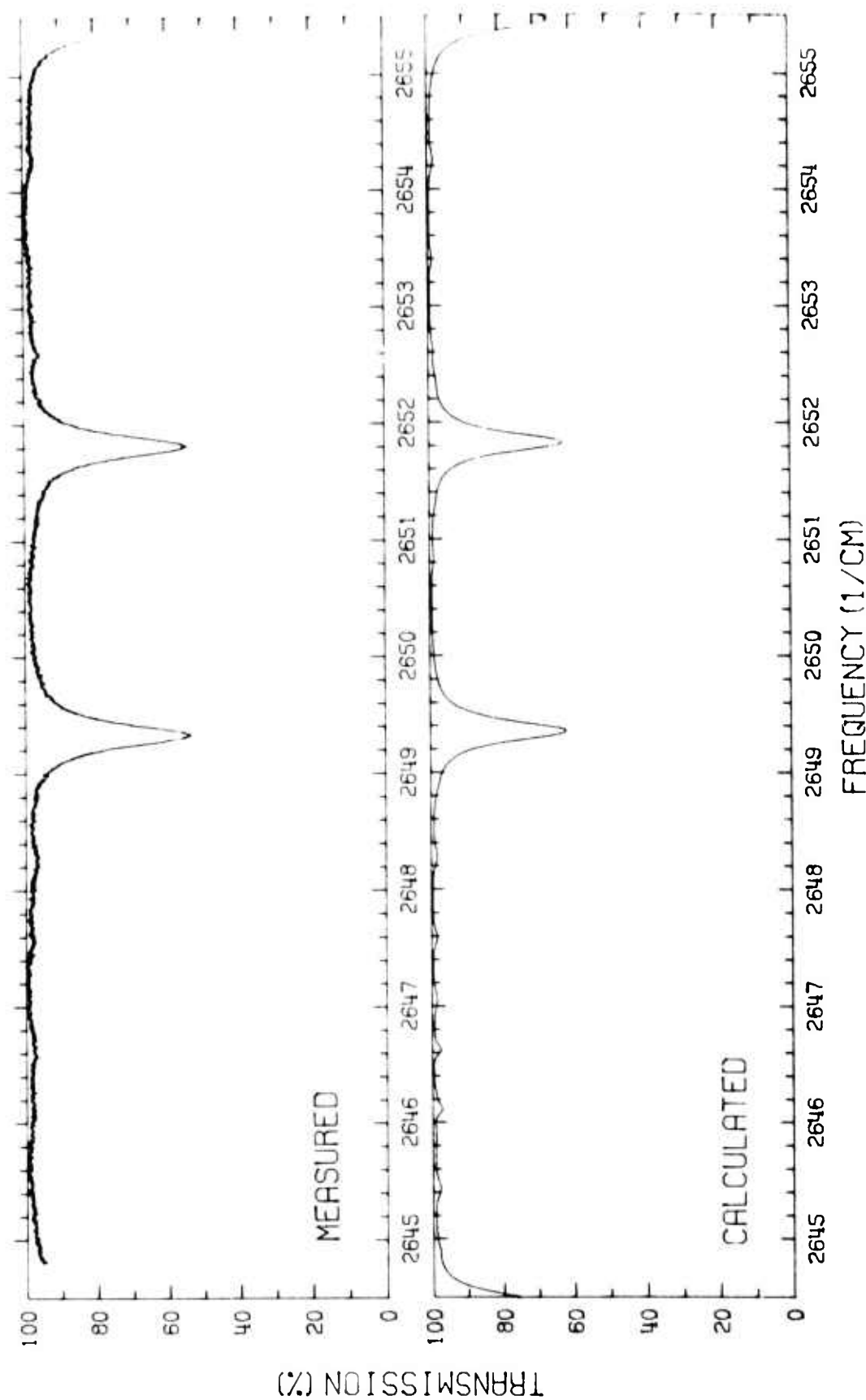


Figure 54. Comparison of Measured and Calculated HDO Spectra.
(100 meter path; .0205 Torr HDO; 760 Torr air; 300°K)

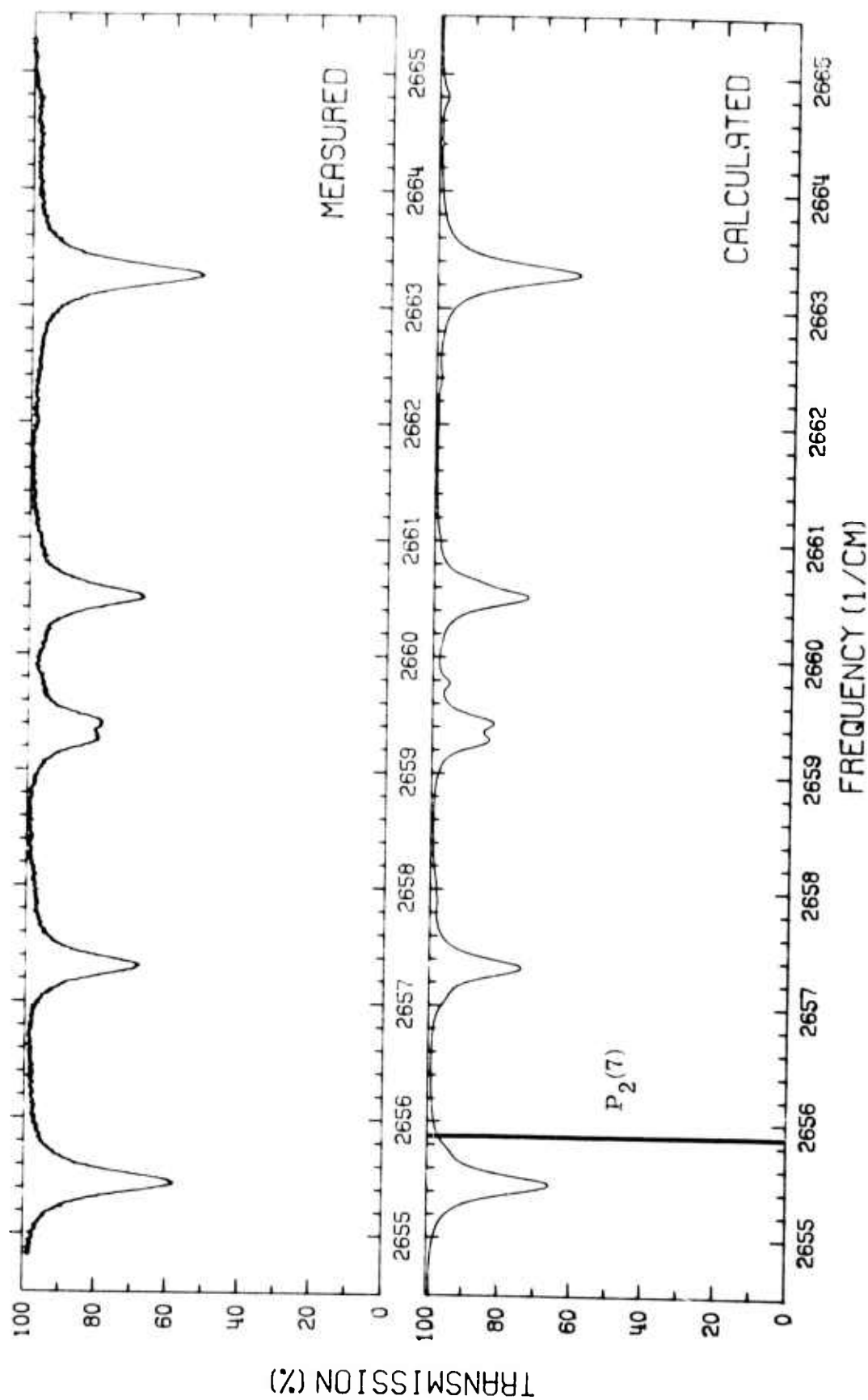


Figure 55. Comparison of Measured and Calculated HDO Spectra.
(100 meter path; .0205 Torr HDO; 760 Torr air; 300°K)

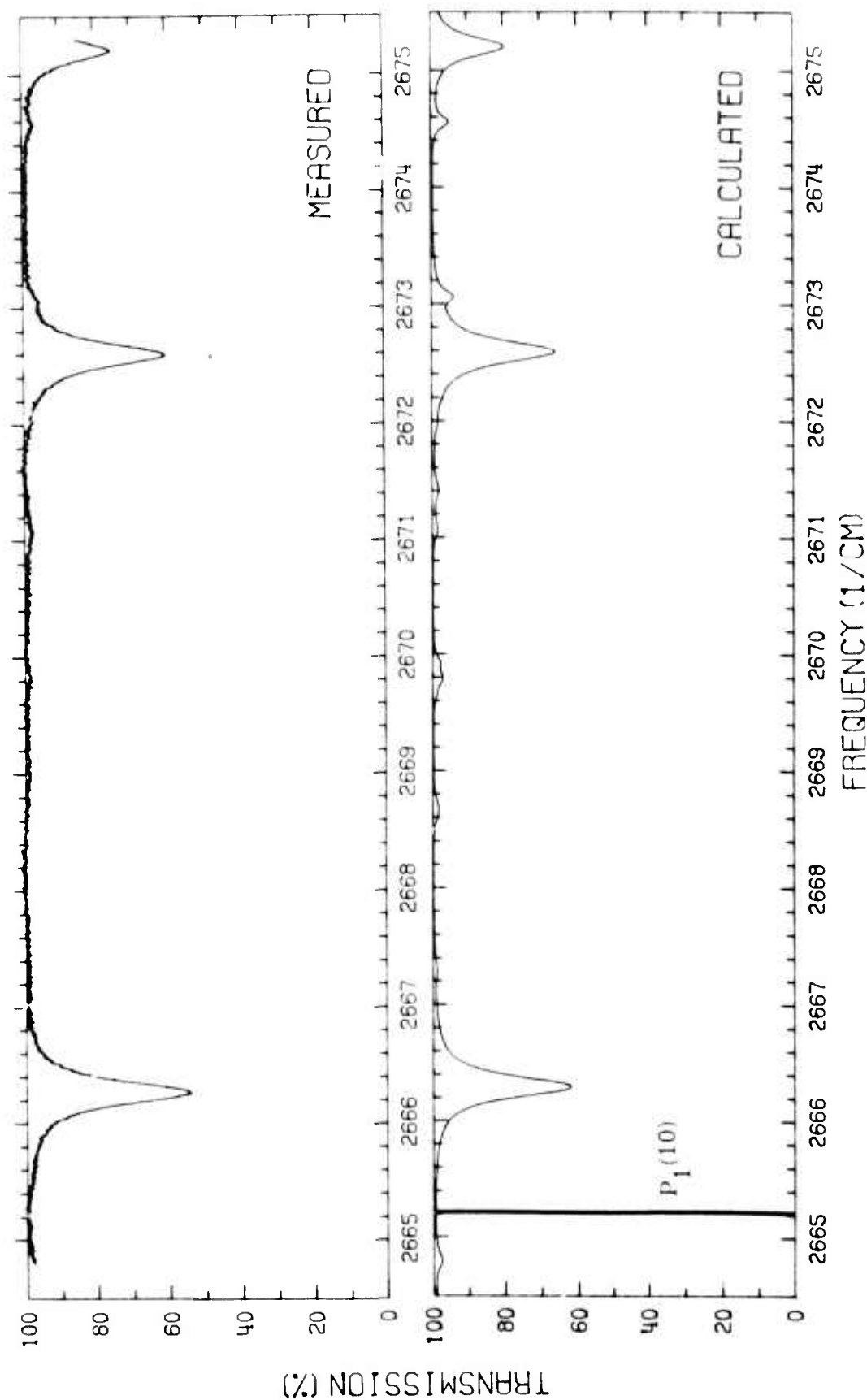


Figure 56. Comparison of Measured and Calculated HDO Spectra.
(100 meter path; .0205 Torr HDO; 760 Torr air; 300°K)

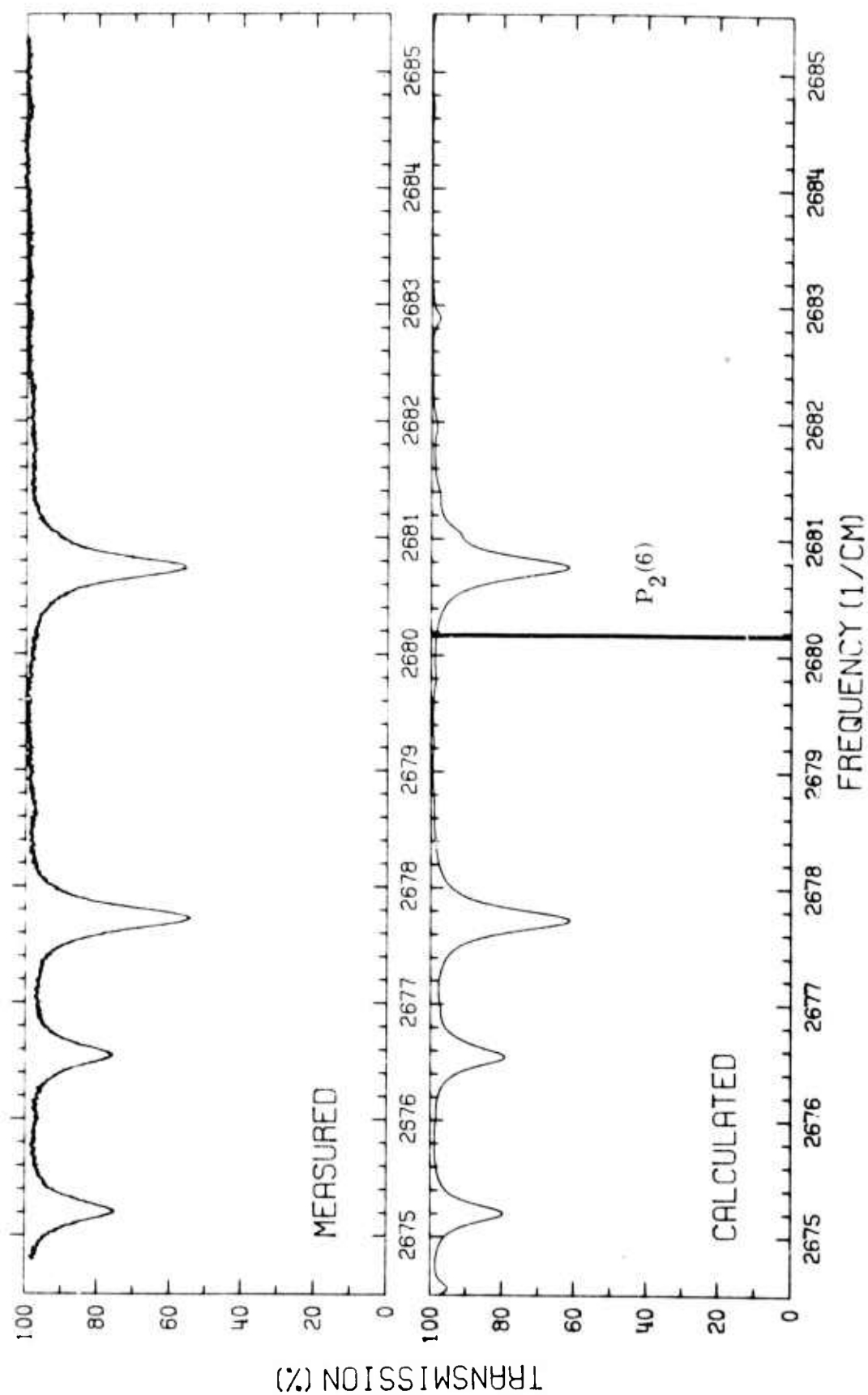


Figure 57. Comparison of Measured and Calculated HDO Spectra.
(100 meter path; .0205 Torr HDO; 760 Torr air; 300°K)

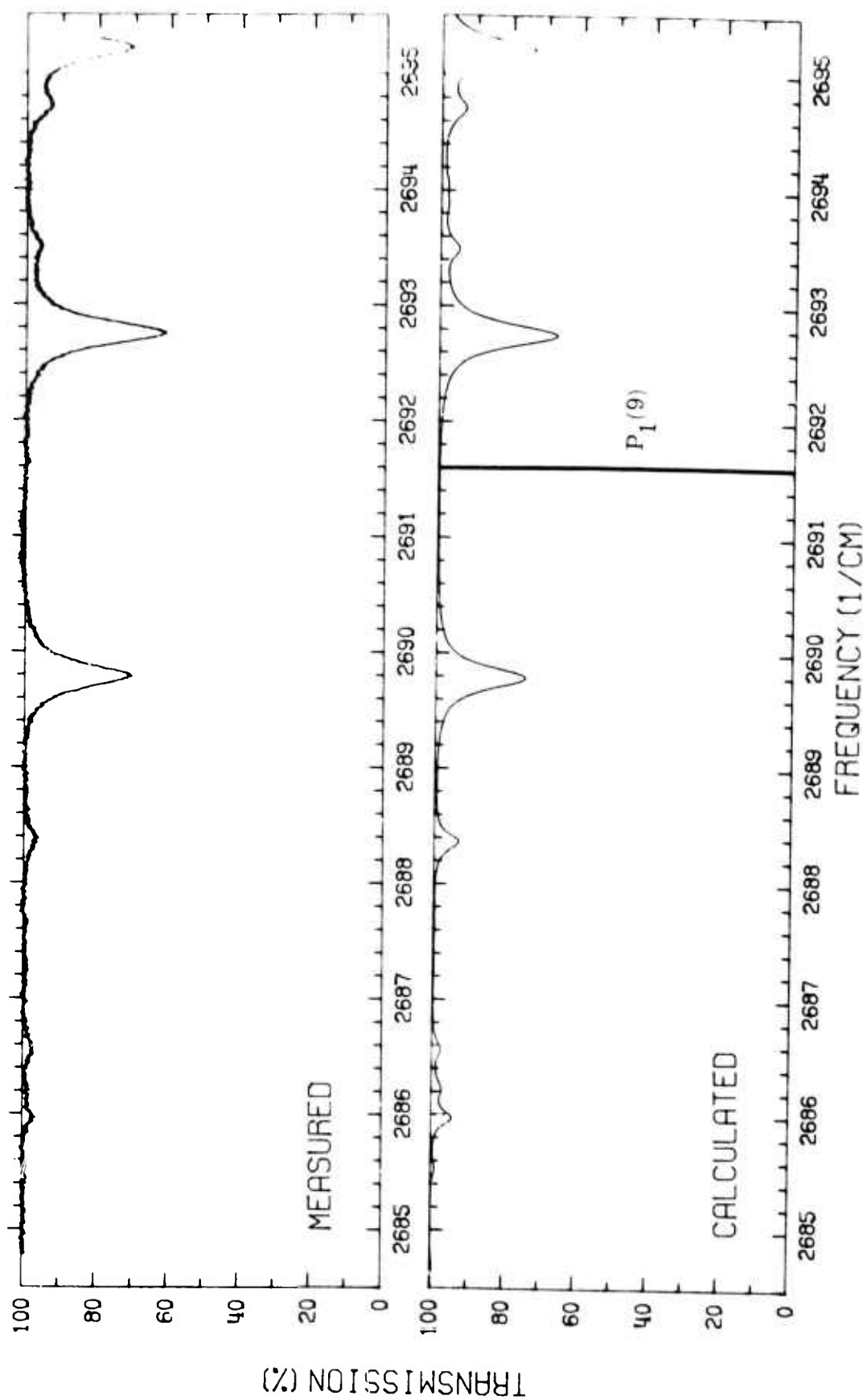


Figure 58. Comparison of Measured and Calculated HDO Spectra.
(100 meter path; .0205 Torr HDO; 760 Torr air; 300°K)

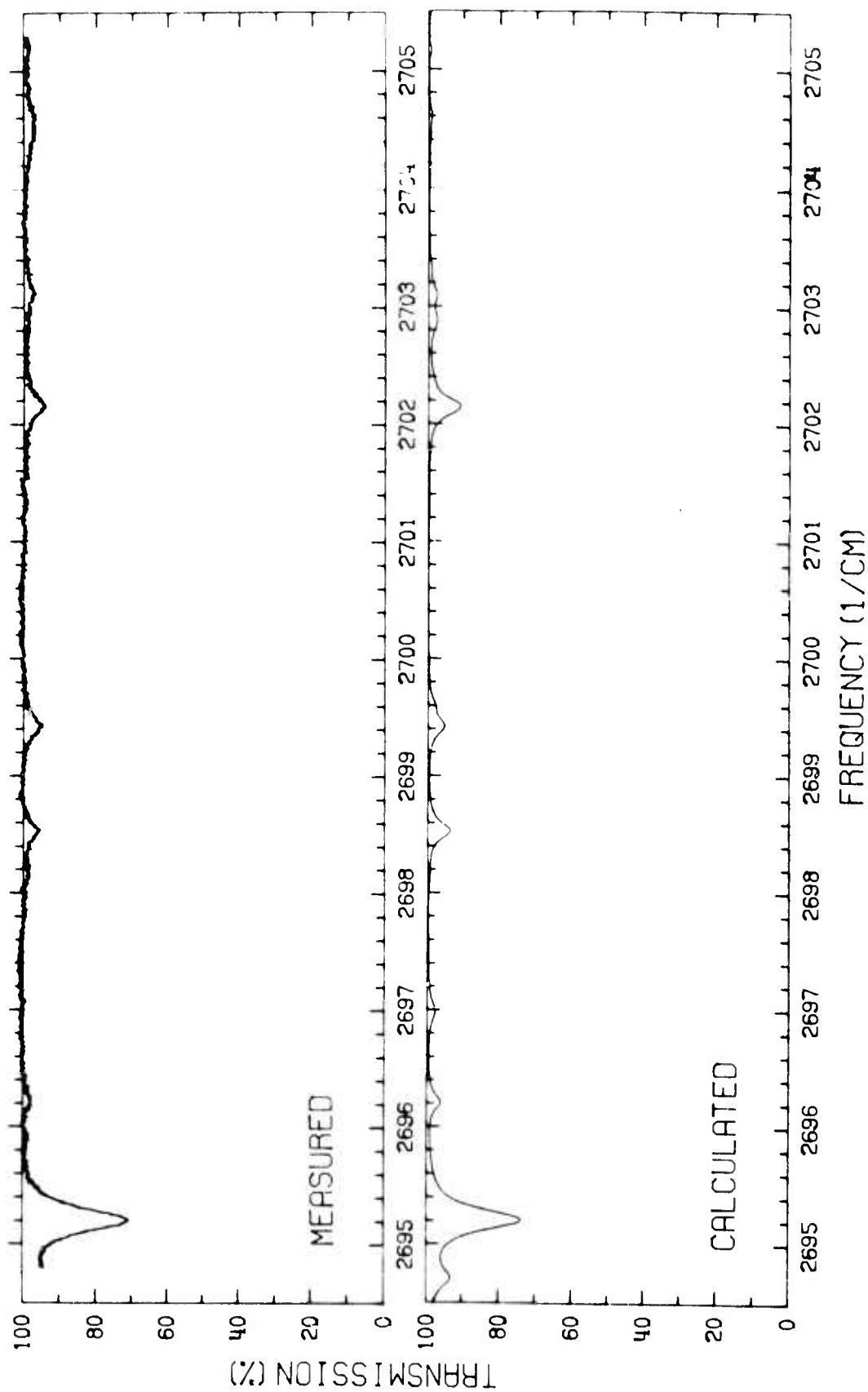


Figure 59. Comparison of Measured and Calculated HDO Spectra.
(100 meter path; .0205 Torr HDO; 760 Torr air; 300°K)

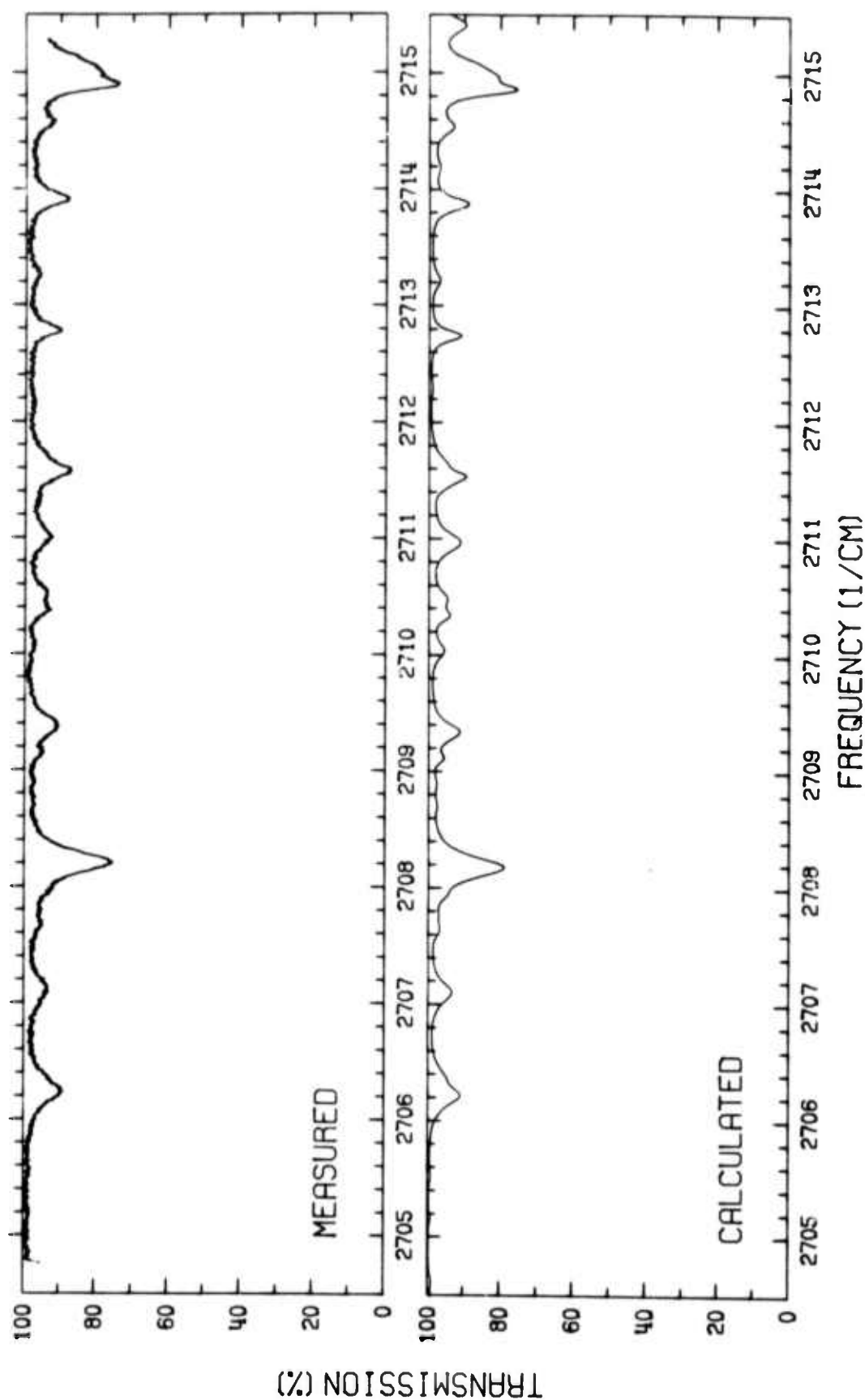


Figure 60. Comparison of Measured and Calculated HDO Spectra.
(100 meter path; .0205 Torr HDO; 760 Torr air; 300° K)

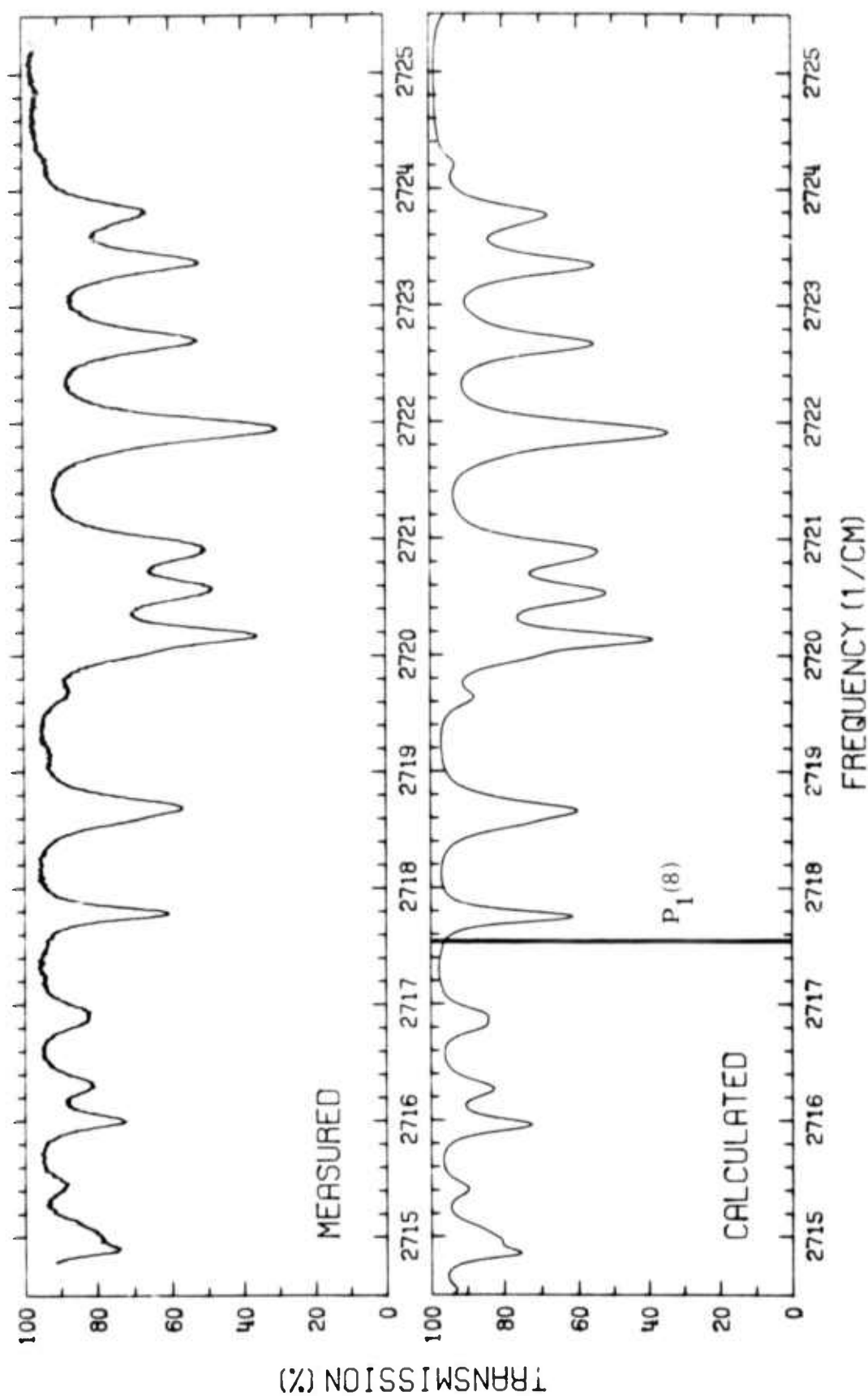


Figure 61. Comparison of Measured and Calculated HDO Spectra.
(100 meter path; .0205 Torr HDO; 760 Torr air; 300°K)

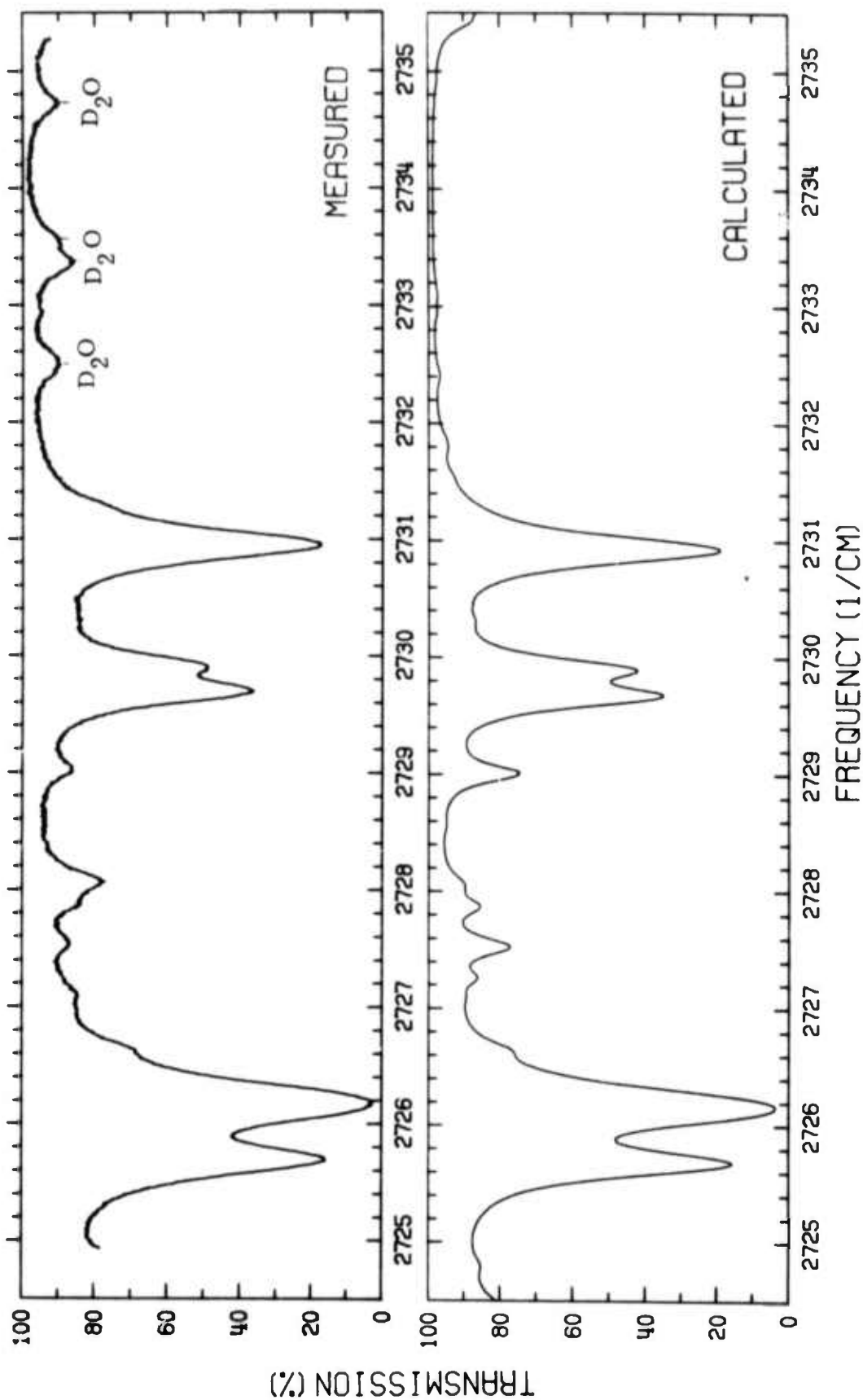


Figure 62. Comparison of Measured and Calculated HDO Spectra.
(100 meter path; .2002 Torr HDO; 760 Torr air; 300°K)

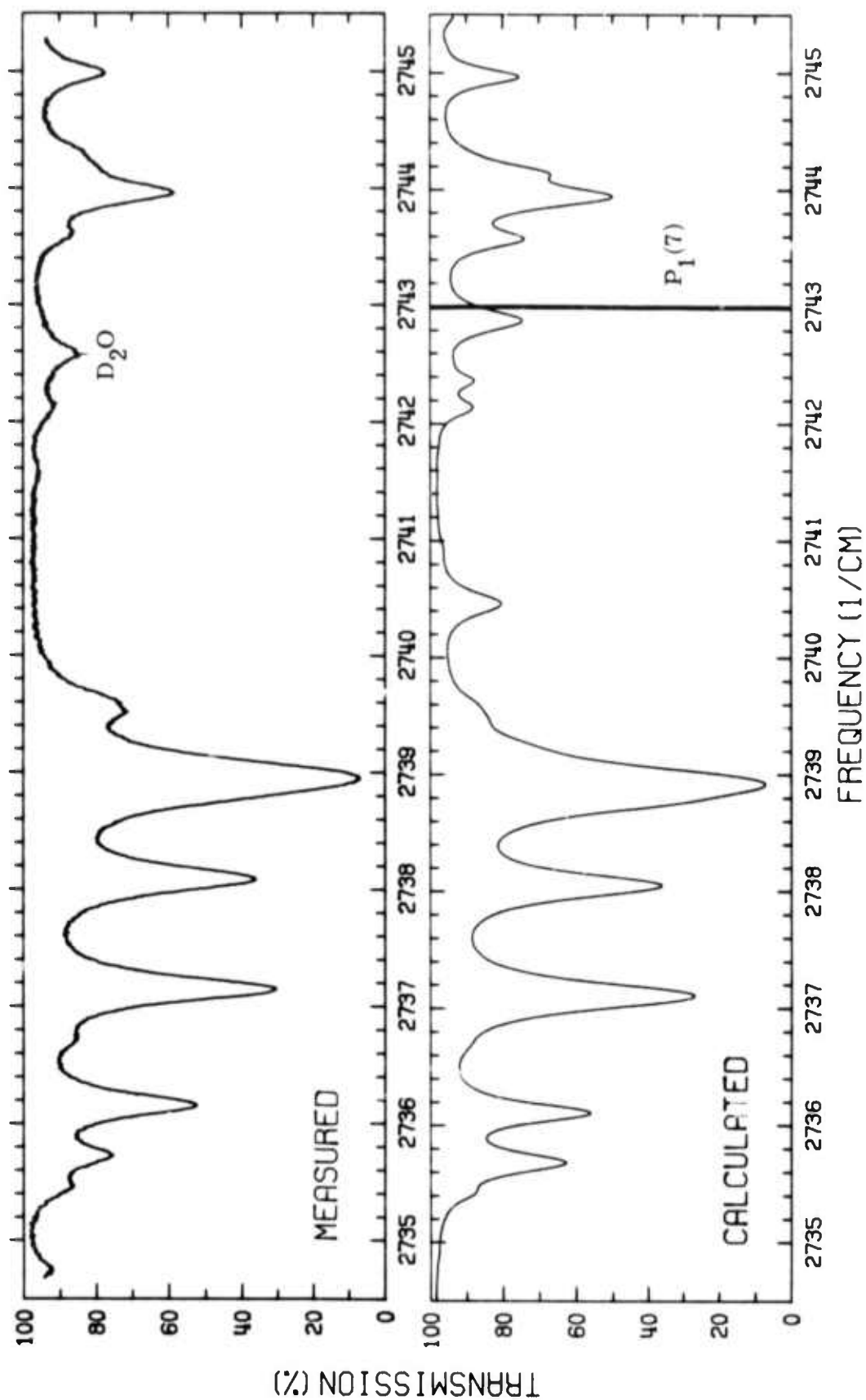


Figure 63. Comparison of Measured and Calculated HDO Spectra.
(100 meter path; .2002 Torr HDO; 760 Torr air; 300°K)

REFERENCES

1. R. E. Meredith, T. W. Tuer, and D. R. Woods, Investigation of DF Laser Propagation, Atmospheric Science Laboratory, U. S. Army Electronics Command, White Sands Missile Range, New Mexico, ECOM 74-4, 1974.
2. This reference is available to qualified military and government agencies on request from RADC (OCSE) Griffiss Air Force Base, New York 13441.
3. K. N. Rao, Bill Heath, The Ohio State University Physics Department Private Communication.
4. D. J. Spencer, G. C. Denault, and H. H. Takimoto, "Atmospheric Gas Absorption at DF Laser Wavelengths", Applied Optics, 13(12), 2855, 1974
5. F. S. Mills, and R. K. Long, Measured N_2O-N_2 Absorption of HF and DF Laser Radiation, RADC-TR-74-89, 1974 (AD778 949).
6. R. A. McClatchey, and J. E. A. Selby, Atmospheric Attenuation of HF and DF Laser Radiation, AFCRL-72-0312, 1972
7. R. A. McClatchey, W. S. Benedict, S. A. Clough, D. E. Burch, R. F. Calfee, K. Fox, L. S. Rothman, and J. A. Garing, AFCRL Atmospheric Absorption Line Parameters Compilation, AFCRL-TR-73-0096, 1973
8. R. K. Long, F. S. Mills, and G. L. Trusty, Calculated Absorption Coefficients for DF Laser Frequencies, RADC-TR-73-389 (AD775 373).
9. R. A. McClatchey, R. W. Fenn, J. E. A. Selby, J. S. Garing, and F. E. Volz, Optical Properties of the Atmosphere, AFCRL-70-0527
10. F. S. Mills, and R. K. Long, Absorption Coefficient Measurements of CO_2 , $HDO-N_2$ and CH_4 -Air Using a DF Laser, RADC-TR-74-295, 1974 (ADA001 097).
11. D. H. Enhalt and H. G. Ostlund, "Deuterium in Hurricane Faith 1966: Preliminary Results", Journal of Geophysical Research, 75(12), April 20, 1970.



MISSION
of
Rome Air Development Center

RADC is the principal AFSC organization charged with planning and executing the USAF exploratory and advanced development programs for information sciences, intelligence, command, control and communications technology, products and services oriented to the needs of the USAF. Primary RADC mission areas are communications, electromagnetic guidance and control, surveillance of ground and aerospace objects, intelligence data collection and handling, information system technology, and electronic reliability, maintainability and compatibility. RADC has mission responsibility as assigned by AFSC for demonstration and acquisition of selected subsystems and systems in the intelligence, mapping, charting, command, control and communications areas.